

Exploiting Piano Acoustics in Automatic Transcription

Tian Cheng

PhD thesis

School of Electronic Engineering and Computer Science
Queen Mary University of London

2016

Abstract

In this thesis we exploit piano acoustics to automatically transcribe piano recordings into a symbolic representation: the pitch and timing of each detected note. To do so we use approaches based on non-negative matrix factorisation (NMF). To motivate the main contributions of this thesis, we provide two preparatory studies: a study of using a deterministic annealing EM algorithm in a matrix factorisation-based system, and a study of decay patterns of partials in real-world piano tones.

Based on these studies, we propose two generative NMF-based models which explicitly model different piano acoustical features. The first is an attack/decay model, that takes into account the time-varying timbre and decaying energy of piano sounds. The system divides a piano note into percussive attack and harmonic decay stages, and separately models the two parts using two sets of templates and amplitude envelopes. The two parts are coupled by the note activations. We simplify the decay envelope by an exponentially decaying function. The proposed method improves the performance of supervised piano transcription.

The second model aims at using the spectral width of partials as an independent indicator of the duration of piano notes. Each partial is represented by a Gaussian function, with the spectral width indicated by the standard deviation. The spectral width is large in the attack part, but gradually decreases to a stable value and remains constant in the decay part. The model provides a new aspect to understand the time-varying timbre of piano notes, but further investigation is needed to use it effectively to improve piano transcription.

We demonstrate the utility of the proposed systems in piano music transcription and analysis. Results show that explicitly modelling piano acoustical features, especially temporal features, can improve the transcription performance.

Acknowledgements

First and foremost, I would like to thank my supervisors, Simon Dixon and Matthias Mauch, for their advice in these four years of research, providing me with useful guidance on the big picture of the thesis and also a great deal of freedom to explore the topics of my choice. I am grateful to Emmanouil Benetos, for his extremely detailed feedback and help that has led to a joint publication.

Special thanks to Roland Badeau, Sebastian Ewert and Kazuyoshi Yoshii for their advice on the work in Chapter 3, 5 and 6, respectively. I am further grateful to Kazuyoshi Yoshii for a very nice stay at the Okuno Lab in Kyoto University.

A big thanks to the members of the Centre for Digital Music who have made these four years a pleasant research experience: Mathieu Barthet, Chris Cannam, Keunwoo Choi, Magdalena Chudy, Alice Clifford, Jiajie Dai, Brecht De Man, Gyorgy Fazekas, Peter Foster, Dimitrios Giannoulis, Steven Hargreaves, Chris Harte, Ho Huen, Holger Kirchhoff, Katerina Kosta, Panos Kudumakis, Beici Liang, Zheng Ma, Andrew McPherson, Ken O'Hanlon, Maria Panteli, Marcus Pearce, Mark Plumbley, Elio Quinton, Andrew Robertson, Mark Sandler, Siddharth Sigtia, Jordan Smith, Janis Sokolovskis, Chunyang Song, Yading Song, Dan Stowell, Bob Sturm, Mi Tian, Robert Tubb, Bogdan Vera, Siying Wang, Sonia Wilkie and Luwei Yang.

Finally, I thank my family and friends (especially Shan) for their support. Many thanks to Hao Li for his unwavering moral support!

This work was supported by a joint Queen Mary/China Scholarship Council Scholarship.

Licence

This work is copyright © 2016 Tian Cheng, and is licensed under the Creative Commons Attribution Non Commercial Share Alike Licence. To view a copy of this licence, visit

<https://creativecommons.org/licenses/by-nc-sa/4.0/>

or send a letter to Creative Commons, 171 Second Street, Suite 300, San Francisco, California, 94105, USA.

Contents

1	Introduction	14
1.1	Automatic music transcription and piano transcription	15
1.2	Research questions	16
1.3	Thesis structure and contributions	18
1.4	Related publications	19
2	Background	21
2.1	Music knowledge	21
2.1.1	Sound generation and perception	21
2.1.2	Piano acoustics	24
2.2	Related work	28
2.2.1	Methods based on periodicity	29
2.2.2	Methods based on harmonics (partials)	31
2.2.3	Methods based on timbre	33
2.2.4	Methods based on high level information	35
2.2.5	Classification-based methods	38
2.2.6	Note tracking	39
2.3	Techniques for NMF-based AMT systems	42
2.3.1	A general framework for NMF-based AMT	43
2.3.2	Constraints	51
2.3.3	Bayesian extension of NMF	56
2.4	Evaluation metrics	59
2.4.1	Frame-level evaluation	59
2.4.2	Note-level evaluation	60
2.4.3	Instrument-level evaluation	60
2.4.4	Public evaluation	61
2.5	Conclusions	61
3	A Deterministic Annealing EM Algorithm for AMT	63
3.1	PLCA and shift-invariant PLCA	64

3.2	Transcription system based on DAEM	65
3.2.1	The baseline PLCA model	65
3.2.2	The DAEM-based model	67
3.3	Experiments	68
3.3.1	Datasets	68
3.3.2	Evaluation	68
3.3.3	Results	69
3.4	Conclusions and discussions	72
4	Modelling the Decay of Piano Tones	74
4.1	Method	75
4.1.1	Finding partials	75
4.1.2	Tracking the decay of partials	76
4.2	Experiment	80
4.2.1	Dataset	81
4.2.2	Metric	81
4.2.3	Modelling the decay	81
4.3	Results	81
4.3.1	R-squared	81
4.3.2	Decay response	83
4.3.3	Decay of different dynamics	84
4.4	Conclusions	84
5	An Attack/Decay Model for Piano Transcription	87
5.1	Method	89
5.1.1	A model of attack and decay	89
5.1.2	Sparsity	92
5.1.3	Onset detection	93
5.1.4	Offset detection	93
5.2	Experiments	96
5.2.1	Experimental setup	97
5.2.2	The main transcription experiment	97
5.2.3	Comparison with state-of-the-art methods	103
5.2.4	Test on repeated notes for single pitches	106
5.2.5	Analysing decay in different dynamics	109
5.3	Conclusion and future work	111
6	Modelling Spectral Widths for Piano Transcription	114
6.1	The proposed model	115
6.1.1	Modelling spectral widths	115
6.1.2	Modelling piano notes	116

6.2	Piano transcription experiment	117
6.2.1	Pre-processing	118
6.2.2	Template training	118
6.2.3	Post-processing	119
6.2.4	Results	122
6.3	Conclusions and future work	127
7	Conclusions and Future Work	129
7.1	Conclusions	129
7.2	Further work	131
A	Beating in the dB scale	135
B	Derivations for the attack/decay model	137
C	Derivations for modelling spectral widths	141

List of Figures

2.1	The first four standing wave modes of an ideal vibrating string fixed at both ends.	22
2.2	Spectra of tones A4 (with the fundamental frequencies of around 440 Hz) generated by different instruments. The dashed lines indicate positions of harmonics (multiples of f_0).	23
2.3	Grand piano structure, http://www.radfordpiano.com/structure/	25
2.4	Time evolution of the spectrum of note A4 (440 Hz).	27
2.5	Different decay patterns of partials from notes (a) F1 (43.7 Hz), (b) G♭2 (92.5 Hz) and (c) A1 (55 Hz). The top and middle panes show the waveforms and spectrograms, respectively. The bottom panes show the decay of selected partials, which are indicated by the arrows on the spectrograms. The dashed lines are estimated by the model in Chapter 4.	28
2.6	Dynamic Bayesian Network structure with three layers of variables: the hidden chords C_t and note combinations N_t , and observed salience S_t	37
2.7	The hybrid architecture of the AMT systems in [Sigtia et al., 2015, 2016].	38
2.8	A general framework for NMF-based transcription.	44
2.9	The waveform and spectrogram of a tone with f_0 of 440 Hz.	49
2.10	Spectral bases and activations obtained using different cost functions.	50
3.1	Box-and-whisker plots of (a) accuracy; (b) onset-only F-measure; and (c) onset-offset F-measure; for the Bach10 dataset.	70
4.1	(a) Partial frequencies of note A1 (55 Hz), (b) Inharmonicity coefficient B along the whole compass estimated for the piano of the RWC dataset.	76

4.2	Linear fitting for: (a) the 3 rd partial of note D1 ($f_0 = 36.7$ Hz); (b) the 2 nd partial of note A♭1 ($f_0 = 51.9$ Hz); (c) the 30 th partial of note D♭2 ($f_0 = 69.3$ Hz).	78
4.3	Multi-phase linear fitting for: (a) the 7 th partial of note B♭0 ($f_0 = 29.1$ Hz); (b) the 4 th partial of note B♭2 ($f_0 = 116.5$ Hz); (c) the 1 st partial of note E5 ($f_0 = 659.3$ Hz).	79
4.4	Non-linear curve fitting for: (a) the 22 nd partial of note D♭1 ($f_0 = 34.6$ Hz); (b) the 10 th partial of note G1 ($f_0 = 49$ Hz); and (c) the 10 th partial of note A1 ($f_0 = 55$ Hz).	80
4.5	Flowchart of partial decay modelling.	82
4.6	Average R^2 of different note groups. f , m , p stand for dynamics, while L and 3 indicate the linear and mixed models, respectively. The order of labels in the legend corresponds to the order of lines from top to bottom.	83
4.7	Decay response: decay rates against frequency. Lower values mean faster decay. The greyscale is used to indicate fundamental frequency, with darker colours corresponding to lower pitches. . .	84
4.8	Decay rates for the first five partials for different dynamics . . .	86
5.1	An example of output from the proposed model.	88
5.2	An example illustrating of the proposed model (note D3 with the MIDI index of 50).	91
5.3	Example of onset detection showing how activations are processed.	94
5.4	Costs and segments for pitch F3 (MIDI index 53).	95
5.5	Attack envelopes.	99
5.6	Detected onsets with different sparsity for pitch G4 (MIDI index 67).	101
5.7	Performance using different sparsity factors and thresholds. The sparsity factors are indicated by different shapes, as shown in the legends. Lines connecting different shapes are results achieved via the same threshold. The threshold of the top-left set is -40 dB, and the bottom-right set is -21 dB. The dashed lines show F-measure contours, with the values decreasing from top-right to bottom-left.	102
5.8	Examples of repeated note detection for low (left) and high (right) pitches at three dynamic levels. Detected onsets are shown as brown impulses, and ground truth onsets as red.	109
5.9	Attack envelopes of different dynamics.	110
5.10	Decay rates as a function of pitch for different dynamics.	111

6.1	Spectra of the signal in Equation 6.1	116
6.2	The response of a Gaussian window	117
6.3	Spectrograms and extracted parameters: templates, activations and spectral widths for notes of different pitches	120
6.4	Trained spectral widths.	121
6.5	Box-and-whisker plots of spectral widths (below 20 frequency bins) at onsets, with pitch in MIDI index on the vertical axis. . .	125
6.6	Box-and-whisker plots of spectral widths (below 20 frequency bins) in decay stages, with pitch in MIDI index on the vertical axis.	126
6.7	An example of the spectral width and activation for one pitch during the first 6 seconds of the piece ‘alb_se2’.	127
7.1	Filters for modelling the frequency response difference between two pianos.	134

List of Tables

2.1	Three levels of music dynamics, adapted from [Rossing, 1990, p. 100]	26
2.2	The usage of the β -divergences in AMT	47
2.3	Relation between divergences and generative models, adapted from [Smaragdis et al., 2014]	57
2.4	Public evaluation results on frame-wise accuracy (Acc_f) and onset-only note-level F-measure F_{on}	61
3.1	Note ranges (in MIDI index) of instruments, adapted from Benetos and Dixon [2012b].	66
3.2	Multiple F0 estimation results (see Section 2.4 for explanation of symbols).	69
3.3	Note-tracking results	70
3.4	Instrument assignment results	72
4.1	Average R^2 of the linear and mixed models. NP is the number of partials above the noise level for each dynamic level.	82
5.1	Variable list	90
5.2	Datasets used in the experiments	98
5.3	Experimental configuration for the training stage	98
5.4	Experimental configuration I for the transcription experiments in Section 5.2.2.	99
5.5	Note tracking results with different fixed sparsity factors (above) and annealing sparsity factors (below).	100
5.6	Note tracking results (onset-offset) and frame-wise results	103
5.7	Comparison of transcription results with two state-of-the-art methods on three public datasets.	105
5.8	Experimental configuration II for test on repeated notes in Section 5.2.4.	106

5.9	Note tracking (onset-only) results for repeated notes in different dynamics.	108
6.1	Comparison of the proposed systems with a standard NMF . . .	123

List of Abbreviations

AMT	Automatic Music Transcription
ARMA	AutoRegressive Moving Average
CQT	Constant-Q Transform
DAEM	Deterministic Annealing Expectation-Maximization
EM	Expectation-Maximization
ERB	Equivalent Rectangular Bandwidth
HMM	Hidden Markov Model
HTC	Harmonic Temporal Structure Clustering
HTTC	Harmonic Temporal Timbral Clustering
IS	Itakura-Saito
KL	Kullback-Leibler
MIDI	Musical Instrument Digital Interface
MIR	Music Information Retrieval
ML	Maximum Likelihood
NMF	Non-negative Matrix Factorization
PLCA	Probabilistic Latent Component Analysis
SI-PLCA	Shift-Invariant Probabilistic Latent Component Analysis
STFT	Short-Time Fourier Transform
SVM	Support Vector Machine

Chapter 1

Introduction

This thesis explores piano acoustics for automatic transcription, using knowledge and techniques from signal processing, machine learning, and the physics of musical instruments. Signal processing provides a time-frequency representation as the front-end of the transcription system and machine learning helps us estimate the specific parameters for our models that relate the time-frequency representation to musical notes. The physics of musical instruments, and piano acoustics in particular, provides us with knowledge about the structure of piano sounds, and informs our research into new features to improve transcription accuracy.

Automatic music transcription (AMT) is important because the transcribed music notation (musical score) is a convenient summarisation of music that allows musicians to efficiently exchange musical ideas and play them. It can be used in many applications, such as karaoke, query by humming (e.g. [midomi](http://www.midomi.com)¹) and music education [Tambouratzis et al., 2008]. In order to limit the scope of the thesis, we decided to focus on a single instrument. Being one of the most commonly-used instruments, the piano was the natural choice. Piano sounds have many specific features, including either ones simplifying the transcription task like discrete frequency and percussive onsets, or others such as time-varying timbre, large frequency and dynamic ranges. The richness of piano sounds makes the topic (piano transcription) interesting to explore. Furthermore, piano acoustics have been well investigated, providing us with ample theoretical findings which we can make use of.

In order to transcribe piano music signals into a symbolic representation, we make use of the non-negative matrix factorisation (NMF) framework to generate transcription systems motivated by piano acoustics. The thesis does not use methods such as simpler template matching, neural networks and hidden

¹<http://www.midomi.com>

Markov models. NMF has been used for AMT for more than one decade. It factorises a spectrogram into two low-rank matrices, representing spectral features and temporal features individually. Unlike simple template-matching models and black-box methods such as neural networks, NMF can explicitly model physical parameters, is easy to extend, and can be combined with a wide range of different methods, such as source/filter models for spectral modelling [Cheng et al., 2014].

In Section 1.1, we introduce automatic music transcription and piano transcription. Then we specify the research questions of the thesis in Section 1.2. Section 1.3 presents the structure of the thesis and contributions associated to each part. In Section 1.4, we list the publications by the author.

1.1 Automatic music transcription and piano transcription

Automatic music transcription converts a musical recording into a symbolic representation using some form of musical notation. AMT is a fundamental task in the music information research (MIR) domain, which is related to many MIR tasks, such as key detection, chord estimation, source separation, instrument recognition, fundamental frequency estimation, beat tracking, and onset/offset detection. They represent different levels and aspects (e.g. melody or rhythm) of music understanding. The task of automatic music transcription produces musical notation at a relatively low level [Benetos, 2012]. Research on AMT mainly focuses on three subtasks with detailed definitions in [Duan and Temperley, 2014, MIREX, 2016]. (1) Multiple F0 estimation (MFE) concentrates on the time frame level information. In this subtask, an audio signal is first divided into frames of equal time durations, then pitches are estimated in each frame. (2) Note tracking produces a list of note events, consisting of onsets, offsets and pitches of the notes. (3) In the third level, the stream or instrument level, systems try to explore the additional property of sound sources, in order to assign notes to their instrument sources [Grindlay and Ellis, 2011, Bay et al., 2012, Benetos et al., 2013b]. In order to step from AMT toward producing the musical score, it is essential to consider high-level information (key detection and chord estimation) and rhythm information (beat tracking).

In comparison to other instruments, working on piano music simplifies the transcription task in several ways, due to features such as discrete pitches and hard onsets. However, piano transcription is still of great challenge. Firstly, the piano covers a large pitch range with fundamental frequencies from 27.5 Hz to 4186 Hz. Secondly, the stiffness of the strings causes inharmonicity of pi-

ano sounds. Thirdly, the number of simultaneous notes can be high in piano music. It is even possible to have over 10 notes at the same time (using the sustain pedal). Lastly, the decaying note energy makes the offsets hard to detect correctly.

In this thesis, we start our studies on automatic music transcription in Chapter 3, in which we analyse results of AMT systems at all three levels (frame level, note level and instrument level). After investigating piano decay in Chapter 4, we focus on piano transcription in Chapter 5 and 6, so that instrument assignment is not needed for these two chapters.

1.2 Research questions

The work in this thesis addresses one main research question (RQ), which we then break down into four more specific questions as detailed below.

RQ: Can automatic transcription of piano music be improved by considering acoustical features of the piano?

This thesis targets the automatic transcription task on a specific piano. Given the situation that we have access to isolated notes produced by the piano (the training dataset), we want to know what we can learn from the training dataset, and how that might be useful for transcribing polyphonic music pieces played on the same piano.

In order to answer the research question, we review both piano acoustics and automatic music transcription methods. The thesis is undertaken from the following four aspects.

RQ1: What are the weaknesses of matrix factorisation-based approaches and how can the weaknesses be addressed?

We review automatic music transcription systems in Section 2.2. Among the methods, non-negative matrix factorisation (NMF) is commonly used since [Smaragdis and Brown, 2003]. NMF can represent the spectral features and temporal features of musical tones individually, is easy to extend, and has been used in a physics-informed piano analysis system [Rigaud, 2013]. NMF is chosen as the fundamental framework for the proposed methods in this thesis. We specify systems based on non-negative matrix factorisation in Section 2.3, and deal with the local minimum problem of probabilistic latent component analysis (PLCA) (the probabilistic counterpart of NMF) in Chapter 3.

RQ2: Which features can we learn associated with piano acoustics?

Piano acoustics studies features associated with the physical structure and excitation mechanism of the piano. We briefly introduce piano acoustics in Section 2.1.2, including inharmonicity, attack noise and temporal evolution of piano tones. Inharmonicity has been studied by Rigaud [2013] for piano transcription and tuning. This thesis will focus on the time-varying spectral structures and the temporal evolution of piano tones.

RQ3: How do piano partials decay in real recordings?

Among the features associated to piano acoustics, we are particularly interested in piano decay. The theory of piano decay was studied by Weinreich [1977] and has been applied for sound synthesis [Aramaki et al., 2001, Bensa et al., 2003, Bank, 2000, 2001, Lee et al., 2010]. Previous studies on decay parameter estimation were only verified on some examples of synthetic notes [Välämäki et al., 1996, Karjalainen et al., 2002]. We do not know how well the theory based on two coupled strings works for all piano tones with different numbers of strings (1-3 strings). In Chapter 4, we track the decay of acoustic piano tones to understand partial decay of all 88 piano notes. We analyse the influence of the frequency range, pitch range and dynamic on decay patterns, to gain insights into how the decay information can be used in piano transcription systems.

RQ4: How can acoustical features be modelled in transcription systems?

Piano acoustics is well understood, but it is not intuitive to analyse and apply the acoustical features in an NMF framework. Previous studies on analysing musical signals using NMF are undertaken in several ways [Rigaud, 2013, Cheng et al., 2014], in which the parametric models attracted our attention. Hennequin et al. [2011a] extend the temporal activations of a standard NMF to be frequency-dependent by using the auto-regressive moving average (ARMA) model. Then the parameters of the ARMA model can be estimated directly. Hennequin et al. [2010] and Rigaud [2013] parameterise each partial by its frequency and the main lobe of the Hamming window, to estimate the frequencies directly for vibratos and inharmonic tones, respectively. In Chapter 5, we parameterise the decay envelope as an exponentially decaying function. In Chapter 6, we model each partial by its frequency and a Gaussian function, with the spectral width represented by the standard deviation of the Gaussian function. Then we can model and directly estimate the decay rate and the spectral width respectively in these proposed parametric models.

1.3 Thesis structure and contributions

The remainder of this thesis is organised as follows, with the associated contributions of the chapters.

Chapter 2 - Background: We present necessary information on piano music and computational methods. First, we introduce sound generation and perception, and specify piano acoustics as the theoretical foundation of our proposed piano transcription systems. Then we give a literature review on related work in the automatic music transcription (AMT) domain. Especially, we present a general framework for AMT systems based on non-negative matrix factorisation (NMF), including front-end, post-processing of standard AMT systems, and parameter estimation methods and constraints imposed in the NMF framework. Finally we describe commonly used evaluation metrics and compare the performance of important methods based on the results of a public evaluation platform.

Chapter 3 - A Deterministic Annealing EM Algorithm for AMT:

We deal with the local minimal problem of PLCA with a Deterministic Annealing Expectation-Maximisation (DAEM) algorithm and show the improvements in transcription performance by doing so.

Contributions: We provide modified update rules for a PLCA-based transcription method [Benetos and Dixon, 2012a] according to the DAEM, with the introduction of a ‘temperature’ parameter. In comparison to the baseline method, the proposed method brings improvements to both frame-level and note-level results.

Chapter 4 - Modelling the Decay of Piano Tones: We track the decay of acoustic piano tone. First, partials are found with inharmonicity considered. Then we track each partial to understand the decay of piano tones in real recordings.

Contributions: We track the decay of acoustic piano tones from the RWC Music Database in detail (first 30 partials of 88 notes played in 3 dynamics). We compare the temporal decay of individual piano partials to the theoretical decay patterns based on piano acoustics [Weinreich, 1977]. We analyse the influence of the frequency range, pitch range and dynamic on decay patterns, and gain insights into how piano transcription systems can make use of decay information.

Chapter 5 - An Attack/Decay Model for Piano Transcription: We propose an attack/decay model motivated by piano acoustics, which models the time-varying timbre and decaying energy of piano notes. We

detect note onsets by peak-picking on attack activations, then offsets for each pitch individually based on the reconstruction errors.

Contributions: The attack/decay method brings three refinements to the non-negative matrix factorisation: (1) introduction of attack and harmonic decay components; (2) use of a spike-shaped note activation that is shared by these components; (3) modelling the harmonic decay with an exponential function.

The results show that piano transcription performance for a known piano can be improved by explicitly modelling piano acoustical features. In addition, the proposed methods help to automatically analyse the decay of piano sounds in different dynamic levels.

Chapter 6 - Modelling Spectral Widths for Piano Transcription: We present a model for piano notes with time-varying spectral widths in an NMF framework. We refine detected onsets by their spectral widths, and analyse the spectral widths of isolated notes and notes in the musical pieces.

Contributions: We present a new feature, the spectral width, which could be potentially used as a cue to indicate the duration of piano notes. The results on isolated notes suggest that the spectral width is large in the attack part, then it decreases and remains stable in the decay part. We use the spectral widths to refine detected onsets in the transcription experiment. We analyse the spectral width distributions at onsets and in the decay parts for notes in the musical pieces and show several directions of future work.

Chapter 7 - Conclusions and further work: This chapter summarises the contributions of the thesis and provides a few directions worthy of further investigation, building on the work in the main chapters and generalising the proposed models for other pianos and instruments.

1.4 Related publications

The publications listed below are closely related to this thesis. The main chapters are based on [5] (Chapter 3), [3] (Chapter 4) and [1] (Chapter 5), respectively. The author was the main contributor to the listed publications, who performed all scientific experiments and manuscript writing, under supervision of SD and MM. Co-authors SD, MM, EB provided advice during meetings and comments on manuscripts. EB provided code of the baseline model in [5] and [6].

Peer-reviewed conference papers

- [1] T. Cheng, M. Mauch, E. Benetos and S. Dixon. An attack/decay model for piano transcription. In *17th International Society for Music Information Retrieval Conference (ISMIR)*, pages 584-590, 2016.
- [2] T. Cheng, S. Dixon and M. Mauch. Improving piano note tracking by HMM smoothing. In *European Signal Processing Conference (EUSIPCO)*, pages 2009-2013, 2015.
- [3] T. Cheng, S. Dixon and M. Mauch. Modelling the decay of piano sounds. In *IEEE International Conference on Acoustics, Speech, and Signal Processing (ICASSP)*, pages 594-598, 2015.
- [4] T. Cheng, S. Dixon and M. Mauch. A comparison of extended source-filter models for musical signal reconstruction, In *International Conference on Digital Audio Effects (DAFx)*, pages 203-209, 2014.
- [5] T. Cheng, S. Dixon and M. Mauch. A deterministic annealing EM algorithm for automatic music transcription. In *14th International Society for Music Information Retrieval Conference (ISMIR)*, pages 475-480, 2013.

Other publication

- [6] T. Cheng, S. Dixon and M. Mauch. MIREX submission: A deterministic annealing EM algorithm for automatic music transcription. *Music Information Retrieval Evaluation eXchange (MIREX)*, 2013.

Chapter 2

Background

The scope of this thesis is the automatic transcription of audio recordings of piano music into symbolic notation. It relates to piano music and computational methods. In this chapter, we present necessary information from both aspects. First, we introduce related music knowledge in Section 2.1. Then in Section 2.2 we give a literature review on related work in the automatic music transcription (AMT) domain. In Section 2.3 we focus on techniques for AMT systems based on non-negative matrix factorisation (NMF). Section 2.4 describes commonly used evaluation metrics. In Section 2.5 we conclude this chapter.

2.1 Music knowledge

We first introduce how sounds are generated and how people perceive them in Section 2.1.1, to understand the observation (input) and expected output of AMT systems. Secondly, in Section 2.1.2 we specify piano acoustics: features related to the piano’s physical structure, which is the theoretical fundament of our proposed piano transcription systems.

2.1.1 Sound generation and perception

In this section, we discuss sounds of music instruments generated via vibrating strings or air columns (pitched instruments).

Given a tense string with fixed ends, when the string is set to vibrate, it excites a series of waves with nodes at both ends of the string, as shown in Figure 2.1. These waves are the *standing waves* of the string; a detailed demonstration can be found online.¹ The frequency of the first wave is called the *fundamental frequency* (f_0) of the string. Compared to the string length L , the

¹<http://newt.phys.unsw.edu.au/jw/strings.html>

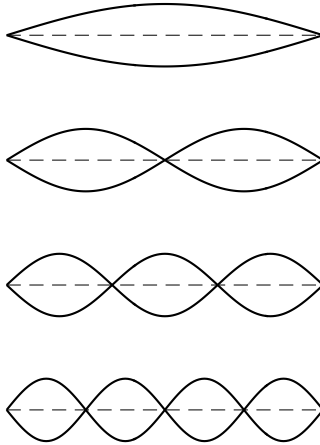


Figure 2.1: The first four standing wave modes of an ideal vibrating string fixed at both ends.

wavelengths of the standing waves are

$$\lambda_n = 2L/n, n = 1, 2, 3, \dots, \quad (2.1)$$

where λ_n is the wavelength of the n^{th} standing wave. Because the frequency is inversely proportional to the wavelength, the frequencies of the standing waves are integer multiples of f_0 . These frequency components are called *harmonics* of the string. The first harmonic f_1 is identical to the fundamental frequency f_0 ; the second harmonic f_2 is the upper *octave* of f_1 ; and the fourth harmonic f_4 is double octave [Roederer, 2009, Chapter 4.1]. The frequency components of a vibrating string are not always harmonically located, such as the spectrum of a piano tone in Figure 2.2(a). We find that its frequency components are stretched a little away from the harmonics because of the stiffness of strings. In this case we call these frequency components *partials*, which include all frequency components of a sound, whether they are harmonics or not [Rossing, 1990, Chapter 4.4]. The waveform generated by the vibrating string is a quasi-periodic signal, which can be assumed as a periodic wave for short durations:

$$x(t) = x(t + T), \quad \forall t, \quad (2.2)$$

where $x(t)$ is the waveform of the signal at time t , and T is the period, equal to $1/f_0$.

A musical sound is a complex tone, consisting of a set of harmonics or partials, as shown in Figure 2.2. The frequency components of a complex tone

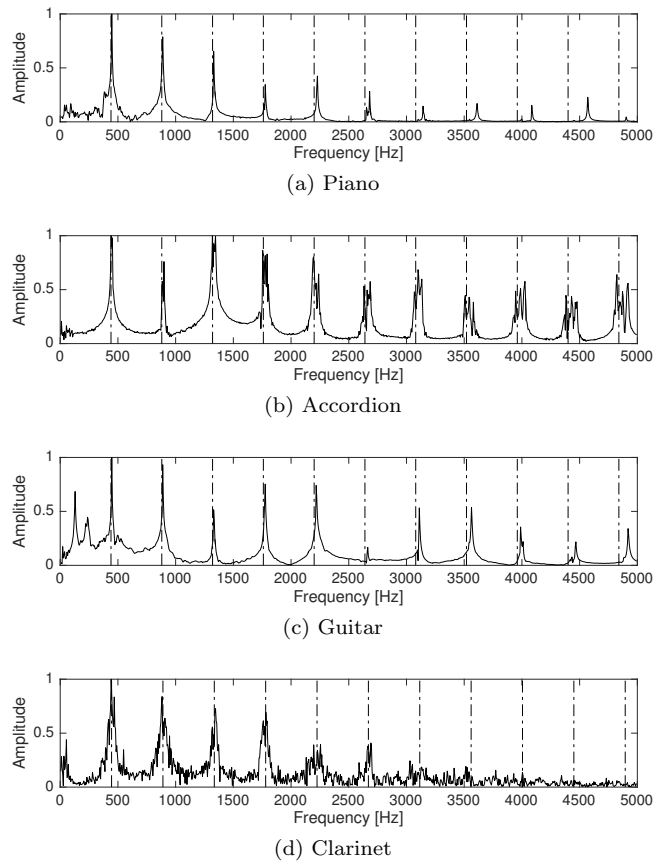


Figure 2.2: Spectra of tones A4 (with the fundamental frequencies of around 440 Hz) generated by different instruments. The dashed lines indicate positions of harmonics (multiples of f_0).

are perceived together as a single *pitch*.² The perception of pitch is related to the fundamental frequency of the tone (the repetition rate of the vibration pattern), but a pitch is also perceptible even when the fundamental frequency is absent. Smoorenburg’s historic pitch-matching experiments show that two neighbouring harmonics of a complex tone can be perceived as a pitch with a missing fundamental frequency [Roederer, 2009, Chapter 2.7]. For example, for two pure tones of frequencies of 800 Hz and 1000 Hz, corresponding to the 4th and 5th harmonics of a pitch of 200 Hz, the perceived pitch is 200 Hz.

In Western music theory, an octave includes 12 semitones. The relation between f_0 and pitch is given as follows:

$$f_0 = 440 * 2^{(m-69)/12}, \quad (2.3)$$

²The American National Standards Institute (1960) defines *pitch* as “that attribute of auditory sensation in terms of which sounds may be ordered on a scale extending from low to high.”

where m is the Musical Instrument Digital Interface (MIDI) index of a pitch. For a piano, the pitch range is $m \in [21, 108]$.

The sounds in Figure 2.2 have the same pitch. However, their spectra vary. The spectral structure of a pitched sound is characterised by the excitation mechanism and physical structure of the instrument [Roederer, 2009, Chapter 4.2, 4.3]. The identification of the instrument is related to *timbre*³ perception, which depends primarily on the precise structure of the spectrum, as studied in psychoacoustic experiments in [Plomp, 1970, 1976, McAdams, 1999]. For example, a musician may describe a tone as dull or stuffy (few upper harmonics), “nasal” (mainly odd harmonics), bright or sharp (many enhanced upper harmonics), or otherwise. These qualifications are associated to actual instrumental tones (fluty, stringy, reedy, brassy, etc.) [Roederer, 2009, Chapter 4.8].

In this section, we briefly introduce how a pitched sound is generated with harmonics (partials) and what is primary to human perception of the pitch and timbre of the sound. Just like human perception of music, an automatic music transcription (AMT) system also works on a waveform of complex tones, to estimate the pitch of each tone. The expected output can be in the form of a time-pitch representation or a list of note events.

2.1.2 Piano acoustics

In this section we investigate piano acoustics, specific properties of sounds associated to piano physics.

A piano mainly consists of a keyboard, keys, hammers, strings and a soundboard, as shown in Figure 2.3. It has 88 keys, with a pitch range of more than 7 octaves (A0 to C8), covering fundamental frequencies from 27.5 Hz to 4186 Hz. Each piano tone is generated by the string(s) vibrating at a specific frequency. The fundamental frequency of a string with fixed ends is given by [Pierce, 1983, Chapter 2]:

$$f = \frac{1}{2l} \sqrt{\frac{T}{\mu}}. \quad (2.4)$$

It is related to the length l , the tension T and the linear density μ (mass per unit length) of the string. This means that for two tones an octave apart, the string length of the lower pitch is twice as long as that of the higher pitch, if the strings have equal tension and density. In this case, the string lengths of low-pitch keys would be too long to fit on the sound board. To build a piano of reasonable size, low bass tones usually use thicker strings, and treble tones (tones in the high pitch range) use thinner strings with higher tensions [Burred,

³The American National Standards Institute (1960) defines *timbre* as “that attribute of auditory sensation in terms of which a listener can judge two sounds similarly presented and having the same loudness and pitch as dissimilar.”

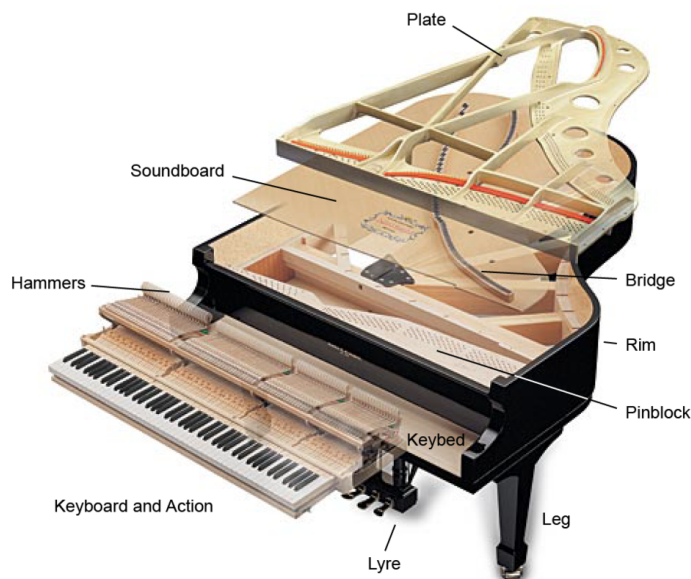


Figure 2.3: Grand piano structure, <http://www.radfordpiano.com/structure/>

2004], [Fletcher and Rossing, 1998, Chapter 12]. The short and thin strings are less resonant than the long and thick strings, therefore, two or three strings are used for a mid or high pitch to produce a louder sound [Livelybrooks, 2007].

Due to the stiffness of the string, partials of piano tones are slightly stretched away from the harmonic positions (shown in Figure 2.2(a)), which is referred to as *inharmonic*ity. The inharmonicity coefficient B is calculated as follows [Fletcher et al., 1962]:

$$B = \frac{\pi^3 Q d^4}{64 l^2 T}, \quad (2.5)$$

where Q is Young's modulus, d is the diameter of the string, l and T are the length and the tension of the string. This shows that the degree of inharmonicity increases with decreased length and increased thickness. Then piano tones of low-pitch and high-pitch ranges have greater inharmonicity than mid-pitch tones. Experiments in the 1960's showed that slight inharmonicity made synthesised piano tones sound more natural, and was one of the characteristics that added certain warmth [Fletcher et al., 1962], richness and quality to the piano sound [Blackham, 1965]. However, the sound quality can be influenced negatively by excessive inharmonicity [Burred, 2004, Chaigne and Kergomard, 2016]. Especially for bass notes, when the partials are very inharmonic, the pitch can be confusing with a less pleasing sound. In an experiment on the audibility of

Table 2.1: Three levels of music dynamics, adapted from [Rossing, 1990, p. 100]

Name	Symbol	Meaning
forte	f	Loud
mezzo forte	mf	Moderately loud
piano	p	Soft

inharmonicities [Järveläinen et al., 2001], inharmonicity was more easily detected for bass tones than treble tones.

Inharmonicity also influences piano tuning [Schuck and Young, 1943]. When tuning a piano, a note’s upper octave is tuned to the frequency of its second partial to eliminate the beats between these two notes. Then the fundamental frequency ratio of an octave is slightly larger than 2. This results in the stretched piano tuning, which allows the piano to sound maximally in tune with itself. In [Rigaud, 2013], a model is proposed and studied, to explain inharmonicity and tuning.

An individual piano tone is generated by the hammer hitting the string(s) of the key. There are three characteristics of piano sounds associated with the attack motion [Meyer, 2009, Chapter 3.4]. Firstly, the strike produces a percussive sound. We can see that the energy distribution is flatter at the attack stage, as shown in Figure 2.4. Secondly, the dynamics of a piano tone are primarily determined by the force of the key attack [Hirschhorn, 2004]. Commonly used dynamics symbols are introduced in Table 2.1. Thirdly, the hammer hits the string at $1/7$ of its whole length, resulting in a particular excitation structure with suppressed 7th, 14th, ..., partials.

Then we look at the sound evolution after the attack. In a grand piano the string is excited into a perpendicular motion to the soundboard because the hammer strikes from below. This perpendicular motion decays quickly. Due to the coupling of the bridge and soundboard, the plane of vibration gradually rotates to a parallel motion which decays more slowly [Weinreich, 1977]. This is referred to as the typical “double decay” of the piano, as shown in Figure 2.5(a). In a piano, most notes have more than one string per note. Usually only the lowest ten or so notes have one string per note. The subsequent (about 18) notes have two strings, and the rest have three strings. For notes with multiple strings, the decay rate will double or treble if the strings are tuned to exactly the same frequency. To make the sound sustain longer, the strings are tuned to slightly different frequencies. Weinreich [1977] studies the coupled oscillation of two strings in detail. If the frequency difference between strings is small, the coupled motion will result in a double decay, as shown in Figure 2.5(b).

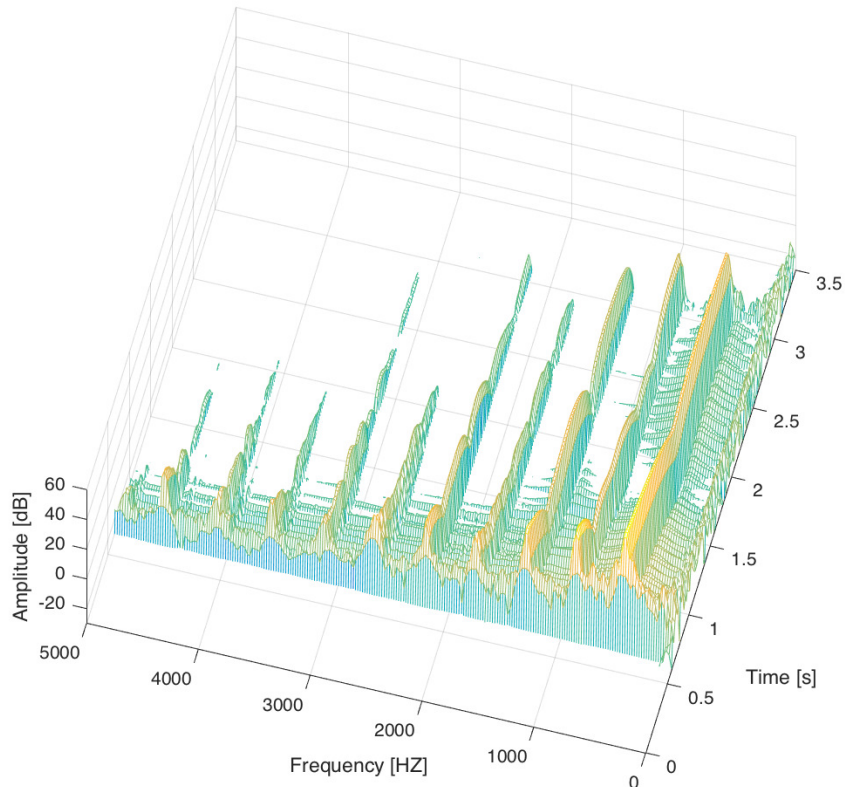


Figure 2.4: Time evolution of the spectrum of note A4 (440 Hz).

When the frequency difference is large, the decay becomes a wave-like curve, as shown in Figure 2.5(c). Half of the frequency difference is defined as the angular frequency *mistuning*, and the amplitude modulation of the decay is called *beats* or *beating* [Weinreich, 1977]. Note that the beat frequency is not equal to the frequency difference between strings, due to the coupled oscillation of strings. We also observe beats in high partials of single string notes. This is known as “false beats” which is caused by imperfections in string wire or problems at the bridge such as loose bridge pins [Capleton, 2004].

We have reviewed spectral and temporal features of piano sounds associated to its excitation mechanism and physical structure. In our work we represent spectral features, such as inharmonicity and the excitation structure, by training on isolated tones, but focus more on the temporal evolution of piano sounds. The decay of real world piano tones is studied in detail in Chapter 4 and its utility for transcription is analysed in Chapter 5. The temporal evolution from

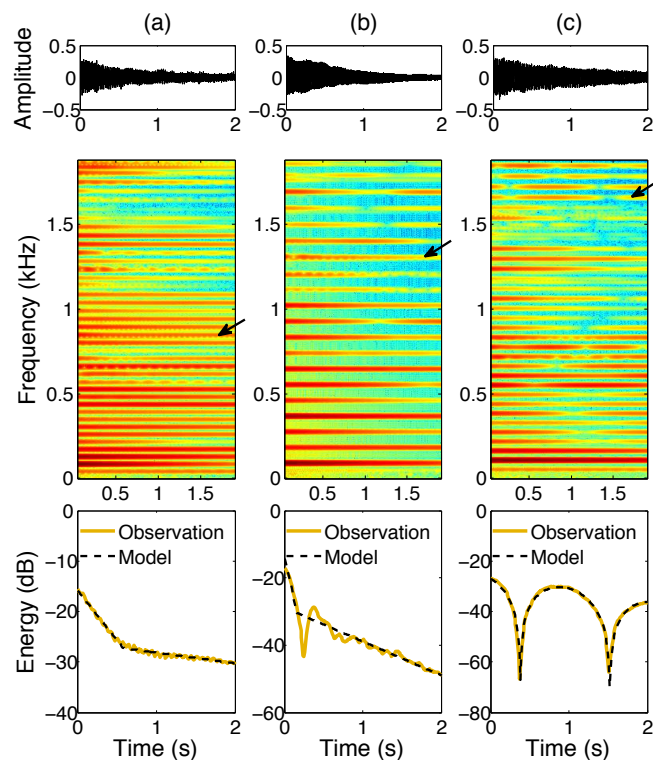


Figure 2.5: Different decay patterns of partials from notes (a) F1 (43.7 Hz), (b) G \flat 2 (92.5 Hz) and (c) A1 (55 Hz). The top and middle panes show the waveforms and spectrograms, respectively. The bottom panes show the decay of selected partials, which are indicated by the arrows on the spectrograms. The dashed lines are estimated by the model in Chapter 4.

the attack to decay stage is modelled in Chapter 6.

2.2 Related work

In this section, we review methods proposed for automatic music transcription. Readers are referred to [Klapuri and Davy, 2006, de Cheveigné, 2006, Christensen and Jakobsson, 2009, Benetos et al., 2013b] for some excellent literature reviews. Here we provide a new aspect to catalogue the methods by the level of music understanding they involve. In the following sections, we introduce methods automatically transcribing musical signals by relating the pitch of a musical tone to its fundamental frequency (period), harmonics (partials) and spectral structure (timbre), modelling musicological information, and making use of classification-based methods. Then in Section 2.2.6, we cover steps to form note events and some note-level methods which model the discrete note events directly.

2.2.1 Methods based on periodicity

Methods reviewed in this section detect the pitch of a musical tone by its period. These methods, which are also referred to as pitch detection algorithms (PDA) [Hess, 1983, Gerhard, 2003], usually work only for single-pitch detection.

As mentioned in Section 2.1.1, a pitched sound is a quasi-periodic signal and can be assumed as a periodic wave for short durations. We rewrite Equation 2.2 as follows:

$$x(t) - x(t + T) = 0, \forall t, \quad (2.6)$$

where $x(t)$ is the waveform of the signal, and T is the period, equal to $1/f_0$. The key for detecting period is to design a period candidate generating function, which should have a maximal or minimal value at the time of the period [Talkin, 1995]. Commonly used functions are based on the autocorrelation function (ACF) [Rabiner, 1977], and the average magnitude difference function (AMDF) [Ross et al., 1974]. In a frame with an integration window of size W , the ACF at time index t is defined as:

$$ACF_t(\tau) = \sum_{j=t+1}^{t+W} x(j)x(j + \tau), \quad (2.7)$$

where τ is the time lag. We show the squared-difference function (SDF) [de Cheveigné, 1998], a variant of AMDF, defined as:

$$SDF_t(\tau) = \sum_{j=t+1}^{t+W} (x(j) - x(j + \tau))^2. \quad (2.8)$$

The *cepstrum* is also a commonly used method for period detection, which is defined as the inverse Fourier transform of the short-time log magnitude spectrum [Noll, 1967, Oppenheim and Schaffer, 2004]. Unlike the previous time-domain method, the cepstrum is performed in the frequency-domain, then inversely transformed back to the time domain. The harmonic peaks are flattened by the log operator on the magnitude spectrum.

The above methods show peaks or valleys at multiples of the period, with the period detected by the first peak of the ACF and cepstrum or first valley of the AMDF and SDF. Associating the pitch with the zero-lag peak and other high-order peaks are the typical errors in these pitch detection algorithms. Several extended methods to solve these problems are introduced as follows.

de Cheveigné and Kawahara [2002] propose a method, YIN, based on ACF with a number of modifications for f_0 estimation. The method first computes a modified ACF with shrunk integration window size, which lowers the high-order peaks. Then the square difference function is applied as the second indicator.

It is argued that the SDF is closer to the representation of the periodic signal in Equation 2.6, which contributes to a significant reduction of the error rate. A cumulative mean normalised difference function is proposed based on SDF to decrease the errors near the zero lag. In the fourth step, an absolute threshold (0.1) is used to find the first dip for the period. The global minimum is selected if no dip is below the threshold. Then parabolic interpolation is used for a better estimation of the period. There is a final smoothing step to reduce the fluctuation of the f_0 estimation. The algorithm outperforms all compared methods, and is simple and computationally efficient with few parameters to be tuned.

McLeod and Wyvill [2005] propose a normalised square difference function (NSDF) to find the pitch, which is defined as:

$$NSDF_t(\tau) = \frac{ACF_t(\tau)}{m_t(\tau)} \quad (2.9)$$

where $m_t(\tau) = \sum_{j=t+1}^{t+W} (x(j)^2 + x(j+\tau)^2)$. This normalised SDF (or normalised ACF) minimises the edge effects of the decreasing window size. The highest positive maxima between pairs of zero crossings are selected as the candidates, and the maximum at delay 0 is ignored. A threshold is set by multiplying the global maximum with a constant $k \in [0.8, 1)$. The delay τ of the first candidate above the threshold is detected as the pitch period. Parabolic interpolation is also applied to find the positions of the maxima more accurately. The method uses a small window for a better representation of a changing pitch, such as vibrato.

The above period detection methods actually find the smallest common period shared by all harmonics of a pitch. If there are two pitches, they detect the smallest common period they share, or a ‘root’ frequency of the two notes [Moorer, 1975]. So these methods usually work only for single-pitch signals.

In the following, we introduce two methods jointly using temporal and spectral representation [Peeters, 2006, Emiya et al., 2007]. The methods are motivated by the observation of inverse octave errors (‘twice the pitch’ and ‘half the pitch’) of the two representations. The pitch detection function is a product of the temporal method and the spectral method, to reduce both octave errors. In [Peeters, 2006], different representations are considered: spectral ones include the Discrete Fourier Transform (DFT) of the signal, the frequency reassignment (REAS), and the Auto-Correlation Functions of DFT and REAS; and temporal ones include the Auto-Correlation Function and Real-Cepstrum of the signal. Then the proposed periodicity function is computed by the product of each of the two kinds of representations. The method is tested on a large test set of over 5000 musical instrument sounds, showing competitive results in comparison to

the YIN estimator [de Cheveigné and Kawahara, 2002].

Emiya et al. [2007] propose a pitch estimation method for a short analysis window and focusing on piano sounds. Both the temporal method (based on the autocovariance function) and spectral method (based on spectral matching) include the inharmonicity factor. The final pitch detection function is a product of the two methods. This model is the first physics-based transcription system for piano. The test dataset contains a large set of isolated piano tones for RWC database [Goto et al., 2003], a PROSONUS and a Yamaha upright piano. Better performance is achieved by the proposed method compared to the YIN estimator [de Cheveigné and Kawahara, 2002], especially for low-pitch and high-pitch notes.

2.2.2 Methods based on harmonics (partials)

We know that a pitched sound actually consists of a set of frequency components, appearing at or near integer multiples of f_0 , as shown in Section 2.1.1. Methods reviewed in this section make use of harmonics (partials) to detect the pitch of the sound.

A subharmonic summation method uses the weighted sum of harmonic amplitudes [Hermes, 1988]:

$$H(f) = \sum_{n=1}^N h_n P(nf), \quad (2.10)$$

where $H(f)$ is the subharmonic sum spectrum, and h_n is the weight for the n^{th} harmonic. P is the spectrum with low frequency noise suppressed. Pitch is detected with f_0 where $H(f)$ is maximum.

Taking harmonics (partials) into account makes it possible to estimate multiple pitches. The first attempt for duets was carried out by Moorer [1975]. The method first detects the root frequency (the greatest common frequency) of the two notes with a periodicity detector. Bandpass filters centred at multiples of the root filter out harmonics of notes. The strongest harmonic and its sub-harmonics are compared to detect the root. Each integer multiple of the root forms a note hypothesis. The hypothesis is tested by the existence of its harmonics.

Klapuri [2003] proposes a multiple fundamental frequency estimation method by iteratively detecting the predominant pitch and cancelling the detected sound. First, the power spectrum is magnitude-warped and noise is suppressed using a moving average filter. Then for each iteration, an f_0 is detected with the highest global weight. The global weight of an f_0 is a sum of its squared band-wise weights with adopted inharmonicity, and the band-wise weight is a sum of its partials' amplitudes modified by a triangular window. The method

assumes a smooth spectrum for a pitched tone. When cancelling a detected pitch, the spectrum of the detected pitch is smoothed to reduce its influence on remaining pitches. The smoothing method replaces the original amplitude value of each partial by the weighted mean of the partials' amplitudes in an octave-wide triangular weighting window if the weighted mean is smaller. Two terms based on the signal-to-noise ratio are used to stop the iteration.

Yeh et al. [2010] propose a joint estimation method for multiple fundamental frequency estimation by progressively combining hypothetical sources and iteratively verifying each combination. The system first applies an adaptive noise level estimation to divide the spectral peaks into partials of harmonic sources and noise. A score function is defined as the weighted sum of the four criteria, which are proposed to prevent sub-harmonic/super-harmonic errors, including harmonicity, mean bandwidth, spectral centroid, and the standard deviation of mean time. The f_0 candidates are selected by iteratively applying a predominant- f_0 estimation and cancelling related partials. A harmonically related f_0 (HRF0) of the extracted f_0 s is also selected as a candidate if it is dominant and disturbs the envelope smoothness. To infer the best combination, f_0 candidates are added to the combination one by one starting with the highest score. The newly added f_0 is considered valid if it either explains more energy than the noise, or significantly improves the envelope smoothness for HRF0s.

Duan et al. [2010] estimate multiple f_0 s by modelling both the spectral peak and non-peak regions. The peak region likelihood helps find f_0 s that have harmonics that explain peaks, and the non-peak region likelihood helps avoid f_0 s that have harmonics in the non-peak region. The method first detects peaks from the spectrum. The f_0 candidates are restricted to be around peaks with the lowest frequencies or (locally) highest amplitudes. To reduce the time complexity, an iterative greedy search strategy is applied to add f_0 s one by one. For each iteration, a set of f_0 s is found which maximises the product of the peak and non-peak region likelihoods. The likelihoods are based on the probabilities of peaks belonging to given f_0 s, which are learned from monophonic and polyphonic training data. A threshold-based method is used to end the iteration. In the post-processing step inconsistent f_0 estimates are removed and the missing f_0 is reconstructed using neighbouring f_0 estimates.

Dressler [2011] proposes a pitch estimation method based on pair-wise analysis of spectral peaks. The method first detects amplitude and instantaneous frequency (IF) of the spectral peaks, with each peak magnitude weighted by its IF. The method finds pitch candidates by assuming two spectral peaks are successive harmonics or successive odd harmonics for wind instruments (suppressed even harmonics because of the open end of wind instruments). A pitch candidate is rated by a multiplication of values of functions indicating the har-

monicity, spectral smoothness, attenuation by intermediate peaks and harmonic impact of the candidate. Each function operates on frequencies or amplitudes of the pitch pair or peaks between them.

2.2.3 Methods based on timbre

Timbre is associated to the spectrum of the musical sound. It primarily explains the human ability of distinguishing instruments, as explained in Section 2.1.1. Methods reviewed in this section represent the spectral structure of each pitch, with the ability to be applied to multi-instrument music signals to identify pitches from different instruments.

All matrix-factorisation-based AMT methods are included in this category, such as non-negative matrix factorisation (NMF) [Smaragdis and Brown, 2003], probabilistic latent component analysis (PLCA) [Smaragdis, 2009], independent component analysis (ICA) [Plumbley and Abdallah, 2003], and sparse coding [Abdallah and Plumbley, 2004]. Spectrogram factorisation methods decompose the spectrogram into two matrices,

$$X_{ft} \approx \sum_{r=1}^R W_{fr} H_{rt}, \quad (2.11)$$

where \mathbf{X} is the observed spectrogram, \mathbf{W} represents spectral bases of pitches and \mathbf{H} are corresponding activations. $f \in [1, F]$ is the frequency bin, $t \in [1, T]$ is the time frame, and $r \in [1, R]$ is the pitch index. A spectral basis has the same dimension as the spectrogram in frequency, and represents the primary timbre information of a pitched sound with a weighted average of its spectrogram over time.

Among these methods, NMF is the most commonly used framework for AMT, and our proposed systems are also based on NMF. We will discuss NMF-based AMT systems in detail in Section 2.3. We briefly introduce some extensions based on matrix factorisation for multi-instrument polyphonic music transcription as follows.

Vincent and Rodet [2004] use a three-layer probabilistic generative model for multi-instrument separation and transcription. The low level is a spectral layer modelled by a non-linear independent subspace analysis (ISA), describing the input spectrum as a sum of weighted spectral components. The middle level is a description layer, connecting the other two layers. The high-level state layer tracks note states using the product of a Bernoulli prior and a factorial Markov chain. This method needs information about instrument types to perform transcription.

Cont et al. [2007] propose a real-time system for multi-pitch and multi-

instrument recognition based on NMF and sparse coding. First, a modulation spectrum representation is learned per pitch and instrument to represent not only short-term features but also long-term features, such as spectral envelope or phase coupling. Then the spectrum is decomposed using learned templates with a sparse non-negative decomposition method.

Grindlay and Ellis [2011] transcribe multi-instrument polyphonic music using a hierarchical probabilistic model. A set of linear subspaces are trained on sounds of instruments. Detected notes can be assigned to their respective sources by mapping the note into a subspace or a hierarchical mixture-of-subspaces. The hierarchical mixtures include far more than just the training points. The system only needs information about the number of instruments. The types of instruments are not necessary but can help the performance.

Bay et al. [2012] present a PLCA-based model for tracking the pitches of individual instruments in polyphonic music. The system first learns a dictionary of spectral basis vectors for each note of various musical instruments, then explains the input spectrum of each frame as a sum of spectral bases in the dictionary. Finally, a Viterbi algorithm is applied to track the most likely pitch sequence for each instrument.

Kirchhoff [2013] investigates instrument-specific transcriptions with a human user involved. Different types of user input are studied to derive timbre models for the instruments by means of NMF, source/filter model and so on.

Benetos et al. [2013a] propose a temporally constrained shift-invariant model for multi-instrument music transcription. For each pitch of a variety of instruments, several spectral templates are learned, corresponding to the attack, sustain and decay states. The templates are able to shift across the log-frequency axis to fit notes with frequency modulations and tuning changes based on a shift-invariant PLCA (SI-PLCA) model. Pitch-wise HMMs constrain the temporal transitions between states. All parameters are jointly estimated in an HMM-constrained SI-PLCA model. With the trained templates on a set of instruments, this method needs no prior information about played instruments.

Beside matrix-factorisation-based methods, there is another way to represent the spectral structure of musical sounds, by means of a Gaussian mixture. Goto [2004] proposes a harmonic structure model for predominant- f_0 estimation (PreFEst). The h^{th} harmonic of a tone with fundamental frequency of f_0 is represented by a Gaussian function centred at $f_0 + \log_2 h$ on a log frequency scale, with the relative amplitude determined by the weight of the Gaussian function. The PreFEst-core uses several types of harmonic-structure tone models to deal with sounds produced by different instruments. The frame level pitch likelihoods are estimated using an expectation-maximisation (EM) algorithm on the MAP (maximum a posteriori probability) mixture weights of the tone models.

A multiple-agent architecture is used to find the most dominant and stable f_0 trajectory. First, an agent is generated by considering salient values of peaks in current and near-future frames. Then each agent allocates peaks of close frequency and is penalised if no peak is found nearby. The global f_0 estimation is obtained by the agent with the highest reliability and greatest total power.

The same harmonic structure is applied in the harmonic temporal structure clustering (HTC) method for multi-pitch analysis [Kameoka et al., 2007]. The HTC method imposes temporal continuity by weighted Gaussian function kernels which are equally spaced after the onset. This two-dimensional geometric model jointly estimates pitch, intensity, onset and duration of each underlying source. The EM algorithm is applied to iteratively decrease the Kullback-Leibler (KL) divergence between the HTC model and the whole observed spectrogram. The model is then extended as a maximum a posteriori (MAP) estimation problem to include prior distributions on the parameters, which helps to prevent sub-harmonic (half-pitch) errors and avoid overfitting.

The HTC model is further extended to Harmonic-Temporal-Timbral Clustering (HTTC) for the analysis of multi-instrument polyphonic music [Miyamoto et al., 2008]. The HTTC model considers multi-pitch analysis and timbre clustering simultaneously. Each acoustic event is modelled by a harmonic structure and a smooth envelope both represented by Gaussian mixtures. Timbres are clustered to form timbre categories based on the similarity of the shape of spectral energy in time and log-frequency space, regardless of pitch, spectral power, onset, and duration. The harmonic, temporal and timbral model parameters are simultaneously updated using the EM algorithm.

2.2.4 Methods based on high level information

A music piece is not a set of independent note events, despite often being modelled so. Temporal or harmonic structure of music can provide useful information for AMT. For example, both key and chords describe harmony, strongly related to corresponding notes. Acoustic models directly extract information from signals, while musicological models model the abstract structure of music. A musicological model is also called a symbolic model or a music language model. We show several AMT systems with musicological models in detail as follows.

Ryynänen and Klapuri [2005] propose a transcription system with three probabilistic models: a note event HMM, a silence model, and a musicological model. First, the system applies a multiple-pitch estimator [Klapuri, 2005] to detect f_0 s and related features frame-by-frame. The 3-state note HMM calculates likelihoods for different notes based on the estimated f_0 s and related

features, and the silence model built on a 1-state HMM is used to skip the silent time regions. The musicological model controls transitions between note HMMs and the silence model according to the key estimated on frame-wise f_0 s. Given a relative-key pair (major and minor keys with the same set of notes), the transition probabilities between note HMMs are trained from a large database of monophonic melodies. Probabilities for the note-to-silence and the silence-to-note transitions are set with the assumption that a note sequence is more likely to start and to end with a frequently occurring note in the musical key. Transcription is done by searching for disjoint paths through the note models and the silence model.

Raczyński et al. [2013] propose a family of probabilistic symbolic polyphonic pitch models, which account for both the temporal and the harmonic pitch structure. In the paper, acoustic modelling is represented as a maximum likelihood estimation process:

$$\hat{N} = \arg \max_N P(S|N), \quad (2.12)$$

where $P(S|N)$ is the acoustic model, S are the observations and N are the note activations. The proposed model includes a symbolic pitch model $P(N)$ as prior knowledge in the posteriori-like estimation by Bayes' rule:

$$\hat{N} = \arg \max_N P(S|N)P(N). \quad (2.13)$$

The distribution of the note sequences $P(N)$ is modelled in a Dynamic Bayesian Network with two layers of hidden nodes: a chord layer and a note activity layer, as shown in Figure 2.6. The symbolic model makes use of a chord model and 5 sub-models for temporal dependencies of notes and chords and harmonic dependencies between notes. Knowledge about chord progressions is modelled in the chord model, and relations between chords and pitches are modelled in a harmony sub-model. Each of the other 4 sub-models deals with a different property of pitch, for note duration, melodic intervals in voices, the degree of polyphony per frame and neighbouring pitches, respectively. In order to effectively deal with the high dimensionality of the distributions, the note combination distribution is factorised into a product of single note distributions. Sub-models are normalised and combined by means of linear or log-linear interpolation for each note distribution. The proposed symbolic model is evaluated on symbolic data and on audio data. The second evaluation is in combination with an NMF-based acoustic model [Raczyński et al., 2007]. In both experiments the proposed model outperforms the baseline Bernoulli model.

Sigtia et al. [2014] use a Music Language Model (MLM) to improve automatic music transcription performance. The MLM is based on Recurrent Neural Networks (RNNs), which can model long-term temporal dependencies,

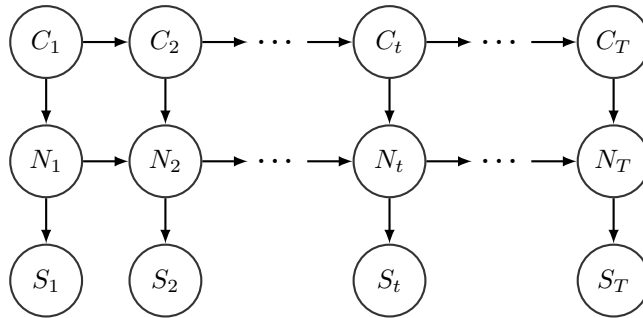


Figure 2.6: Dynamic Bayesian Network structure with three layers of variables: the hidden chords C_t and note combinations N_t , and observed salience S_t

and the acoustic AMT model is based on probabilistic latent component analysis (PLCA) [Benetos et al., 2013a]. First, the pre-trained MLM generates a prediction based on the results of the PLCA-based acoustic model (a pitch activation distribution). Then, the prediction is combined with the pitch activation distribution via a Dirichlet prior. Finally the combined pitch activation is weighted and added to the output of the acoustic model. With the RNN trained on symbolic music data from the Nottingham dataset,⁴ the proposed hybrid models outperform the baseline acoustic AMT system by 3 percentage points in terms of note-wise F-measure on the Bach10 dataset [Duan et al., 2010] of multiple-instrument polyphonic music.

Sigtia et al. [2015, 2016] employ a hybrid architecture for polyphonic music transcription, as shown in Figure 2.7. The proposed model also comprises an acoustic model and a music language model. The acoustic model (the posterior distributions $p(y_t|x_t)$) is modelled using different neural networks to identify the pitches in a frame of audio. The MLMs model the prior $p(y_t|y_0^{t-1})$ using a generative RNN for the correlations between pitch combinations over time. Both the acoustic and the language models are jointly trained under a single objective with the hybrid RNN framework. Sigtia et al. [2015] compare three acoustic models based on the deep feed-forward neural network (DNN) and RNN. A high dimensional beam search algorithm is used to perform inference over the output variables. Sigtia et al. [2016] also include convolutional neural nets (ConvNets) as the acoustic model, and an efficient version of the beam search algorithm is presented to reduce decoding time by an order of magnitude. The experiments on the MAPS database [Emiya et al., 2010] show that the hybrid architecture offers better results than applying a threshold or HMM on the same acoustic models and outperforms state-of-the-art transcription systems.

⁴<http://ifdo.ca/~seymour/nottingham/nottingham.html>

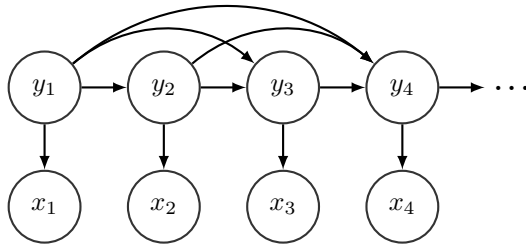


Figure 2.7: The hybrid architecture of the AMT systems in [Sigitia et al., 2015, 2016].

2.2.5 Classification-based methods

The acoustic models in [Sigitia et al., 2015, 2016] are also classification methods based on neural networks. In this section, we introduce several more classification-based methods in which classifiers are trained on spectral features.

Poliner and Ellis [2007] propose a supervised classification system based on a Support Vector Machine (SVM) for polyphonic piano transcription. The system employs separate one-versus-all SVM classifiers for each of the 87 piano keys (the highest note is not included), then the classifier outputs are temporally constrained via hidden Markov models. The classification is performed at the frame level, with each frame of the input audio represented by a 255-element feature vector. The binary note classifiers are trained from spectral features, and the input feature vectors of different notes correspond to different frequency ranges: the first 63 piano keys use normalised spectrograms below 2 kHz; the next 12 notes between 1 kHz and 3 kHz; and the rest of the notes between 2 kHz and 4 kHz. The classifiers are trained, tested, and validated on music pieces generated by MIDI files and a Yamaha Disklavier piano. A two-state, on/off, HMM is used to temporally smooth the output of each note independently. The HMM parameters are learned on the ground-truth transcriptions of the training set. The experiment shows that using a larger and more diverse training set can improve the classification accuracy.

Nam et al. [2011] further extend the previous classification-based approach of Poliner and Ellis [2007] in two ways: (1) by using learned feature representations for note classifiers and (2) by jointly training the classifiers for multiple notes. Firstly, mid-level features are learned on spectrogram frames via deep belief networks (DBNs) of one or two layers and then used to feed into the SVM classifier. The networks are fine-tuned with the error from the SVM for each piano note (single-note training). Secondly, multiple SVM classifiers are trained at the same time (multiple-note training). A two-state HMM is adopted to temporally smooth the SVM output for each note. Experiments show that

better transcription results can be achieved by using the learned feature from a DBN, especially the one-layer DBN, in comparison to the normalised spectrogram used by Poliner and Ellis [2007]. Multiple-note training improves training speed and classification performance in comparison to single-note training. The classification approach outperforms compared piano transcription methods.

Böck and Schedl [2012] propose a method to simultaneously detect onsets and pitches of piano notes based on a recurrent neural network. The compressed input of the neural network is obtained by filtering two magnitude spectrograms of different window lengths with semitone filter-banks. The system is built on a Bidirectional Recurrent Neural Network (BRNN) which models both the past and future context of the notes. A Long Short-Term Memory (LSTM) unit is used to ensure that the BRNN only use input values inside the memory cell. The system has three bidirectional hidden layers with 88 LSTM units each. The regression output layer has 88 units for all piano pitches. Onsets of each pitch are detected by applying a standard local maximum peak picking algorithm on the smoothed neural network output. Solo piano music pieces from different piano datasets are used for training and testing. Evaluation indicates that the reduction on note detection errors is mainly related to the single regression output layer which detects piano notes simultaneously.

2.2.6 Note tracking

Automatic music transcription methods usually work in two steps. In the first step, the music piece is segmented into frames of equal intervals, and pitches are estimated in each frame. In the second step, estimated pitches of adjacent frames are grouped together to form note events, then hence onsets and offsets. There are also note-level systems which directly model the discrete note events. In the following, we first introduce some basic methods for converting frame-wise results into note events, then we illustrate several note-level systems.

Thresholding

For some methods, for example matrix-factorisation-based methods, a threshold is applied to obtain a binary output [Wang et al., 2008, 2009, Grindlay and Ellis, 2011]. The threshold is usually adapted to the maximum value of each piece [Vincent et al., 2010, O’Hanlon and Plumbley, 2013]:

$$Thre = \delta \max_{k,t} H_{k,t}^a. \quad (2.14)$$

the optimal value for parameter δ is usually determined by training.

Tavares et al. [2016] provide an unsupervised way to choose the threshold for NMF-based piano transcription. Ideally for an activation matrix, its values are sparse with only a few notes active at any given time, and high activation values are related to true positives. The system assumes that the envelope of a histogram of the activation matrix has the rough shape of a reverse sigmoid. In order to find the elbow of the envelope, the method uses 10 threshold candidates equally located between the maximum and minimum values in the activation matrix (from 0 to 1 for normalised activations). For each piece, the candidate with least second differential is found as the elbow:

$$i_e = \arg \min_i [(th^{i+1} - th^i) - (th^i - th^{i-1})], \quad (2.15)$$

where th^i indicates the number of active pitches using the i^{th} threshold candidate. While using the elbow value as a threshold leads to a low mean F-measure with high Recall and low Precision rates, then the optimal threshold is adjusted to $i_e + 0.3$ with tests on three datasets. In the experiments, the method provides better results than using a threshold trained on a different dataset.

Minimum-duration pruning

After thresholding, notes are detected in the time-pitch representation by converting pitches found in consecutive frames into notes. There are some short false-alarm notes brought by fluctuations of the activations. Minimum duration pruning is applied to remove those short notes that fail to reach a duration threshold [Dessein et al., 2010].

HMM smoothing

Hidden Markov models (HMMs) [Rabiner, 1989] are frequently employed to provide a smooth output at the post-processing step. In order to decrease the search space, HMMs are usually applied in a pitch-wise fashion, either using two states per pitch to detect that a note is active or not [Poliner and Ellis, 2007, Benetos and Dixon, 2012a], or using states corresponding to several stages of a note (attack, decay, sustain and release) which follow a certain sequence [Ryynänen and Klapuri, 2005, Cheng et al., 2015b]. Pitch-wise HMM parameters (state transitions and priors) are learned on symbolic representations, such as a ground-truth training set or MIDI files, while the observation probability is set based on the frame-wise transcribed results. The most likely state sequence is estimated using the Viterbi algorithm.

Note-level methods

Several note-level systems are built with temporal evolution modelling. The HTC [Kameoka et al., 2007] and HTTC [Miyamoto et al., 2008] methods model the observed power envelope of a single source by weighted Gaussian function kernels. Chen et al. [2012]’s preliminary work uses an exponential model for energy evolution of notes. Berg-Kirkpatrick et al. [2014] represent the energy evolution of a piano note by a trained envelope. Ewert et al. [2015] represent both time-varying timbre and temporal evolution of piano notes by time-frequency patches. In these systems, a note event is represented by a single amplitude parameter for its whole duration with the modelled temporal evolution, which provides promising transcription results. In addition, Cogliati and Duan [2015] propose a note level system informed by detected onsets, which also approximates decays of piano partials with a sum of two decaying exponentials. The HTC and HTTC methods have been already described in Section 2.2.3. We will introduce the other four systems in detail as follows.

Chen et al. [2012] extend the hierarchical eigeninstrument model of Grindlay and Ellis [2011] for multi-instrument music transcription using note-level templates. In this method, musical notes are assumed to consist of a relatively invariant attack, and a decay that depends on the overall duration of the note. In order to represent notes with various durations for each pitch of different sources, the system applies a parametric transformation step, controlling the spectral evolution and amplitude envelope. In the parametric form, a non-linear time warp is used to match notes of varying durations and to describe the nonuniformity across attack and decay. In addition, the overall amplitude decay is formulated by an exponential decay function. The method provides a significant improvement compared to a frame-level system, with better note-level transcription results on real woodwind excerpts and piano music pieces.

Berg-Kirkpatrick et al. [2014] present a probabilistic model comprising discrete musical events. The generative system is built on three models. For each pitch, there are (1) an event model, including discrete note events having a velocity and duration, (2) an activation model, generated based on the event model and an envelope parameter, and (3) a spectrogram model, generated by the activations and spectral parameters of the pitch. The observed spectrogram is reconstructed by adding the component spectrograms of all pitches. A block-coordinate ascent procedure is performed to estimate the unknown parameters. The spectral and envelope parameters are learned on isolated, synthesised, piano sounds. The event parameters are learned by counting note occurrences in numerous symbolic music data. The pre-learned parameters are updated during the decoding to predict transcriptions with fitted parameters. The approach

outperforms state-of-the-art methods on piano music transcription, especially on onset-wise metrics.

Ewert et al. [2015] present a novel transcription method based on non-negative matrix deconvolution with the variable note lengths modelled by a dynamic system. The system assumes that recordings of individual notes of played instruments are available, and uses the spectrogram of the whole note as a time-frequency patch. Frames in a patch are identified with states in a dynamic system. The system performs transcription by operating the following two steps iteratively. First, the best fitting state sequence is tracked pitch by pitch using dynamic programming to form notes with various lengths. Then note objects of all pitches are updated jointly in a global optimisation, with frames of each note object sharing the same activation parameter. The joint estimation helps to avoid degenerate local minima caused by parameter decoupling in the first step. The system is tested on 10 MIDI files from a piano playing competition.⁵ Both the test dataset and training dataset (individual piano notes) are generated by Native Instruments Vienna Concert Grand VST plugin using MIDI files. The note-wise onset F-measure achieves as high as 88% in the experiment.

Cogliati and Duan [2015] propose a note-level spectrogram factorisation method exploiting the temporal evolution of piano notes. The method detects note onsets from the audio spectral flux using an artificial neural network. The audio signal is segmented by the detected onsets. In each segment, partials of notes lasting from the previous segment are set to zeros; only partials of notes starting at the current segment are processed by a greedy search algorithm. Notes are successively added with the lowest cost. An additional note is valid only if the cost function decreases by more than 5%; otherwise the search stops. During dictionary learning, a sum of two decaying exponentials is used to approximate the amplitude evolution of active partials. Frequency bins fitting this parametric evolution are retained; and noisy bins are set to zeros. In addition, a new cost function is proposed for spectrogram similarity. The cost function weights the reconstruction error according to the energy present in the original spectrogram, which works better than the L^1 -norm, L^2 -norm and KL-divergence in the experiments.

2.3 Techniques for NMF-based AMT systems

In this section, we review techniques applied to non-negative matrix factorisation for automatic music transcription (AMT). First we present a general frame-

⁵<http://www.piano-e-competition.com>

work for AMT systems based on NMF in Section 2.3.1, including front-end, post-processing of standard AMT systems, and parameter estimation methods in the NMF framework. Then in Section 2.3.2 we specify constraints used to impose sparsity, smoothness and harmonicity/inharmonicity, which lead to more meaningful decompositions. In Section 2.3.3, we introduce the Bayesian extension of NMF, and show ways of using prior information to enforce constraints, especially methods which impose temporal continuity on activations.

2.3.1 A general framework for NMF-based AMT

An AMT system starts from an audio signal and ends with a symbolic representation, in the form of a time-pitch representation. NMF is the key part of the system, which works on the time-frequency representation matrix of the signal, and provides an activation matrix as a mid-level representation of the symbolic output. The general framework of an NMF-based AMT system consists of three main parts: the front-end providing the time-frequency representation of the signal, the NMF model for estimating unknown parameters, and the post-processing step with a binary output, as shown in Figure 2.8. We will describe each part individually in the following sections.

Time-frequency representation

The front-end of an NMF-based transcription system produces a non-negative time-frequency (TF) representation of the signal. NMF decomposes the TF representation into a linear combination of spectral bases with non-negative constraints. The transform \mathcal{F} to produce the TF representation should also exhibit linearity, that is $\mathcal{F}(ax + by) = a\mathcal{F}(x) + b\mathcal{F}(y)$, or at least $\mathcal{F}(ax + by) \approx a\mathcal{F}(x) + b\mathcal{F}(y)$. Among various transform methods, we focus on three TF representations as follows.

Short-Time Fourier Transform (STFT)

The Short-Time Fourier Transform (STFT) is a common TF representation with a linear frequency scale. As reviewed by Bay et al. [2009], most AMT systems employ STFT as a front-end. To obtain a spectrogram by STFT, the signal is segmented into overlapping frames by a window function. The discrete Fourier transform is performed on each frame to get the short-time spectrum.

This method is a fundamental transform method with many available implementations. The frequency bins are linearly spaced, giving an intuitive TF image. AMT systems usually work on the magnitude spectrogram or power spectrogram. Only a few papers use the complex spectrogram with complex NMF [Kameoka et al., 2009, Kirchhoff et al., 2014].

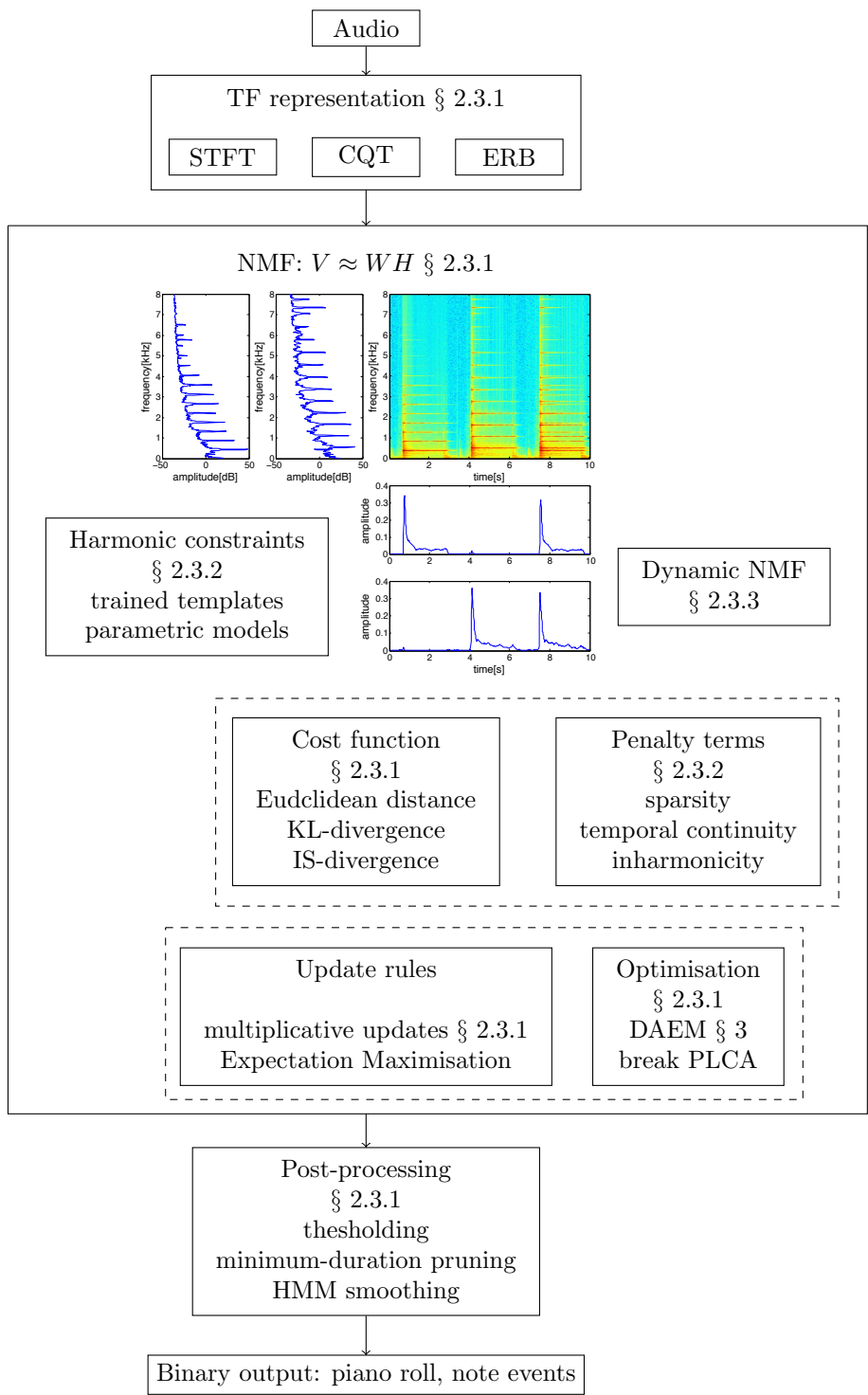


Figure 2.8: A general framework for NMF-based transcription.

Constant-Q Transform (CQT)

Constant-Q transform (CQT) provides a TF representation on a log-frequency scale. The Q in CQT indicates the quality factor, defined as [Brown, 1991]:

$$Q = f_k / \delta f_k, \quad (2.16)$$

where f_k and δf_k are the central frequency and the frequency resolution of the k^{th} bin, respectively. Then the window length of the k^{th} bin is given by

$$N[k] = \frac{f_s}{\delta f_k} = \left(\frac{f_s}{f_k}\right)Q, \quad (2.17)$$

where f_s is the sampling rate. In the constant-Q transform, the central frequencies of the frequency bins are geometrically spaced and the Q value is constant. The geometrically spaced frequency bins are in line with the musical scale, because the fundamental frequencies (f_0 s) of musical pitches are equally spaced in the log frequency scale. Constant Q means that the window sizes of the frequency bins are inversely proportional to their centre frequencies. This results in varying time and frequency resolutions along the frequency axis, with better frequency resolution at low frequencies and better time resolution at high frequencies. This frequency scale is closer to human auditory perception than the STFT [Schörkhuber and Klapuri, 2010].

Because of the geometrically spaced frequency bins in the CQT, the intervals between f_0 s and harmonics are constant for all pitches, which allows the note spectra to be shiftable along the log-frequency axis. However, simply shifting a spectrum for all pitches is not practical for AMT, because the spectra of different pitches usually have different harmonic distributions. This shift-invariant characteristic has been used successfully to shift templates among a small frequency range [Benetos and Dixon, 2012a].

Some efficient implementations of CQT can be found in [Schörkhuber and Klapuri, 2010, Fillon and Prado, 2012, Schörkhuber et al., 2014].

Equivalent Rectangular Bandwidth-scale (ERB-scale) TF representation

The ERB-scale TF representation is an auditory-motivated TF representation, with the ERB scale defined by [Moore and Glasberg, 1996]

$$f_{ERB} = 9.26 \log(0.00437 f_{Hz} + 1). \quad (2.18)$$

As applied in musical source separation [Vincent, 2006, Duong et al., 2010] and automatic music transcription [Vincent et al., 2008, Bertin et al., 2009a, 2010,

Vincent et al., 2010], the ERB-scale TF representation is computed as follows. The signal $x(t)$ is passed through a bank of filters $H_f(t)$, providing subband signals $x_f(t)$ of the f^{th} filter:

$$x_f(t) = \sum_{\tau} H_f(t)x(t - \tau). \quad (2.19)$$

The centre frequencies of the filters are linearly spaced on the ERB scale. The distribution of the filters is approximately linear in the low frequency range (below 500 Hz), and approximately constant-Q at high frequencies (above 2000 Hz) [Necciari et al., 2013]. The main-lobe bandwidth of each filter is set to four times the frequency difference between the centre frequencies of adjacent filters. The magnitude frequency response G_f of the f^{th} filter can then be analytically computed as a combination of sine cardinal (sinc) functions.

It is shown that in comparison to the STFT, the ERB scale provides a representation of better temporal resolution in the higher frequency range with smaller size [Vincent et al., 2008]. In addition, tests on AMT show that better or at least similar performance can be achieved at lower computational cost using the ERB-scale representation [Vincent et al., 2008, O’Hanlon and Plumbley, 2013, Benetos and Weyde, 2015b].

‘The ERBlet transform’, an alternative implementation of an invertible ERB-scale representation, is available in [Necciari et al., 2013].

Non-negative matrix factorisation

After obtaining the TF representation, for example the spectrogram, the transcription systems employ NMF to represent the spectrogram \mathbf{V} as a linear combination of spectral bases \mathbf{W} :

$$V_{ft} \approx \sum_{r=1}^R W_{fr}H_{rt}, \quad (2.20)$$

where $\mathbf{V} \in \mathbb{R}^{F \times T}$, $\mathbf{W} \in \mathbb{R}^{F \times R}$ and $\mathbf{H} \in \mathbb{R}^{R \times T}$ are non-negative matrices, and f , t and r are indices of the frequency bin, time frame and latent component, respectively. R is chosen in order to perform a low-rank matrix approximation ($R(F + T) \ll FT$).

Cost functions

We denote $\hat{\mathbf{V}} = \mathbf{W}\mathbf{H}$ as the reconstruction. NMF estimates \mathbf{W} and \mathbf{H} by minimising the distance between \mathbf{V} and $\hat{\mathbf{V}}$. This distance is called the cost function or the objective function [Lee and Seung, 1999], which is initially represented

Table 2.2: The usage of the β -divergences in AMT

Cost function	literature
Euclidean distance	[Vincent et al., 2008] (Weighted EUC)
KL-divergence	[Hennequin et al., 2010, Rigaud et al., 2012, 2013a,b] [Yoshii and Goto, 2012]
IS-divergence	[Bertin et al., 2009b, Yoshii and Goto, 2012]
β -divergence	[Dessein et al., 2010]

as:

$$D(\mathbf{V}|\hat{\mathbf{V}}) = \sum_{f,t} (V_{ft} \log(\hat{V}_{ft}) - \hat{V}_{ft}). \quad (2.21)$$

There are two other cost functions, Euclidean distance and Kullback-Leibler (KL) divergence, discussed in [Lee and Seung, 2000], shown as follows,

$$D_{Euc}(\mathbf{V}|\hat{\mathbf{V}}) = \sum_{f,t} (V_{ft} - \hat{V}_{ft})^2, \quad (2.22)$$

$$D_{KL}(\mathbf{V}|\hat{\mathbf{V}}) = \sum_{f,t} (V_{ft} \log \frac{V_{ft}}{\hat{V}_{ft}} - V_{ft} + \hat{V}_{ft}). \quad (2.23)$$

In addition, the Itakura-Saito (IS) divergence is also widely-used [Févotte et al., 2009]:

$$D_{IS}(\mathbf{V}|\hat{\mathbf{V}}) = \sum_{f,t} (\frac{V_{ft}}{\hat{V}_{ft}} - \log \frac{V_{ft}}{\hat{V}_{ft}} - 1). \quad (2.24)$$

These three cost functions are included in a β -divergence family, with $\beta = 2, 1, 0$ for the Euclidean distance, KL divergence and IS divergence, respectively [Dessein et al., 2010]. The β -divergence is defined as follows:

$$d_{\beta}(x|y) = \begin{cases} \frac{1}{\beta(\beta-1)}(x^{\beta} + (\beta-1)y^{\beta} - \beta xy^{\beta-1}) & \beta \in \mathbb{R} \setminus \{0, 1\} \\ x \log \frac{x}{y} - x + y & \beta = 1 \\ \frac{x}{y} - \log \frac{x}{y} - 1 & \beta = 0 \end{cases} \quad (2.25)$$

Systems with different cost functions are summarised in Table 2.2.

The scaling property of the β -divergence is usually analysed when choosing the cost function, which can be derived from the definition in Equation 2.25:

$$d_{\beta}(\lambda x|\lambda y) = \lambda^{\beta} d_{\beta}(x|y). \quad (2.26)$$

The Itakura-Saito divergence ($\beta = 0$) is known to be scale-invariant, which means that small and large coefficients of \mathbf{V} are weighted equally in the cost

function [Févotte et al., 2009]. When $\beta > 0$, more emphasis is put on the frequency components of higher energy, and the emphasis increases with β . When $\beta < 0$, the effect is the converse [Dessein et al., 2010].

We apply a simple test of different $\beta \in \{2, 1, 0\}$ using an isolated piano tone from the ‘ENSTDkCl’ subset of the MAPS database [Emiya et al., 2010]. The piano tone with the fundamental frequency of 440Hz (MIDI index 69) is produced by a Disklavier piano. The waveform and spectrogram (normalised to a maximum of 1) of the signal are shown in Figure 2.9. A rank-one NMF is performed on the amplitude spectrogram with different $\beta \in \{2, 1, 0\}$, and the maximum of the activation is normalised to 1. The spectral basis is also normalised to a maximum of 1 after the iterations for an intuitive comparison. The results are illustrated in Figure 2.10, which are basically in line with the analysis in previous literature. The activation of $\beta = 2$ resembles more the envelope of the partial with largest energy, as shown in the fundamental frequency amplitude in the spectrogram of Figure 2.9. By contrast, the activation of $\beta = 0$ is equally sensitive to energy changes of all frequencies, therefore the trajectory fluctuates. The activation of $\beta = 1$ is somewhere in between. It smoothly represents the decaying energy of the signal.

Update rules

There are several ways to estimate parameters in NMF. Here we employ multiplicative update rules for parameter estimation. The rules can be obtained by choosing an adaptive step in gradient descent [Lee and Seung, 2000]. The derivative of the cost function D with respect to (w.r.t) θ , $\nabla_{\theta} D(\theta)$, is written as a difference of two non-negative functions:

$$\nabla_{\theta} D(\theta) = \nabla_{\theta}^{+} D(\theta) - \nabla_{\theta}^{-} D(\theta), \quad (2.27)$$

where $\nabla_{\theta}^{+} D(\theta)$ and $\nabla_{\theta}^{-} D(\theta)$ are the absolute values of the positive and negative parts of the derivative, respectively. The multiplicative algorithm is given by:

$$\theta \leftarrow \theta \cdot \frac{\nabla_{\theta}^{-} D(\theta)}{\nabla_{\theta}^{+} D(\theta)}. \quad (2.28)$$

For the β -divergence, the derivative is derived as:

$$\nabla_{\theta} D(\theta) = (\hat{V}^{\beta-1} - V\hat{V}^{\beta-2})\nabla_{\theta}\hat{V}. \quad (2.29)$$

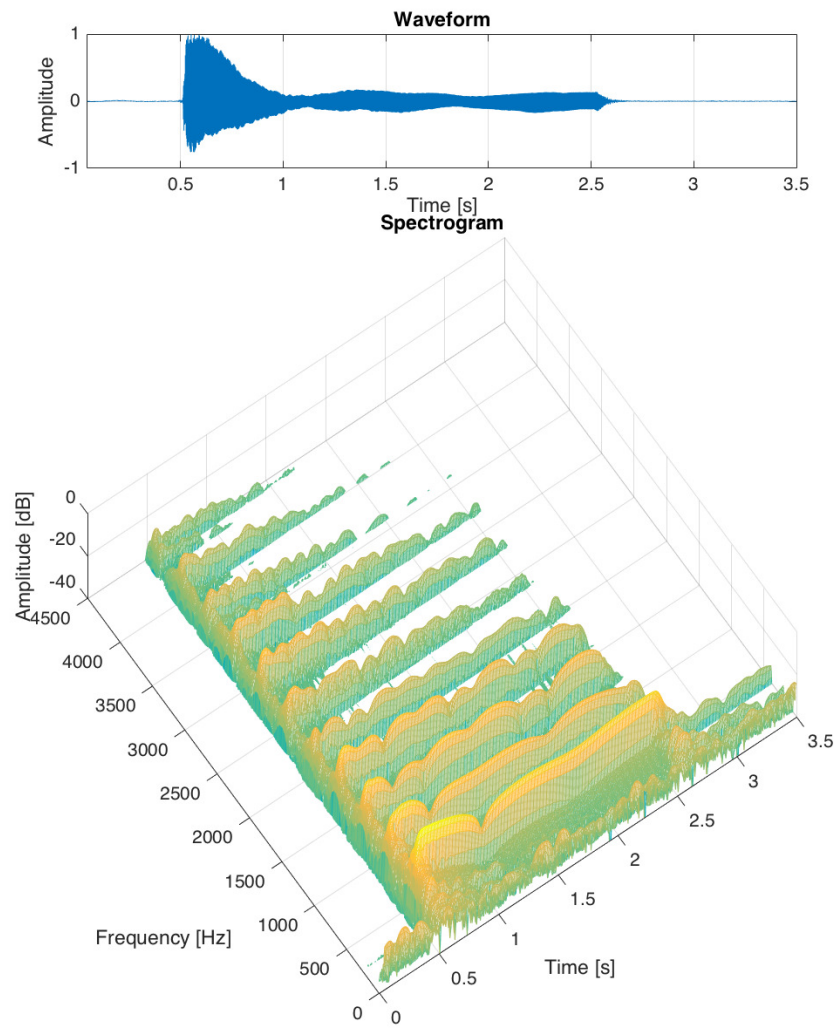


Figure 2.9: The waveform and spectrogram of a tone with f_0 of 440 Hz.

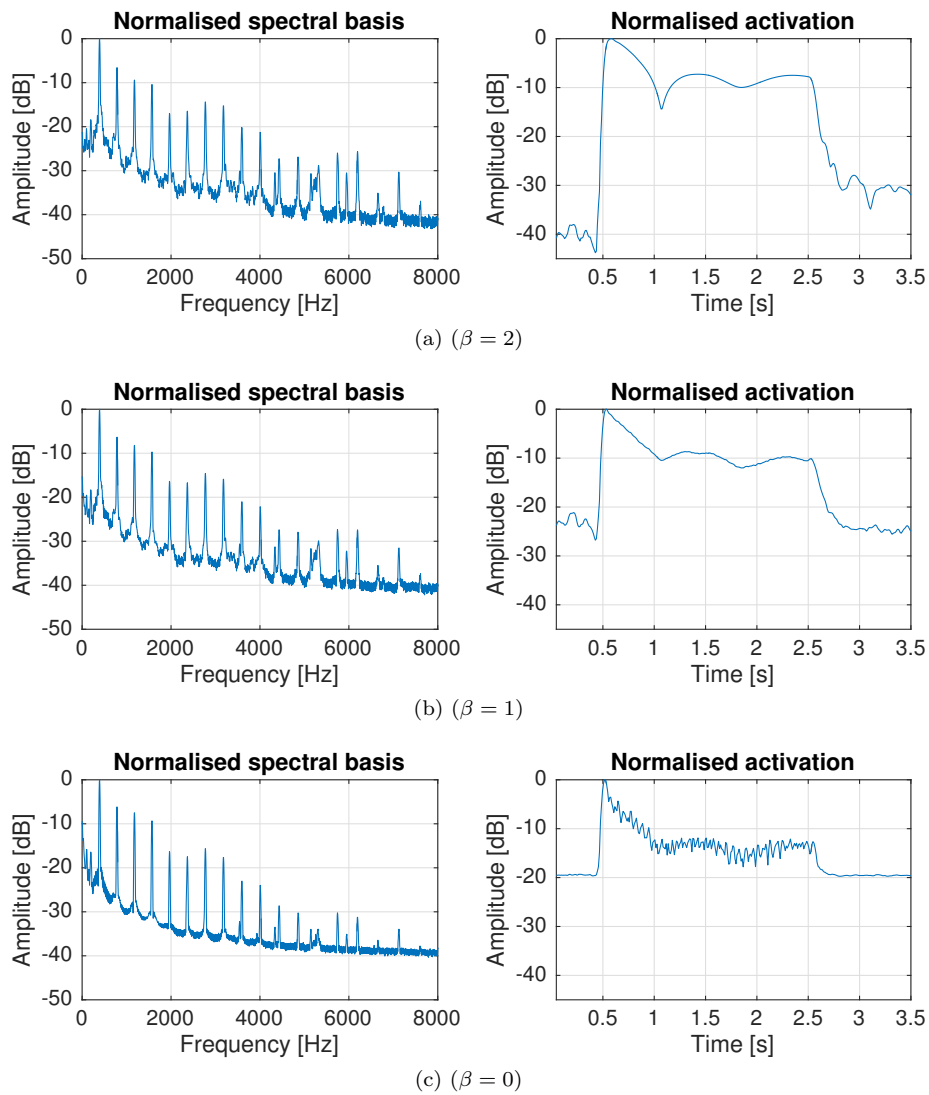


Figure 2.10: Spectral bases and activations obtained using different cost functions.

Then the updates for W and H with β -divergence are as follows [Févotte, 2011],

$$H \leftarrow H \cdot \frac{W^T [(WH)^{\cdot(\beta-2)} \cdot V]}{W^T [WH]^{\cdot(\beta-1)}}, \quad (2.30)$$

$$W \leftarrow W \cdot \frac{[(WH)^{\cdot(\beta-2)} \cdot V] H^T}{[WH]^{\cdot(\beta-1)} H^T}. \quad (2.31)$$

The update rules are iterated alternately until convergence.

Optimisation

Parameter estimation is achieved by finding the minimum of the cost function. Optimisation methods can help to find the global minimum or at least a better local minimum when the problem is non-convex. We will discuss the local minimum problem of matrix-factorisation-based methods in Chapter 3, and introduce an optimisation method to deal with this problem.

Post-processing

The activations indicate the volumes of different pitches. In order to provide a binary output, we can simply apply a threshold on the activations. After that minimum-duration pruning is commonly used to reduce erroneous notes with short duration. To smooth the output, many systems apply Hidden Markov Models to track the optimal state sequences. Readers are referred to Section 2.2.6 for our summaries of these methods.

2.3.2 Constraints

The non-negative constraint allows NMF to provide part-based and meaningful decompositions, but the result is not unique. It is related to the cost function, estimation method, initialisation, scaling, constraints and so on. In this section, we will discuss several commonly-used constraints. Besides non-negativity, sparsity and continuity are also proper assumptions for many real-world applications. For music, another primary characteristic is the harmonic (or quasi-harmonic) structure in the spectrum.

Bertin et al. [2010] summarise three ways to enforce constraints: adding penalty terms to cost functions, using parametric models and choosing prior distributions in the statistical Bayesian NMF. In this section, we review the first two methods for constraints. We individually describe incorporating priors in the Bayesian extension of NMF in Section 2.3.3.

Sparsity

Sparsity is the most common constraint for NMF, which can be enforced on either decomposed matrix, depending on the specific application. We usually assume the activation of each time frame is sparse in AMT.

Hoyer [2004] proposed to project the column of W or the row of H to achieve a desired level of sparsity after each iteration. The sparsity is measured by the relation between the L_1 norm and the L_2 norm:

$$g(\mathbf{x}) = \frac{\sqrt{n} - \|\mathbf{x}\|_1 / \|\mathbf{x}\|_2}{\sqrt{n} - 1}, \quad (2.32)$$

where L_p -norm is given by $\|\mathbf{x}\|_p := (\sum_{i=1}^n |x_i|^p)^{1/p}$, and n is the dimension of the vector \mathbf{x} . The method is used for multiple pitch estimation with modified sparsity measures [Cont, 2006, Cont et al., 2007].

An alternative method is to add a penalty term to the cost function [Eggert and Körner, 2004], which is adapted from non-negative sparse coding [Hoyer, 2002]:

$$C_s(\mathbf{H}) = \sum_{r,t} g(H_{rt}),$$

$$C = D(\mathbf{V}|\mathbf{W}\mathbf{H}) + \lambda_s C_s(\mathbf{H}), \quad (2.33)$$

where $g(x) = |x|$ is the L_1 -norm regularisation for measuring sparsity and λ_s controls the degree of sparsity. Because all values are non-negative in NMF, the L_1 -norm function can be expressed as $g(x) = x$. Note that the scaling problem of choosing λ_s can be fixed by normalising W_r . Similarly, the L_0 -norm and L_2 -norm are applied in [Peharz and Pernkopf, 2012] and [Smaragdis and Brown, 2003] for sparsity constraints, respectively.

In the equivalent probabilistic model (PLCA), the sparsity is enforced by applying a power larger than 1 to the distribution [Benetos and Dixon, 2012a]:

$$H_{rt} \leftarrow H_{rt}^{\lambda_s}. \quad (2.34)$$

where λ_s is larger than 1. When we normalise the sum of the activations in each frame to be 1, the activations in NMF can be seen as probabilities. So the method in Equation 2.34 can also be applied in normalised NMF to enforce sparsity.

Continuity

We review methods to enforce temporal continuity and spectral continuity on the activations and spectral bases, respectively.

Temporal continuity

To enforce temporal continuity, Virtanen [2007] proposed to add a penalty on the activations \mathbf{H} to the cost function :

$$C_t(\mathbf{H}) = \sum_{r=1}^R \frac{1}{\delta_r^2} \sum_{t=2}^T (h_{r,t} - h_{r,t-1})^2. \quad (2.35)$$

This constraint prevents a large change between activations in adjacent frames. The standard deviation estimate $\delta_r = \sqrt{(1/T) \sum_{t=1}^T h_{rt}^2}$ is used for normalisation, so the cost is not affected by scaling. The IS divergence of amplitudes of adjacent frames is also used as a penalty to impose temporal continuity, which is also scale-invariant [Févotte, 2011]. The cost function is written as:

$$C(\mathbf{W}, \mathbf{H}) = D(\mathbf{V}|\mathbf{WH}) + \lambda_t C_t(\mathbf{H}), \quad (2.36)$$

where λ_t controls the degree of continuity.

Another temporal flatness term is proposed for temporal continuity, motivated by spectral flatness [Becker et al., 2014]. The proposed term is presented as:

$$C_t(\mathbf{H}) = \sum_{r=1}^R \frac{1}{T} \frac{\sum_{t=1}^T H_{rt}}{\sqrt[T]{\prod_{t=1}^T H_{rt}}}. \quad (2.37)$$

Spectral continuity

Two spectral terms are employed to enforce spectral continuity to penalise large spectral variations [Becker et al., 2014], which take the same forms as the previous temporal terms. One is the spectral-wise squared difference motivated by the temporal squared difference, Equation 2.35. The other penalty is the inverted spectral flatness descriptor, written as:

$$C_{sp}(\mathbf{W}) = \sum_{r=1}^R \frac{1}{F} \frac{\sum_{f=1}^F W_{fr}}{\sqrt[F]{\prod_{f=1}^F W_{fr}}}. \quad (2.38)$$

This penalty term is also added to the cost function:

$$C(\mathbf{W}, \mathbf{H}) = D(\mathbf{V}|\mathbf{WH}) + \lambda_{sp} C_{sp}(\mathbf{W}), \quad (2.39)$$

where λ_{sp} controls the degree of spectral continuity.

Harmonic constraints

A pitched sound generates frequency components at or near the multiples of its fundamental frequency, i.e. the harmonics or partials, with a comb-shaped spectrum. In NMF-based systems, the harmonic structure is constrained by each spectral basis \mathbf{w}_r . In this section, we show several ways to enforce harmonicity or inharmonicity.

Training templates

The harmonic structure of a pitch can be obtained by template training. A template is an average of the spectral distribution over the duration of the note, which is usually learned on an isolated note. When we have access to sound samples of the sources, we can train the templates first and then keep them fixed to perform supervised NMF, or semi-automatic transcription [Kirchhoff, 2013].

The previously-trained templates can be adapted to the test data. Benetos et al. [2014] proposed a template adaptation system to match the test dataset. The system first transcribes the test music pieces with trained templates. Then activations of high values are fixed, and corresponding templates are updated using the test data. Finally music pieces are transcribed again with the adapted templates.

Parametric models

The harmonic structure can be parameterised as a harmonic comb, with peaks at harmonic positions. The spectral basis is given as:

$$W_{fr} = \sum_k a_{kr} g(f - f_{kr}), \quad (2.40)$$

where W_{fr} is the value of spectral basis r in the f^{th} frequency bin. k is the index of the partial. f_{kr} and a_{kr} are the frequency and amplitude of the k^{th} partial of the r^{th} spectral basis, respectively. $g(f)$ represents the frequency response of the window function. The frequency response covers the whole frequency range, but usually only a certain range is used, such as the main lobe of the hamming window [Rigaud et al., 2012, 2013a,b].

This parametric harmonic comb has been employed in music transcription [Vincent et al., 2008, Hennequin et al., 2010, Yoshii and Goto, 2012, Rigaud et al., 2013b], music source separation [Hennequin et al., 2011b] and piano sound analysis [Rigaud et al., 2012, 2013a]. The harmonicity or inharmonicity of the music sounds is enforced by the relation between f_{0r} and f_{kr} . Usually three

harmonic settings are considered [Vincent et al., 2008, Rigaud et al., 2013b]:

- harmonicity:

$$f_{kr} = kf_{0r} \quad (2.41)$$

- inharmonicity with fixed inharmonicity factor B :

$$f_{kr} = kf_{0r} \sqrt{1 + Bk^2} \quad (2.42)$$

- inharmonicity with pitch-variant inharmonicity factor B_r :

$$f_{kr} = kf_{0r} \sqrt{1 + B_r k^2} \quad (2.43)$$

With the explicitly modelled window response, this model can update the fundamental frequencies f_0 directly, to represent vibrato [Hennequin et al., 2010] or for stretched tuning [Rigaud, 2013]. The inharmonicity parameter, especially for piano tones, is also analysed by adding an inharmonic penalty to the cost function in [Rigaud et al., 2012, 2013a,b]. The inharmonic penalty is given by:

$$C_h = \sum_r \frac{1}{K_r} \sum_{k=1}^{K_r} (f_{kr} - kf_{0r} \sqrt{1 + B_r k^2})^2, \quad (2.44)$$

where K_r is the number of partials considered for pitch r , and B_r is the inharmonicity factor for pitch r . The influences of inharmonicity on transcription systems are tested in different systems for piano music. The experiments suggest that the inharmonic constraints even decrease the transcription performance [Vincent et al., 2008], while Rigaud et al. [2013b] show that the results are sensitive to the initialisations of the B_r and f_{0r} , and a pitch-wise inharmonicity parameter can help the transcription performance on piano music.

Adaptive spectral basis

A spectral basis can be represented as a linear combination of narrowband spectra [Vincent et al., 2008, Bertin et al., 2009a, 2010, Vincent et al., 2010],

$$W_{fr} = \sum_m E_{rm} P_{rmf} \quad (2.45)$$

where, P_{rmf} is the m^{th} narrowband spectrum and E_{rm} is the weight of the narrowband spectrum. Each narrowband spectrum P_{rmf} contains a certain number of partials to enforce spectral smoothness as well as to enable adaptation to different instruments. In [Vincent et al., 2008], the subbands are uniformly spaced on the ERB scale, with the centre frequency of the first subband at

the fundamental frequency f_{r1} and subsequent subbands linearly spaced, for example by 3 ERB. The subband spectral shape is defined as the symmetric approximation of the response of the gammatone filter of the corresponding bandwidth.

In comparison to the weighted sum of each partial, the number of free parameters of this model is reduced. It keeps the harmonic structure and flexibility to adapt to various instruments, and also helps to enforce spectral smoothness.

2.3.3 Bayesian extension of NMF

In previous sections we illustrate how NMF works with penalty terms and deterministic constraints. In this section we introduce a Bayesian extension of NMF, which interprets NMF from a statistical perspective and offers a principled way to incorporate prior knowledge.

Initially in NMF, Lee and Seung explained the cost function

$$D(\mathbf{V}|\mathbf{WH}) = \sum_{f,t} (V_{ft} \log(\mathbf{WH})_{ft} - (\mathbf{WH})_{ft}) \quad (2.46)$$

as a generative model, in which V_{ft} is generated by adding Poisson noise to the product $(\mathbf{WH})_{ft}$ [Lee and Seung, 1999]. The cost function is related to the likelihood of generating \mathbf{V} from bases \mathbf{W} and activations \mathbf{H} . The correspondence between the cost functions and probabilistic generative models is analysed in [Abdallah and Plumbley, 2004, Virtanen et al., 2008, Cemgil, 2009, Schachtner et al., 2014, Smaragdis et al., 2014], which is given by

$$-\log p(\mathbf{V}|\mathbf{WH}) = aD(\mathbf{V}|\mathbf{WH}) + b, \quad (2.47)$$

where a and b are constants with respect to \mathbf{WH} , and $a > 0$. This means that minimising the cost function $D(\mathbf{V}|\mathbf{WH})$ is equivalent to maximising the log likelihood $\log p(\mathbf{V}|\mathbf{WH})$. We adapt a summary of the relation between the cost functions and generative models from [Smaragdis et al., 2014] as shown in Table 2.3. In AMT, \mathbf{V} , $\hat{\mathbf{V}}$ indicate the observed and reconstructed spectrograms, respectively.

In the probabilistic model, parameters \mathbf{W} and \mathbf{H} can be estimated by the maximum a posteriori (MAP) method.

$$(\mathbf{W}, \mathbf{H}) = \arg \max_{\mathbf{W}, \mathbf{H}} \log(P(\mathbf{W}, \mathbf{H}|\mathbf{V})). \quad (2.48)$$

Table 2.3: Relation between divergences and generative models, adapted from [Smaragdīs et al., 2014]

Divergence $D(\mathbf{v}_t \hat{\mathbf{v}}_t)$	Generative model $p(\mathbf{v}_t \hat{\mathbf{v}}_t)$
Squared Euclidean Distance $\frac{1}{2\delta^2} \sum_f (V_{ft} - \hat{V}_{ft})^2$	Additive Gaussian $\prod_f N(V_{ft} \hat{V}_{ft}, \delta^2)$
Generalised KL Divergence $\sum_f (V_{ft} \log \frac{V_{ft}}{\hat{V}_{ft}} - V_{ft} + \hat{V}_{ft})$	Poisson $\prod_f P(V_{ft} \hat{V}_{ft})$
IS Divergence $\sum_f (\frac{V_{ft}}{\hat{V}_{ft}} - \log \frac{V_{ft}}{\hat{V}_{ft}} - 1)$	Multiplicative Gamma $\prod_f G(V_{ft} \alpha, \alpha/\hat{V}_{ft})$

The posterior density is given by Bayes' rule:

$$p(\mathbf{W}, \mathbf{H}|\mathbf{V}) = \frac{p(\mathbf{V}|\mathbf{W}, \mathbf{H})p(\mathbf{W}, \mathbf{H})}{p(\mathbf{V})}, \quad (2.49)$$

where $p(\mathbf{W}, \mathbf{H}) = p(\mathbf{W})p(\mathbf{H})$, $p(\mathbf{W})$ and $p(\mathbf{H})$ indicate the prior distributions and are assumed independent [Bertin et al., 2010]. It shows that the Bayesian inference of the model is equivalent to NMF, if ignoring the prior [Cemgil, 2009].

Prior knowledge is enforced by hierarchical structure in Bayesian NMF [Cemgil, 2009]:

$$p(\mathbf{V}|\Theta) = \int d\mathbf{W}d\mathbf{H} \sum_s p(\mathbf{V}|\mathbf{S})p(\mathbf{S}|\mathbf{W}, \mathbf{H})p(\mathbf{W}, \mathbf{H}|\Theta), \quad (2.50)$$

where Θ is the hyperparameter and \mathbf{S} is the latent component, with the assumption of independence between $p(\mathbf{W})$ and $p(\mathbf{H})$, $p(\mathbf{W}, \mathbf{H}|\Theta) = p(\mathbf{W}|\Theta)p(\mathbf{H}|\Theta)$. There are several ways to enforce the prior information on spectral bases $p(\mathbf{W}|\Theta)$ or activations $p(\mathbf{H}|\Theta)$. A Gamma prior is used for spectral bases of drums [Virtanen et al., 2008]. More generally for pitched notes, the spectral bases are harmonically-spaced. A deterministic harmonic structure is suitable for this prior, as shown in Section 2.3.2. For temporal continuity on activations, Gamma-chain [Virtanen et al., 2008] and inverse-Gamma distributions [Bertin et al., 2009a] are used, with more details to be discussed in the next subsection.

If the hyperparameter Θ is arbitrarily fixed or trained, parameters can be estimated by an EM-based algorithm [Bertin et al., 2010] or multiplicative updates [Virtanen et al., 2008, Bertin et al., 2009a]. In this case the prior can be seen as a penalty term [Bertin et al., 2009a]. If the hyperparameters are unknown and need to be estimated, a variational Bayes method can be applied [Cemgil, 2009]. Yoshii and Goto [2012] propose a model in which Bayesian hyper parameters are estimated using variational Bayes, while the NMF parameters are estimated by multiplicative optimisation. Beside incorporating priors, Bayesian NMF can

employ statistical features of Bayesian models, such as non-parametric models [Hoffman et al., 2010, Yoshii and Goto, 2012].

Dynamic models

In basic NMF, the activations of different time frames are assumed independent. Temporal continuity is achieved by post-processing the gains or by a constraint in the cost function as shown in Section 2.3.2. In Bayesian NMF, temporal continuity can be modelled by the prior for the activations. These models are called dynamic models [Smaragdis et al., 2014], which are represented as:

$$\mathbf{h}_t \sim p(\mathbf{h}_t | \mathbf{h}_{t-1}, \theta), \quad (2.51)$$

$$\mathbf{v}_t \sim p(\mathbf{v}_t | \mathbf{W}\mathbf{h}_t), \quad (2.52)$$

where \mathbf{h}_t is the activation vector at time frame t . The second equation represents a probabilistic view of the NMF model, with $\mathbb{E}[\mathbf{V} | \mathbf{W}\mathbf{H}] = \mathbf{W}\mathbf{H}$. The first equation indicates that the activation of the current frame is related to previous frames by a Markov model, where θ denotes the prior parameters. Gamma-chain constraints are used for the activation continuity [Virtanen et al., 2008, Yoshii and Goto, 2012], and an inverse-Gamma distribution is employed in [Bertin et al., 2009a, 2010], defined as:

$$p(h_{rt} | h_{rt-1}) = \mathcal{IG}(h_{rt} | \alpha_r, (\alpha_r + 1)h_{rt-1}), \quad (2.53)$$

where \mathcal{IG} is the inverse-Gamma distribution, and α_r is arbitrarily fixed to control the degree of smoothness.

Other approaches apply Hidden Markov Models for temporal continuity [Ozerov et al., 2009, Nakano et al., 2010, Mysore et al., 2010, Mohammadiha et al., 2013]. With a probabilistic representation, the idea is formulated as:

$$q_t \sim p(q_t | q_{t-1}), \quad (2.54)$$

$$\mathbf{h}_t \sim p(\mathbf{h}_t | q_t), \quad (2.55)$$

where q_t is the hidden state at time frame t . This model can use higher-level information with hidden states [Smaragdis et al., 2014]. Benetos and Dixon [2013] use a probabilistic version (temporally-constrained PLCA) for multi-instrument music transcription. The unknown parameters of the matrix factorisation methods and HMM are estimated jointly in this model.

2.4 Evaluation metrics

In order to evaluate the performance of the AMT methods, two levels of metrics are commonly used, frame-level metrics (for multiple f_0 estimation) and note-level metrics (for note tracking). As transcription systems are now pursuing higher-level representations, more systems are expected to include the instrument information in the output. In this case, instrument-based evaluation is also performed. We will introduce these three levels of metrics in the following. They are also described in an annual evaluation campaign ‘Music Information Retrieval Evaluation eXchange’ (MIREX) for Multiple Fundamental Frequency Estimation & Tracking [MIREX, 2016].

2.4.1 Frame-level evaluation

For a frame-level evaluation, performance is evaluated frame by frame with an interval of 10 ms. If a detected f_0 is in a range of $\pm 3\%$ of the ground truth frequency, it is labelled as a correct detection. The overall accuracy (Acc) is indicated using the definition in [Dixon, 2000]:

$$Acc = \frac{N_{tp}}{N_{tp} + N_{fp} + N_{fn}} \quad (2.56)$$

where N_{tp} is the number of true positives, N_{fp} and N_{fn} are the numbers of false positives and false negatives respectively. The frame-wise precision (P), recall (R) and F-measure (F) are also used as accuracy metrics, defined in [Vincent et al., 2010] as:

$$P = \frac{N_{tp}}{N_{sys}}, \quad R = \frac{N_{tp}}{N_{ref}}, \quad F = \frac{2 \times R \times P}{R + P} \quad (2.57)$$

where $N_{sys} = N_{tp} + N_{fp}$ denotes the number of detected pitches and $N_{ref} = N_{tp} + N_{fn}$ is the number of ground-truth pitches.

Apart from the accuracy, the metrics below are defined for the frame-based evaluation as well [Poliner and Ellis, 2007], including the rates of total errors (E_{tot}), substitution errors (E_{subs}), missed detections (E_{miss}) and false alarms

(E_{fa}):

$$E_{subs} = \frac{\sum_{t=1}^T \min(N_{ref}^t, N_{sys}^t) - N_{tp}^t}{\sum_{t=1}^T N_{ref}^t} \quad (2.58)$$

$$E_{miss} = \frac{\sum_{t=1}^T \max(0, N_{ref}^t - N_{sys}^t)}{\sum_{t=1}^T N_{ref}^t} \quad (2.59)$$

$$E_{fa} = \frac{\sum_{t=1}^T \max(0, N_{sys}^t - N_{ref}^t)}{\sum_{t=1}^T N_{ref}^t} \quad (2.60)$$

$$E_{tot} = E_{subs} + E_{miss} + E_{fa} \quad (2.61)$$

where t is the frame index and T is the total number of frames.

2.4.2 Note-level evaluation

To perform a note-level evaluation, the output is represented as a list of note events, where each note event consists of an onset, an offset and a pitch. In the MIREX public evaluations for Multiple Fundamental Frequency Estimation & Tracking [MIREX, 2016], a note is considered correctly detected if the note is within the following ranges of ground truth.

pitch range $\pm 3\%$

onset range ± 50 ms

offset range $\pm \max \{20\% \text{ of the duration, } 50 \text{ ms} \}$

The algorithms are evaluated in terms of onset-only and onset-offset using the note-wise accuracy metrics, which are defined in a similar way to (2.56) and (2.57). The onset-only precision, recall, F-measure and overall accuracy are denoted as P_{on} , R_{on} , F_{on} and Acc_{on} , respectively. The onset-offset metrics are P_{off} , R_{off} , F_{off} and Acc_{off} .

2.4.3 Instrument-level evaluation

To evaluate a system at the instrument level, the output notes need to be labelled with their corresponding instruments. Then, the performance for each instrument can be measured using previous frame-wise and note-wise metrics. Considering that the contribution of each instrument is often monophonic, melody extraction evaluation metrics are also used for this task [Bay et al., 2012]. The evaluation metrics are calculated over all frames and all instruments, given as

Table 2.4: Public evaluation results on frame-wise accuracy (Acc_f) and onset-only note-level F-measure F_{on} .

Year	Baseline method	Acc_f	F_{on}
2011	[Yeh et al., 2010]	0.683	0.560
2013	[Cheng et al., 2013]	0.620	0.507
2014	[Duan et al., 2010]	0.553	0.451
2014	[Böck and Schedl, 2012]	-	0.547
2014	[Dressler, 2011]	0.680	0.659
2015	[Benetos and Weyde, 2015a]	0.654	0.601
2016	[Benetos and Dixon, 2012a]	0.486	0.503

follows:

$$P = \frac{\sum_{i,t} N_{tpc}^{i,t}}{\sum_{i,t} N_{tp}^{i,t} + N_{fp}^{i,t}} \quad (2.62)$$

$$R = \frac{\sum_{i,t} N_{tpc}^{i,t}}{\sum_{i,t} N_{tp}^{i,t} + N_{fn}^{i,t}} \quad (2.63)$$

$$F = \frac{2 \times P \times R}{P + R} \quad (2.64)$$

$$Acc = \frac{\sum_{i,t} N_{tpc}^{i,t} + N_{tn}^{i,t}}{\sum_{i,t} N_{tp}^{i,t} + N_{fp}^{i,t} + N_{tn}^{i,t} + N_{fn}^{i,t}} \quad (2.65)$$

where N_{tp} , N_{tn} , N_{fp} and N_{fn} are the numbers of true positives, true negatives, false positives and false negatives for pitched/unpitched detection, N_{tpc} denotes the number of correct f_0 in N_{tp} , and i and t are the instrument index and the frame index, respectively.

2.4.4 Public evaluation

Some systems reviewed in this chapter have been submitted to the Music Information Retrieval Evaluation eXchange (MIREX) for the task of Multiple Fundamental Frequency Estimation & Tracking [MIREX, 2016]. We show the results of the latest submissions based on the reviewed systems in Table 2.4. The frame-wise accuracies Acc_f is evaluated on 40 test pieces and note-level F-measures (onset-only) F_{on} is evaluated on 34 test pieces.

2.5 Conclusions

In this chapter, we first give a brief introduction to sound generation and perception, by which we know that human perception of a musical tone is related

to its fundamental frequency, harmonics (partials) and spectrum. Then in Section 2.1.2 we specify acoustical features of piano tones which are related to the excitation mechanism and physical structure of the piano. We review AMT systems according to the level of information employed by the system in Section 2.2. First we introduce systems detecting a pitch using its period, harmonics (partials) and spectrum, respectively. Then we review systems using high level information, i.e. musicological models, for transcription, and also several typical classification-based methods. At last, we present post-processing methods to generate note events and note-level systems which model discrete note events directly. In Section 2.3, we present a general framework for NMF-based transcription in detail, with commonly-used constraints. In Section 2.4 we summarise commonly-used evaluation metrics of three levels (frame level, note level and instrument level), and give a summary on public evaluation results.

In Chapter 3, we will address the local minimum problem of matrix decomposition methods as indicated in Section 2.3.1. We work on an existing transcription system based on the PLCA, the probabilistic counterpart of NMF, with an optimisation method. Based on the theoretical analysis in Section 2.1.2, we will study piano decay in Chapter 4, and model temporal evolution for piano notes for transcription in Chapter 5 and Chapter 6.

Chapter 3

A Deterministic Annealing EM Algorithm for AMT

In this chapter, we use a deterministic annealing EM (DAEM) algorithm to deal with the local minimum problem of PLCA and show the improvement in transcription performance by doing so. Matrix factorisation methods (such as NMF and PLCA) are initialisation-sensitive and tend to converge to a local minimum. There are several approaches to address this local minimum problem. Hofmann [1999] proposes a model based on a tempered EM algorithm to avoid overfitting in probabilistic latent semantic analysis. Bertin et al. [2009b] use the tempering scheme to favour the convergence of the Itakura-Saito (IS) divergence to global minima. Experiments on music transcription show that the IS-NMF can provide a good result by choosing a suitable temperature parameter. The deterministic annealing EM algorithm is proposed to optimise the parameter estimation of EM-based methods [Ueda and Nakano, 1998]. It has been used in a harmonic-temporal-structured clustering (HTC) model for audio feature extraction [Kameoka et al., 2005], and to estimate the parameters of Gaussian mixture models (GMMs) and hidden Markov models (HMMs) for speaker and speech recognition [Itaya et al., 2005]. In the latter method DAEM is shown to be effective for GMM and HMM-based acoustic models. Smaragdis and Raj [2007] state that using ‘annealing’ in PLCA helps to get ‘meaningful’ decompositions and quick convergence.

Here we focus on an existing PLCA-based transcription model [Benetos and Dixon, 2012a], and apply the DAEM algorithm to tackle the local minimum problem. In the proposed model, the PLCA update rules are modified by introducing a ‘temperature’ parameter. At higher temperatures, general areas of the search space containing good solutions are found. As the temperature is

gradually decreased, distinctions in the data are sharpened, resulting in a more fine-grained optimisation at each successive temperature.

We describe transcription systems based on PLCA in Section 3.1. In Section 3.2 we introduce the baseline transcription system and modify the update rules according to DAEM. The proposed method is tested in three transcription subtasks and compared to the baseline method in Section 3.3. Finally conclusions and discussions are indicated in Section 3.4.

3.1 PLCA and shift-invariant PLCA

Two basic PLCA models, PLCA and shift-invariant PLCA, are presented in [Smaragdis et al., 2008]. For automatic music transcription, the spectrogram is decomposed in PLCA as:

$$V(\omega, t) \approx P(\omega, t) = P(t) \sum_p P(\omega|p)P(p|t) \quad (3.1)$$

where $V(\omega, t)$ is the input spectrogram, $P(\omega, t)$ the approximated spectrogram, ω is the frequency bin, and t is the frame number. $P(t)$ is the energy of each time frame, $P(\omega|p)$ is the spectral basis corresponding to pitch p , and $P(p|t)$ the gain function.

To build a shift-invariant PLCA model, the spectrogram needs to be presented on a logarithmic frequency scale, such as the constant-Q transform. Assuming that the energy distributions of adjacent pitches are similar for any given instrument, the spectral basis can be shifted in frequency very easily, as the pattern of partial spacings is the same for all pitches, due to the logarithmic frequency axis. The spectrogram is approximated by:

$$\begin{aligned} V(\omega, t) \approx P(\omega, t) &= \sum_z P(z)P(\omega|z) *_\omega P(f, t|z) \\ &= \sum_z P(z) \sum_f P(\omega - f|z)P(f, t|z) \end{aligned} \quad (3.2)$$

where $P(\omega|z)$ and $P(f, t|z)$ are the spectral templates and time-dependent shifted variant f of component z , ‘*’ indicates the convolution, and $P(z)$ is the prior distribution of the components.

In many recent systems the PLCA model is extended by introducing an instrument distribution, with templates trained per pitch per instrument. The spectrogram is approximated by:

$$V(\omega, t) \approx P(\omega, t) = P(t) \sum_{p,s} P(\omega|s, p)P(s|p, t)P(p|t) \quad (3.3)$$

where $P(\omega|s, p)$ represents the spectral templates corresponding to each instrument s and pitch p , $P(s|p, t)$ the instrument contribution to each pitch in the t^{th} frame, and $P(p|t)$ the pitch probability distribution for each frame.

The parameters of the PLCA models are estimated by iteratively decreasing the KL divergence of the input spectrogram $V(\omega, t)$ and the reconstruction $P(\omega, t)$ using the EM algorithm. The KL divergence is convex in one variable, but not convex in multiple variables [Lee and Seung, 2001]. In this case, the EM algorithm can only guarantee to find a local minimum for these parameters, so the results depend on the initialisation. The use of spectral templates is an effective way to deal with the initialisation sensitivity of the algorithm. Taking the model described in Equation 3.1 for example, if the templates are fixed as constant, the gain function will be convex. This means that when we formulate the model as the product of the spectral bases and a gain function, we obtain a unique gain function corresponding to a fixed set of templates. On the one hand, the templates lead to a stable decomposition for automatic music transcription; on the other hand, the templates also limit the performance of the transcription. However, when encountering the extended model as described in Equation 3.3, the instrument contribution and the pitch contribution still face the risk of converging to local minima, even with fixed templates.

3.2 Transcription system based on DAEM

To deal with the local minimum problem of PLCA models, we derive update rules according to the deterministic annealing EM algorithm [Ueda and Nakano, 1998], which introduces a temperature parameter into the EM algorithm. The temperature parameter is employed on the posterior probability density in the E-step. Then by gradually reducing the temperature, the EM steps are iteratively executed until convergence at each temperature, leading the result to a global or better local minimum. We apply this method to a baseline PLCA-based model proposed in [Benetos and Dixon, 2012a]. The temperature parameter is applied to the posterior probability density of the instrument distribution with fixed templates.

3.2.1 The baseline PLCA model

Benetos and Dixon [2012a] propose a model that adds an instrument distribution variable to shift-invariant PLCA. The time-frequency representation of the input signal is computed with the Constant-Q Transform [Schörkhuber and Klapuri, 2010] using 120 bins per octave. Templates are trained for 10 instruments allowing shifts within a semitone range, in order to deal with arbitrary tuning

Table 3.1: Note ranges (in MIDI index) of instruments, adapted from Benetos and Dixon [2012b].

	instrument	lowest note	highest note
1	Bassoon	34	72
2	Cello	26	81
3	Clarinet	50	89
4	Flute	60	96
5	Guitar	40	76
6	Horn	41	77
7	Oboe	58	91
8	Piano	21	108
9	Tenor Sax	44	75
10	Violin	55	100

and frequency modulations. The model is formulated as:

$$P(\omega, t) = P(t) \sum_{p,s} P(\omega|s, p) *_{\omega} P(f|p, t) P(s|p, t) P(p|t) \quad (3.4)$$

where $P(\omega, t)$ is the approximated spectrogram, $P(t)$ is the energy distribution of the spectrogram. $P(\omega|s, p)$ are the templates of instrument s and pitch p , $P(f|p, t)$ selects the shifted variant for each p , $P(s|p, t)$ is the instrument contribution for each pitch, and $P(p|t)$ is the pitch probability distribution for each time frame. The templates $P(\omega|s, p)$ are trained using the MAPS dataset [Emiya et al., 2010] and RWC dataset [Goto et al., 2003], covering the instruments shown in Table 3.1.

The update rules are derived from the EM algorithm. For the E-step, the posterior probability density is:

$$P(p, f, s|\omega, t) = \frac{P(\omega - f|s, p) P(f|p, t) P(s|p, t) P(p|t)}{\sum_{p,f,s} P(\omega - f|s, p) P(f|p, t) P(s|p, t) P(p|t)} \quad (3.5)$$

For the M-step, each parameter is estimated.

$$P(f|p, t) = \frac{\sum_{\omega,s} P(p, f, s|\omega, t) V(\omega, t)}{\sum_{f,\omega,s} P(p, f, s|\omega, t) V(\omega, t)} \quad (3.6)$$

$$P(s|p, t) = \frac{(\sum_{\omega,f} P(p, f, s|\omega, t) V(\omega, t))^{\alpha_1}}{\sum_s (\sum_{\omega,f} P(p, f, s|\omega, t) V(\omega, t))^{\alpha_1}} \quad (3.7)$$

$$P(p|t) = \frac{(\sum_{\omega,f,s} P(p, f, s|\omega, t) V(\omega, t))^{\alpha_2}}{\sum_p (\sum_{\omega,f,s} P(p, f, s|\omega, t) V(\omega, t))^{\alpha_2}} \quad (3.8)$$

The templates $P(\omega|s, p)$ are not updated as they are previously trained and kept fixed. The parameters α_1 and α_2 used in Equation 3.7 and 3.8 are used to enforce sparsity, where $\alpha_1, \alpha_2 > 1$. We follow the original setting, $\alpha_1 = 1.3$ and $\alpha_2 = 1.1$, from Benetos and Dixon [2012a]. The final piano-roll matrix $P(p, t)$ and the pitches assigned to each instrument $P(p, t, s)$ are given by:

$$P(p, t) = P(p|t)P(t) \quad (3.9)$$

$$P(p, t, s) = P(s|p, t)P(p|t)P(t) \quad (3.10)$$

For post-processing, instead of using an HMM, the note events are extracted by performing thresholding on $P(p, t)$ and using minimum-length pruning (deleting notes shorter than $50ms$). The instrument-wise note events are detected in the same way using $P(p, t, s)$.

3.2.2 The DAEM-based model

Despite using fixed templates, there are still two free parameters, the instrument contribution and the pitch contribution, to estimate in the baseline method. They face the risk of converging to local minima. Here, we use the DAEM algorithm instead of the EM algorithm to derive update rules. In the E-step, the posterior probability density in Equation 3.5 is modified by introducing a temperature parameter τ :¹

$$P_\tau(p, f, s|\omega, t) = \frac{(P(\omega - f|s, p)P(f|p, t)P(s|p, t)P(p|t))^{1/\tau}}{\sum_{p, f, s} (P(\omega - f|s, p)P(f|p, t)P(s|p, t)P(p|t))^{1/\tau}} \quad (3.11)$$

And the update rules are extended by adding a τ -loop:

1. Set $\tau \leftarrow \tau_{max} (\tau_{max} > 1)$.
2. Iterate the following EM-steps until convergence:
 - E-step: calculate $P_\tau(p, f, s|\omega, t)$.
 - M-step: estimate $P(f|p, t)$, $P(s|p, t)$ and $P(p|t)$ by replacing $P(p, f, s|\omega, t)$ with $P_\tau(p, f, s|\omega, t)$ in Equation 3.6, 3.7 and 3.8, respectively.
3. Decrease τ .
4. If $\tau \geq 1$, repeat from step 2; otherwise stop.

The process starts from a high temperature ($\tau_{max} > 1$), then the temperature is reduced by gradually decreasing τ . At each value of τ , we apply the EM-steps until convergence. At higher temperatures, the distributions are smoothed

¹The parameter used in [Ueda and Nakano, 1998] is β , and the temperature is indicated by $1/\beta$. The reason for using τ here is because we want to indicate the temperature directly by τ and distinguish the proposed method from the β -divergence.

and general areas of the search space containing good solutions are found. As the temperature is gradually decreased, distinctions in the data are sharpened, resulting in a more fine-grained optimisation at each successive temperature.

Considering the properties of this particular model, we simplify the posterior probability density to:

$$P_\tau(p, f, s|\omega, t) = \frac{P(\omega - f|s, p)P(f|p, t)P(s|p, t)^{1/\tau}P(p|t)}{\sum_{p, f, s} P(\omega - f|s, p)P(f|p, t)P(s|p, t)^{1/\tau}P(p|t)} \quad (3.12)$$

The convolution of the templates and the pitch impulse distribution, giving the terms $P(\omega - f|s, p)P(f|p, t)$, works as the shift-invariant templates here. These are not modified by the temperature parameter, as the templates are fixed during the iterative process.² In addition, having observed that the instrument distribution $P(s|p, t)$ is dependent on the pitch distribution $P(p|t)$ in this model, we only modify one of them in the posterior probability density.

In the experiment, the parameter τ took the values $10/i$, $i \in \{8, 9, 10\}$. When τ finally decreases to 1, the update rules agree with the original ones.

3.3 Experiments

3.3.1 Datasets

We used the Bach10 Dataset [Duan et al., 2010] and the MIREX Multi-F0 Development Dataset (MIREX dataset) [MIREX, 2016] to test the performance of the proposed method. The Bach10 dataset consists of 10 quartet recordings performed on violin, clarinet, saxophone and bassoon. Ground truth for the Bach10 dataset was automatically generated for each individual instrument by YIN [de Cheveigné and Kawahara, 2002] with some manual corrections by Duan and Pardo. The MIREX dataset is an excerpt from a woodwind quintet recording, played on bassoon, clarinet, flute, horn and oboe. The ground truth for this dataset was manually created by Benetos and Grindlay.

3.3.2 Evaluation

The performance of the proposed system is evaluated in three subtasks: multiple F0 estimation, note tracking and instrument assignment. The corresponding metrics are referred to Section 2.4 for details. We compare the performance of the proposed method to that of the baseline PLCA model introduced in Section 3.1 (mentioned as BD(2012) below). We provide results for the three subtasks on the two different datasets in the following section.

²This was also confirmed by test experiments where the power $1/\tau$ was also applied to the pitch impulse distribution $P(f|p, t)$, giving similar transcription results to Equation 3.12.

Table 3.2: Multiple F0 estimation results (see Section 2.4 for explanation of symbols).

Dataset	Methods	P	R	F	Acc	E_{tot}	E_{subs}	E_{miss}	E_{fa}
Bach10	BD(2012)	0.784	0.791	0.787	0.650	0.311	0.116	0.093	0.102
	Proposed	0.819	0.796	0.807	0.677	0.282	0.098	0.106	0.078
MIREX	BD(2012)	0.748	0.537	0.625	0.455	0.486	0.158	0.305	0.023
	Proposed	0.769	0.561	0.649	0.480	0.461	0.146	0.292	0.023
Both	BD(2012)	0.781	0.768	0.772	0.632	0.327	0.120	0.112	0.094
	Proposed	0.814	0.775	0.793	0.659	0.299	0.102	0.123	0.074

The proposed system was also submitted to the task of multiple fundamental frequency estimation and tracking in MIREX 2013.³ Readers are referred to Table 2.4 for results and comparison to other submissions.

3.3.3 Results

Multiple F0 estimation

The results for multiple F0 estimation using the Bach10 and MIREX datasets are shown in Table 3.2. It can be seen that the proposed method outperforms the BD(2012) method in terms of accuracy (Acc) on both individual datasets by at least 2.5 percentage points, leading to an overall accuracy of 0.659 (up 2.7 percentage points). The total error decreases by 2.8 percentage points. On the Bach10 dataset improvements are mainly due to a reduced false alarm rate (E_{fa}), which decreases from 10.2% to 7.8%. This is also reflected by increased precision (P) and stable recall (R). The improvement for the MIREX dataset mainly comes from reduction in both substitution error (E_{subs}) and missed detection error (E_{miss}) rates, leading to higher precision and recall.

In order to determine if the increase in accuracy (Acc) is significant we ran a Friedman test for this subtask. The resulting p -value of $0.0009 < 0.01$ indicates that the difference is highly significant. The distribution of Acc of the ten files in the Bach10 dataset is shown in Figure 3.1a.

Note tracking

For the note tracking subtask, we found that the F-measure was improved by almost 5 percentage points for onset-only evaluation and around 4 percentage points for onset-offset evaluation for both datasets, as shown in Table 3.3. We ran a Friedman test with regard to the F-measures (F_{on} and F_{off}) for this

³http://www.music-ir.org/mirex/wiki/2013:Multiple_Fundamental_Frequency_Estimation_%26_Tracking_Results.

Table 3.3: Note-tracking results

(a) onset-only accuracy

Dataset	Methods	P_{on}	R_{on}	F_{on}	Acc_{on}
Bach10	BD(2012)	0.319	0.339	0.328	0.197
	Proposed	0.399	0.354	0.374	0.231
MIREX	BD(2012)	0.628	0.420	0.503	0.336
	Proposed	0.690	0.459	0.551	0.380
Both	BD(2012)	0.347	0.346	0.344	0.209
	Proposed	0.427	0.364	0.391	0.245

(b) onset and offset

Dataset	Methods	P_{off}	R_{off}	F_{off}	Acc_{off}
Bach10	BD(2012)	0.217	0.230	0.223	0.126
	Proposed	0.281	0.249	0.263	0.152
MIREX	BD(2012)	0.487	0.326	0.391	0.243
	Proposed	0.537	0.357	0.429	0.273
Both	BD(2012)	0.242	0.239	0.238	0.137
	Proposed	0.305	0.259	0.279	0.163

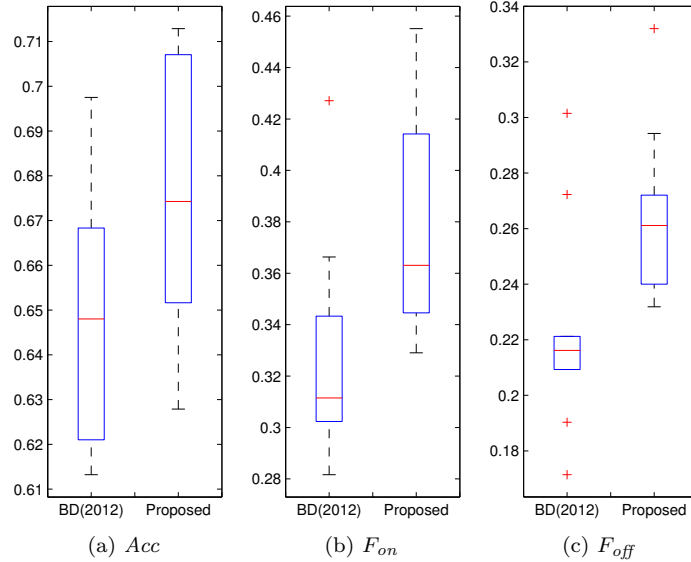


Figure 3.1: Box-and-whisker plots of (a) accuracy; (b) onset-only F-measure; and (c) onset-offset F-measure; for the Bach10 dataset.

subtask. For both onset-only and onset-offset metrics, the p -values are less than 0.01, showing that—here, too—the differences are significant. The distributions of F_{on} and F_{off} for the Bach10 dataset are shown in Figures 3.1b and 3.1c.

The note tracking evaluation shows that both methods under consideration perform better on the MIREX dataset, whereas according to the frame-based evaluation they perform better on the Bach10 dataset. This result has the same trend as the results from other methods on the same data,⁴ and is likely to stem from the unusual co-occurrence of trills and legato notes that dominates the MIREX piece.

Instrument assignment

The results for instrument assignment for the two datasets are shown in Table 3.4. In this subtask, we cannot identify a systematic advantage of either method, with the F-measure means over all instruments being very close (20.7% and 20.9% on the Bach10 dataset, and 35.1% and 34.3% on the MIREX dataset). Slight differences between the methods for particular instruments do not show a consistent advantage of one method either; we will therefore focus on the proposed method in the rest of the discussion. The most obvious differences in F-measure occur between instruments. For example, the results for the Bach10 dataset show that instrument assignment works better for the clarinet and bassoon than for the violin and saxophone. Also, since the note templates include instruments not present in the pieces, false positives occur for these instruments, with the largest ratio of false positives occurring for horn (18.6%) and piano (16.4%). The problem instrument in the MIREX dataset is the oboe, to which few notes are assigned, leading to a low F-measure of around 12-13%. Notes are detected in three instruments that do not feature in the music, with the largest ratio of false positives found in the piano (47.9%) and guitar (34.5%). No false positives were detected for saxophone or violin.

The discrepancy between the multiple F0 estimation results and the comparatively low results for instrument assignment is due to the fact that often the correct pitch is detected, but assigned to a wrong instrument or combination of instruments. That is, note templates from different instruments are combined to approximate the observed spectra. The proposed method provides a better reconstruction of the observed data using combinations of templates at the correct pitches, resulting in better performance for frame level and note tracking tasks.

⁴as published on the MIREX website [MIREX, 2016].

Table 3.4: Instrument assignment results

(a) Bach10					
F-measure	Violin	Clarinet	Saxophone	Bassoon	Mean
BD(2012)	0.175	0.313	0.092	0.246	0.207
Proposed	0.190	0.275	0.127	0.243	0.209

(b) MIREX						
F-measure	Bassoon	Clarinet	Flute	Horn	Oboe	Mean
BD(2012)	0.292	0.444	0.485	0.409	0.125	0.351
Proposed	0.294	0.420	0.489	0.385	0.129	0.343

3.4 Conclusions and discussions

We examine the utility of an optimisation method in a PLCA-based AMT system. The optimisation method, deterministic annealing EM, is based on the EM algorithm and aims to tackle the local minimum problem. The key idea is to decrease the ‘temperature’ gradually, which means to increase the sparse exponent gradually in the AMT system. The transcription experiments show that the proposed method outperforms the baseline method on tasks of multi-pitch estimation (accuracy increases by 2.7 percentage points) and note tracking (F-measure increases by 4 percentage points). Although results on an additional instrument assignment task show no significant difference between the methods, they reveal that both methods use mixtures of instrument templates to approximate observed spectra in the test data. In this work we have used DAEM with only one configuration of three temperature steps set by considering the strategy in [Ueda and Nakano, 1998] and the result of a small preliminary test. In the future, we would like to explore different configurations to see whether we can further improve the transcription results.

In a preliminary experiment, we update both the spectral bases and gain functions of the basic PLCA model in Equation 3.1 based on DAEM. The cost function is smaller than that obtained using the EM algorithm, but the transcription results are not always better, because it becomes difficult to associate the updated spectral bases to pitches in this case. In comparison to the results in Section 3.3, we find that the previously-trained templates are important and work as a good initialisation for the spectral bases. The risk of updating the templates during the iteration is that an updated template might no longer accord with its labels (pitch, instrument). Due to the different ways a note can be played and differences in sound transmission, templates will never match observations precisely. Spectral decomposition algorithms compensate for this

mismatch by finding mixtures of templates which provide a better approximation of the data (see Section 3.3.3). In order to capture the variations of instrument sounds, we would like to refer to information from musical acoustics and physics. In Chapter 4, we will focus on piano tones to explore the decay patterns in detail.

The use of the temperature parameter τ that is central to the DAEM algorithm in Equation 3.11 is similar to the use of the sparsity parameters in Equation 3.7 and Equation 3.8. In fact, the sparsity method used here is related to the tempered EM algorithm [Grindlay and Ellis, 2012]. Both the DAEM and sparsity equations ‘put an exponent on a distribution’. When the exponent is larger than one, the distribution becomes sharper and sparser; when the exponent is smaller than one, the distribution is smoothed, as in the case of high-temperature stages of DAEM.

The PLCA model is a probabilistic variant of NMF, which is used in a probabilistic framework. In the remainder of this thesis, we develop our own transcription approach based on NMF, in consideration of the way that note energy decays over time. The optimisation method can also be adapted to NMF. In Chapter 5, we will use this exponential form for a sparsity constraint in an NMF-based transcription system. The decreasing temperature is indicated by the increasing exponent. The ‘annealing’ will be applied using a continuously increasing exponent, which will reach the desired value at the end of iteration.

Chapter 4

Modelling the Decay of Piano Tones

In this chapter, we compare the temporal decay of individual piano partials in real-world recordings to the theoretical decay patterns based on piano acoustics revised in Section 2.1.2. We mainly focus on the decay behaviour associated with coupled piano strings [Weinreich, 1977]. The acoustics of piano decay is well understood and has been applied for synthesising piano sounds. For instance, the digital waveguide is used in synthetic models to generate a set of quasi-harmonic exponentially decaying sinusoids produced by a single string [Smith, 1992]. A piano note with multiple strings is modelled using coupled digital waveguides [Aramaki et al., 2001, Bensa et al., 2003], or using one digital waveguide with resonators for partials of beats and double decay [Bank, 2000, 2001, Lee et al., 2010]. Recently, incorporating the decay information for piano music analysis has also gained increasing attention. A non-negative source-filter-decay model is proposed to analyse music sounds by assuming a frequency-dependent decaying (decay response) [Klapuri, 2007]. The decay envelopes of piano tones or partials are modelled for automatic music transcription with promising results [Chen et al., 2012, Berg-Kirkpatrick et al., 2014, Cogliati and Duan, 2015].

For estimating decay parameters, Välimäki et al. [1996] first propose to estimate the decay rates of harmonics by linear regression on a logarithmic magnitude scale. Karjalainen et al. [2002] present both linear and non-linear regressions to estimate the decay of piano partials with noise, but the experiments only include some examples of synthetic notes and no conclusion is drawn on the general decay characteristics of piano notes. Here, we track the decay of real piano tones from the RWC Music Database [Goto et al., 2003] in detail (first 30

partials below the Nyquist frequency¹ of 88 notes played in 3 dynamics). We analyse fitness between theoretical models and real world data, and the influence of the frequency range, pitch range and dynamic on decay patterns. The goal of this work is to understand piano decay in real recordings and to gain insights into how piano transcription systems can make use of decay information.

The methods for finding and modelling decays of partials are introduced in Section 4.1. The experimental setup and results are described in Sections 4.2 and 4.3, respectively. Section 4.4 concludes this chapter.

4.1 Method

In order to track the decay of piano notes, we first find the frequencies of partials for each note, taking inharmonicity into account. Then, the decay of the partials is fitted to three typical patterns: linear decay, double decay (modelling the two directions of polarization, vertical and horizontal) and curves (modelling beats due to mistuning). We track partials below the Nyquist frequency, but only the first 30 partials for a note if there are more than 30 partials.

4.1.1 Finding partials

Because of string stiffness, partials of piano notes occur at higher frequencies than the harmonics (integer multiples of the fundamental frequency), which is known as inharmonicity. The partial frequencies are given by [Fletcher et al., 1962]:

$$f_n = nf_0\sqrt{1 + Bn^2}, \quad (4.1)$$

where f_n is the n^{th} partial of the note with fundamental frequency f_0 and B is the inharmonicity coefficient which varies from note to note. Moreover, during the course of a sounded note partial frequencies can diverge from their ideal inharmonic frequencies due to the coupling between bridge and soundboard.

To get the frequencies of partials, we estimate B and f_0 in a non-negative matrix factorisation framework proposed by Rigaud et al. [2013a]. The model represents each partial of a piano tone using the main lobe magnitude spectrum of a Hanning window. In each iteration, the central frequency of each partial is updated to fit the observed spectrum. An inharmonicity constraint is added to the cost function by means of a sum of the mean square error between the estimated partial frequencies and those given by the inharmonicity relation in Equation 4.1. Then the inharmonicity coefficient B is also updated by taking all updated partial frequencies into account. We provide an implementation of

¹The Nyquist frequency is half of the sample rate f_s .

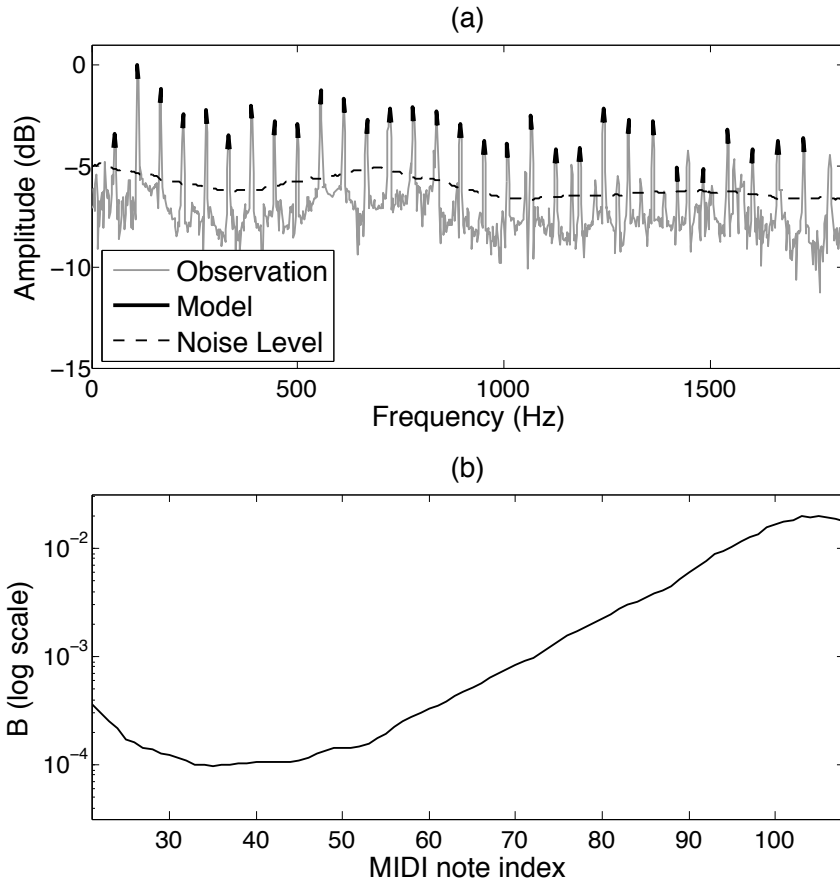


Figure 4.1: (a) Partial frequencies of note A1 (55 Hz), (b) Inharmonicity coefficient B along the whole compass estimated for the piano of the RWC dataset.

this method for download.² When detecting frequencies of partials, errors are likely to arise at partials below the noise level, and even when the frequencies of these partials are detected correctly, they tend to behave noisily. So only partials above the noise level are tracked.

Figure 4.1(a) shows the detected frequencies of the first 30 partials of the note A1 (55 Hz). The estimated inharmonicity coefficient along the piano compass (all 88 piano notes) is given in Figure 4.1(b).

4.1.2 Tracking the decay of partials

The vibrations of the strings are influenced by many factors, which results in a variety of decay patterns of piano notes. We fit the decay of partials with the following three models: linear decay, multi-phase linear decay, and non-linear

²<https://code.soundsoftware.ac.uk/projects/inharmonicityestimation>

curve decay based on the theoretical analysis of coupled oscillation of two piano strings [Weinreich, 1977]. Partial decay of notes with three strings is also fitted by these three models.

Linear decay is suitable for partials of single string notes, notes with well-tuned strings and also notes with large mistunings, with examples shown in Figure 4.2. Multi-phase linear decay is mainly used for double decay caused by transmission direction changes and mistuned strings. It can also be applied for partials with fast decay. In this case, the partial decays to the noise level quickly, and the noisy part is detected as a second line, as shown in Figure 4.3. Partial of notes with mistuned strings exhibit a decay with beats, and is fitted by the non-linear curvy decay. Some high partials of single-string notes also exhibit a decaying periodic curve because of false beating. Readers are referred to Section 2.1.2 for related information on piano decay.

Time-frequency representation

A piano tone starts with a percussive sound with a sharp increase of energy generated by the impact of the hammer on the string(s). In order to discard the attack onset, we use a sound clip beginning at the frame with largest energy for each note. In the RWC dataset [Goto et al., 2003], each piano note lasts about 2 seconds. The length of the clip is set to 2 s, while if the clip is shorter than 2 s the length is restricted to its duration. The sampling rate is $f_s = 44100$ Hz. Frames are segmented by a 4096-sample Hamming window with a hop-size of 441. A discrete Fourier Transform is performed on each frame with 2-fold zero-padding. The power spectrogram is represented on the log scale:

$$S_{dB} = 20 \log_{10}(S), \quad (4.2)$$

where S is the magnitude spectrogram.

The energy of each partial is found according to the frequencies detected in Section 4.1.1. Then the decays are fitted by the following models. The decay rate is measured by the power change per second (dB/s).

Linear regression

In most situations, the decay of partials follows a linear function of time, which is modelled by

$$y(t) = at + b, \quad (4.3)$$

where y is the linear function along time t , a is the decay rate and b is the initial power. The regression parameters are estimated using ordinary least squares.

Figure 4.2 shows three kinds of decay which can be fitted in the linear model:

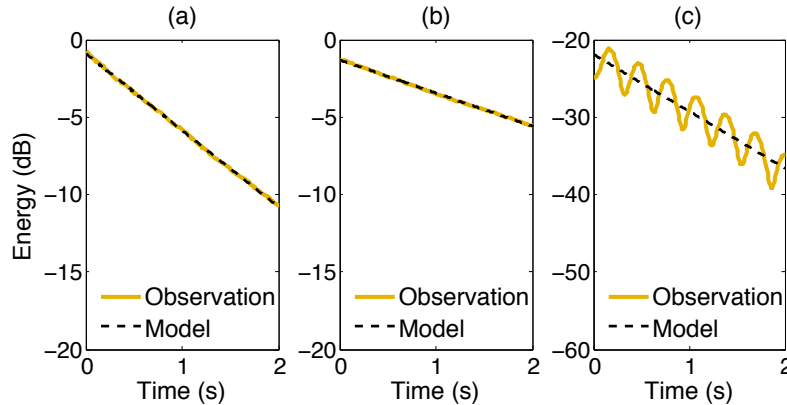


Figure 4.2: Linear fitting for: (a) the 3rd partial of note D1 ($f_0 = 36.7$ Hz); (b) the 2nd partial of note Ab1 ($f_0 = 51.9$ Hz); (c) the 30th partial of note Db2 ($f_0 = 69.3$ Hz).

(a) is a partial of a single-string note; (b) is a partial of a note with well-tuned strings; and (c) is a partial of a note with large mistuning between strings. When the mistuning is large, there is more than one beat in the decay, but the overall decay rate can be detected correctly using the linear model.

Multi-phase linear regression

A multi-phase linear model is employed to model double decay as well as fast decay with noise. Despite the misleading name this is a non-linear regression problem. The decay is modelled by two straight lines, formulated as follows:

$$y(t) = \begin{cases} a_1t + b_1 & : t_s < t < t_{dp} \\ a_2t + b_2 & : t_{dp} < t < t_e \end{cases} \quad (4.4)$$

where y is the estimated function; a_1 , a_2 and b_1 , b_2 are the decay rates and the initial energies of the two lines, respectively; t_{dp} is the demarcation point of the two lines; and t_s and t_e are the starting time and the ending time, respectively. Parameters are estimated using an existing method.³ The method first finds all possible t_{dp} values,

Figure 4.3(a) shows the fit for a partial with two parts, decay and noise. This partial decays quickly, having a low initial amplitude due to the hammer impulse position being near a node of the partial's vibration mode, and the late portion is noise which should be discarded. Fitting this decay with the multi-phase model helps to automatically detect the ending time of the partial decay and discard the noisy part. Figures 4.3(b) and (c) indicate two kinds of double

³<http://research.gansee.org/datasci/mplr/>

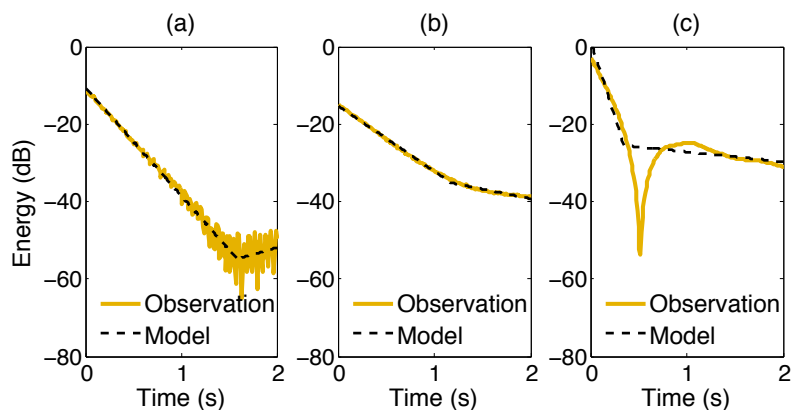


Figure 4.3: Multi-phase linear fitting for: (a) the 7th partial of note Bb0 ($f_0 = 29.1$ Hz); (b) the 4th partial of note Bb2 ($f_0 = 116.5$ Hz); (c) the 1st partial of note E5 ($f_0 = 659.3$ Hz).

decay. The rate change in (b) is caused by the transmission direction switching from vertical to horizontal, while the reason for the double decay in (c) is a small frequency difference between the strings.

For double decay, the slope of the line which covers the larger part of the time duration is recorded as the decay rate, i.e. the first part in Figure 4.3(b) and the second part in Figure 4.3(c). We assume that the decay lasts longer than noise in the situation of fast decay with noise, so the larger part strategy also works in this case, i.e. the first decay rate in Figure 4.3(a).

Non-linear curve fitting

When there are small frequency differences between the strings of a note, partials decay with amplitude modulation as the vibrations of the different strings move in and out of phase with each other. We use a non-linear curve fitting model to fit these decays with beats. The objective function of the curve fitting is more complex than the first two situations. Based on the theory of coupled strings [Weinreich, 1977], the formula is simplified as follows:

$$y(t) = at + b + A \log_{10}(|\cos(ft + \varphi)| + \varepsilon). \quad (4.5)$$

The derivation from the physical model [Weinreich, 1977] to the proposed model is included in Appendix A. This function describes the coupled motion of two strings. There are two parts: the decay part is still modelled by a linear function, $at + b$, and the remaining term models the amplitude modulation, where A and f are the amplitude and frequency of the curve, respectively. φ is the initial phase of the curve, and $\varepsilon = 0.01$ is added to avoid taking the log of 0.

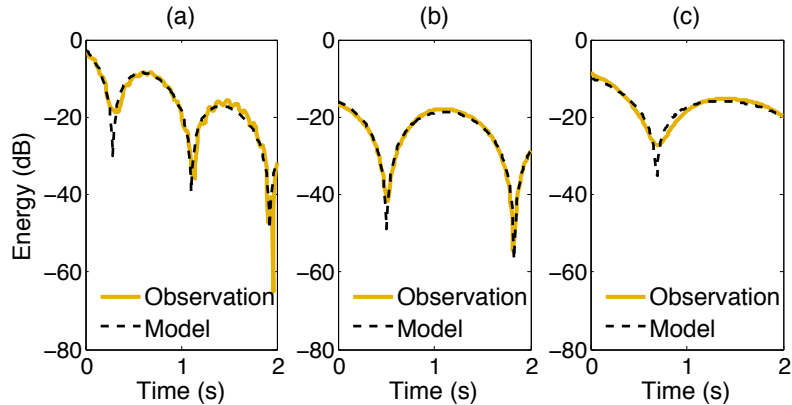


Figure 4.4: Non-linear curve fitting for: (a) the 22nd partial of note Db1 ($f_0 = 34.6$ Hz); (b) the 10th partial of note G1 ($f_0 = 49$ Hz); and (c) the 10th partial of note A1 ($f_0 = 55$ Hz).

Figure 4.4 gives three examples of decay with beats: (a) false beats of a high partial of a single string note; (b) and (c) show beats with different frequencies, which are caused by mistuning of the strings of each note.

The parameters are estimated using a non-linear least squares algorithm [Fox and Weisberg, 2010]. This method requires a good initialisation and ranges for parameters to get a reasonable result. The linear part (a, b) is initialised using the result of the linear model. The amplitude A is initialised to 40 which is the amplitude of purely resistive coupling in dB, as shown in Appendix A. The period ($1/f$) consists of two lobes because of taking the absolute value in Equation 4.5. If there is more than one trough found in the decay, as shown in Figure 4.4(a) and (b), we initialise the curve period to be double the time gap between two adjacent troughs. If only one trough is detected (Figure 4.4(c)), we assume the position of the trough from the onset to be one quarter of the period. The initial phase φ is usually initialised to 0, while sometimes manually adjusted to a value between 0 and π according to the observation.

The coupling between 3 strings is far more complex than for 2 strings. It is out of the scope of this chapter to explore the details of the motion of 3 strings, which we approximate using the models described above. It turns out that the approximation is very close to our observations, as shown in the results of Section 4.3.

4.2 Experiment

In this section, we introduce the dataset, metric for evaluation and the steps of decay modelling.

4.2.1 Dataset

We use the piano sounds from the RWC Musical Instrument Sound Database [Goto et al., 2003]. The notes are played at three dynamics: loud (forte, f), moderate (mezzo, m) and soft (piano, p). Each set consists of 88 isolated notes, covering the whole compass of the piano.

4.2.2 Metric

The coefficient of determination (R-squared) is used for evaluating the fit between the data and model. It is defined as follows:

$$R^2 = 1 - \frac{SS_{res}}{SS_{tot}} = 1 - \frac{\sum_{t=1}^T (o_t - y_t)^2}{\sum_{t=1}^T (o_t - \bar{o})^2}, \quad (4.6)$$

where o_t is the observation of time frame t , y_t is the modelled function and $\bar{o} = \frac{1}{T} \sum_{t=1}^T o_t$ is the mean of the observations. SS_{tot} is the total sum of squares, which is proportional to the variance of the observed data, and SS_{res} is the residual sum of squares, explaining the difference between the observations and the modelled values. The larger R-squared is, the better the data is explained by the model.

4.2.3 Modelling the decay

For each detected partial, we fit it to our models according to the process shown in Figure 4.5. The process is referred to as the mixed model, in which the R^2 of the three models is computed one by one. We first compute the R^2 s of the linear model and the multi-phase linear model. If the larger R^2 of these two models is over 0.9, we assume the decay is fitted well and no curve fitting is needed. Otherwise, we continue to compute the R^2 of the non-linear curve model. We find the largest R^2 of the three models as the R^2 of the mixed model.

4.3 Results

We illustrate the results of decay tracking in this section. Then the estimated decay rates are used to parameterise the decay response and to explore the influence of dynamics.

4.3.1 R-squared

We compare the average coefficient of determination, R^2 , between the linear model and the combination of all three models (referred to as the mixed model

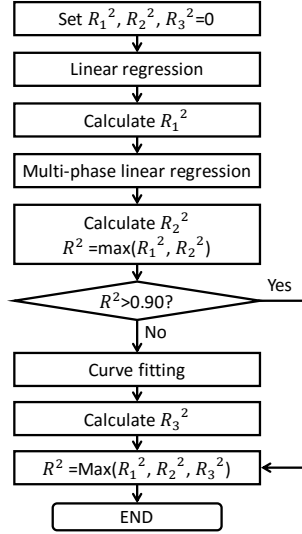


Figure 4.5: Flowchart of partial decay modelling.

Table 4.1: Average R^2 of the linear and mixed models. NP is the number of partials above the noise level for each dynamic level.

Dynamics	NP	linear model	mixed model
<i>f</i>	1572	0.721	0.867
<i>m</i>	1501	0.699	0.853
<i>p</i>	1187	0.644	0.824

as in Figure 4.5). The results are presented in Table 4.1, which indicate that the mixed model has a better fit to the data by around 15 percentage points. We also note that the performance is influenced by dynamics. If the note starts at a lower energy, it will decay to the noise level more quickly, resulting in fewer data available for modelling, not only fewer partials above the noise level, but also shorter duration of notes. This reduction in data makes parameter estimation more difficult, resulting in worse performance for lower dynamics. Although longer notes would help us to observe the decay pattern, we did not look beyond 2s, which is already longer than the duration of most notes in normal music performance. It remains to be investigated how well our model performs on shorter notes.

In order to provide a more detailed investigation of the results for different notes, we divide the notes into 8 groups, with every adjacent 11 notes in a group. The average R^2 of each group is shown in Figure 4.6. We find that the mixed

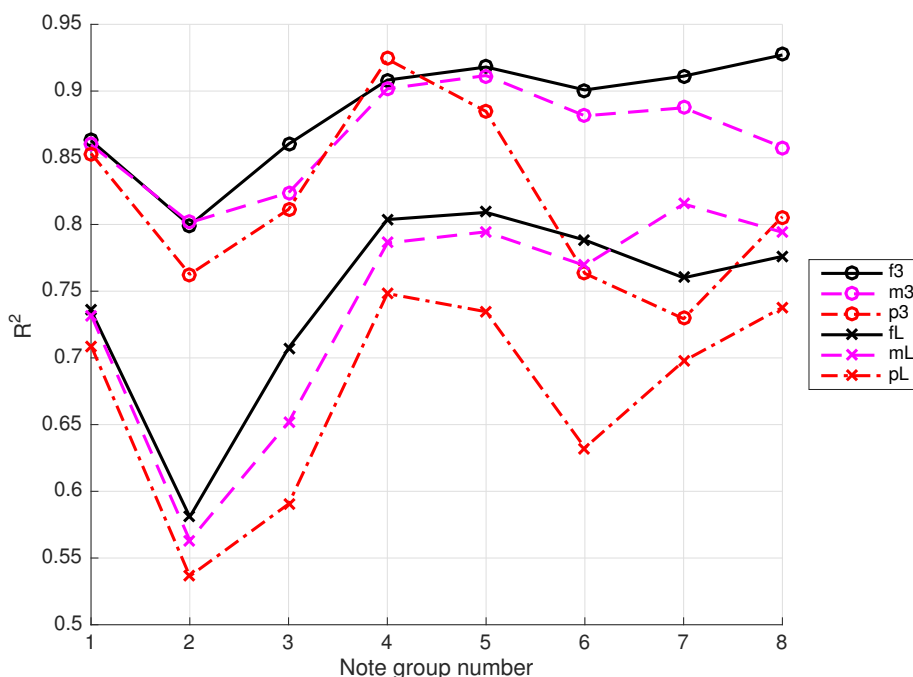


Figure 4.6: Average R^2 of different note groups. f , m , p stand for dynamics, while L and 3 indicate the linear and mixed models, respectively. The order of labels in the legend corresponds to the order of lines from top to bottom.

model improves the performance of all note groups, with the biggest improvement of around 0.2 occurring at Group 2 for all dynamics, corresponding to the observation of clear beats in the decay of these notes. For most pianos, notes in Group 1 have a single string per note, notes in Group 2 and the lower half of Group 3 have two strings per note and the rest have 3 strings. Beats appear extensively in notes from Groups 2 and 3, hence the linear model performs poorly on these notes and the largest improvements are attained by the mixed model. Although we don't explicitly model the details of motion in notes with three strings, the results show that the decays of these notes are approximated quite well by the mixed model.

4.3.2 Decay response

Figure 4.7 shows the decay rates of all partials along the whole compass of the piano for notes played forte. The figure illustrates the well-known fact that high frequency partials decay faster. The spread of observed decay rates is large, and increases with frequency. Note that some frequencies in the low range, around 80 Hz (MIDI index 41) and 150 Hz (MIDI index 50), exhibit particularly fast decay rates. As partials from different notes may have the same frequency,

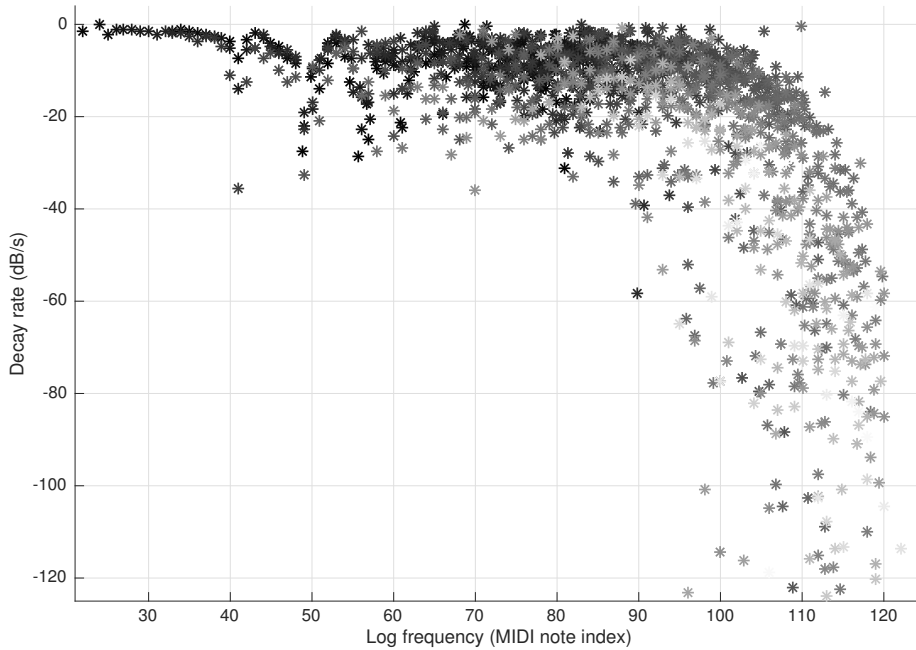


Figure 4.7: Decay response: decay rates against frequency. Lower values mean faster decay. The greyscale is used to indicate fundamental frequency, with darker colours corresponding to lower pitches.

different decay rates of these partials could be used as a clue to decide which note the partial belongs to. However, in musical performances, overlapped partials increase the difficulty of tracking partial decay, which is a topic needing further investigation.

4.3.3 Decay of different dynamics

Figure 4.8 shows the decay rates of the first five partials of notes played at different dynamics. We observe that dynamics have no significant absolute effect on the decay rate. In the low pitch range, the decay rates of different dynamics are almost identical, while in the high pitch range this is less clear, partly due to higher measurement error because of fewer data for modelling.

4.4 Conclusions

We model the decay of piano notes based on piano acoustics theory. Two non-linear models (a multi-phase linear model and a non-linear curve fitting model) are used to fit double decay and beats of piano tone partials, respectively. The results show that the use of non-linear models provides a better fit to the data, especially for notes in the low register. The decay response of the piano shows

that decay increases with frequency. The results also indicate that dynamics have no significant effect on the decay rate.

Based on the observation that linear regression fits data with $R^2 \approx 70\%$ and works well for notes in the middle and high pitch ranges, we assume an exponential decay in the next chapter for piano transcription. According to analysis on decay response and dynamic influence, notes of different pitches will be modelled with different decay rates, while notes of the same pitch played by different dynamics share the same decay rate.

In [Cheng et al., 2015a], we track the decay after 200 ms of the onsets. We think that 200 ms is too long for high-pitch notes, because they decay quickly. In this chapter, we use the sound clip starting from the frame with the largest energy for each note. We apply the model twice on slightly different data, and get similar results and conclusions. We believe that the proposed model is reproducible by following the method described in Section 4.1. For future work, to extend the model to other instruments, such as guitar, harpsichord and harp, would also be a good topic to explore.

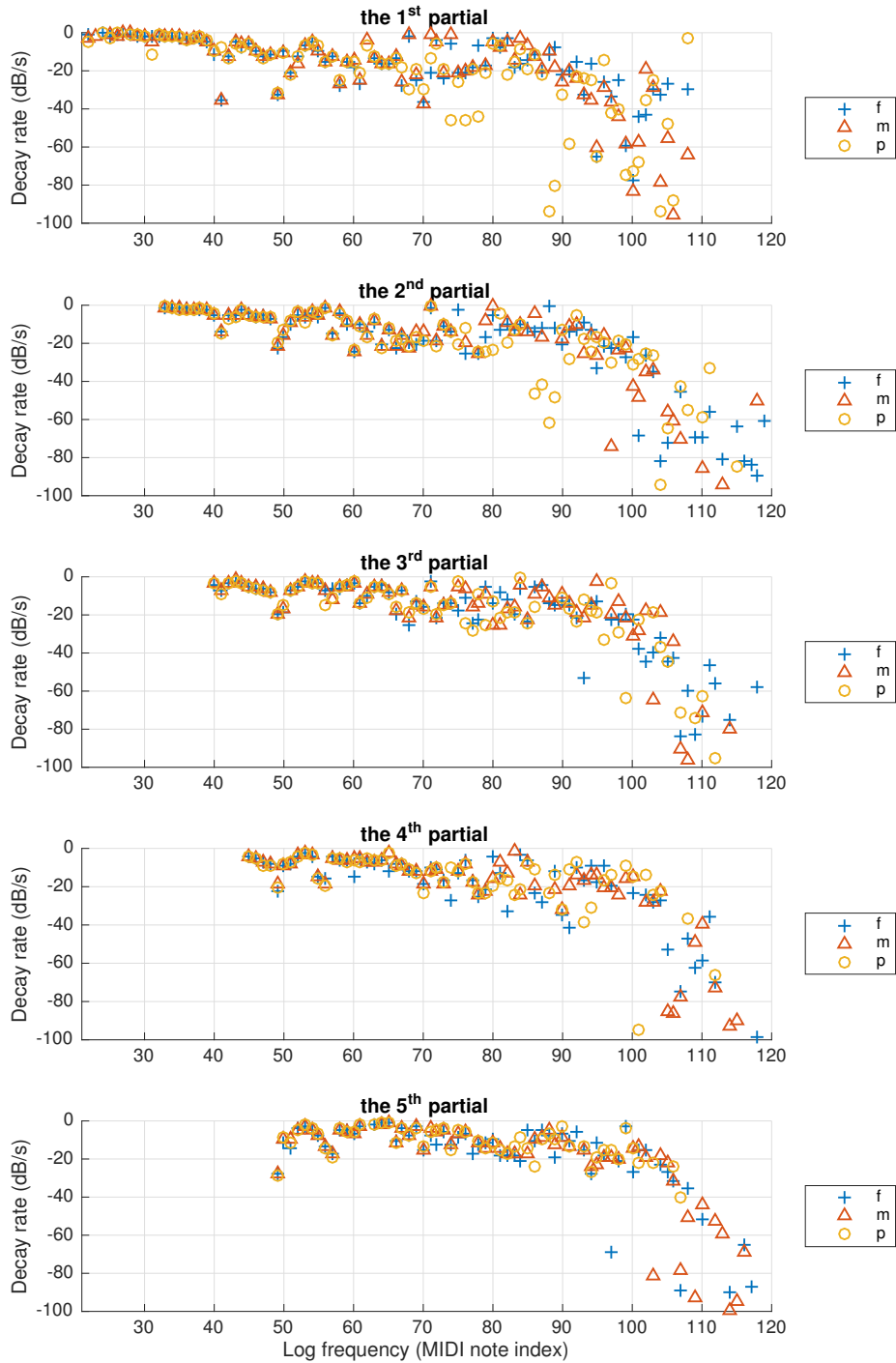


Figure 4.8: Decay rates for the first five partials for different dynamics

Chapter 5

An Attack/Decay Model for Piano Transcription

In this chapter, we demonstrate that piano transcription performance for a known piano can be improved by explicitly modelling piano acoustical features. The proposed method is based on non-negative matrix factorisation, with the following three refinements: (1) introduction of attack and harmonic decay components; (2) use of a spike-shaped note activation that is shared by these components; (3) modelling the harmonic decay with an exponential function. Transcription is performed in a supervised way, with the training and test datasets produced by the same piano.

Several features associated with piano acoustics, such as inharmonicity, time-varying timbre and decaying energy, are examined for their utilities for transcription. Rigaud et al. [2013b] show that an explicit inharmonicity model leads to improvement in piano transcription, while a note-dependent inharmonicity parameter is needed for initialisation. Modelling time-varying timbre not only provides a better reconstruction of the spectrogram, but also improves note tracking results by imposing constraints between note stages (attack, sustain and decay) [Benetos et al., 2013a, Cheng et al., 2015b]. For decaying energy, Chen et al. [2012]’s preliminary work uses an exponential model for energy evolution of notes. Berg-Kirkpatrick et al. [2014] represent the energy evolution of a piano note by a trained envelope. Ewert et al. [2015] represent both time-varying timbre and temporal evolution of piano notes by time-frequency patches. Temporal evolution modelling allows a note event to be represented by a single amplitude parameter for its whole duration, enabling the development of note-level systems with promising transcription results [Chen et al., 2012, Berg-Kirkpatrick et al., 2014, Ewert et al., 2015]. In addition, Cogliati and Duan

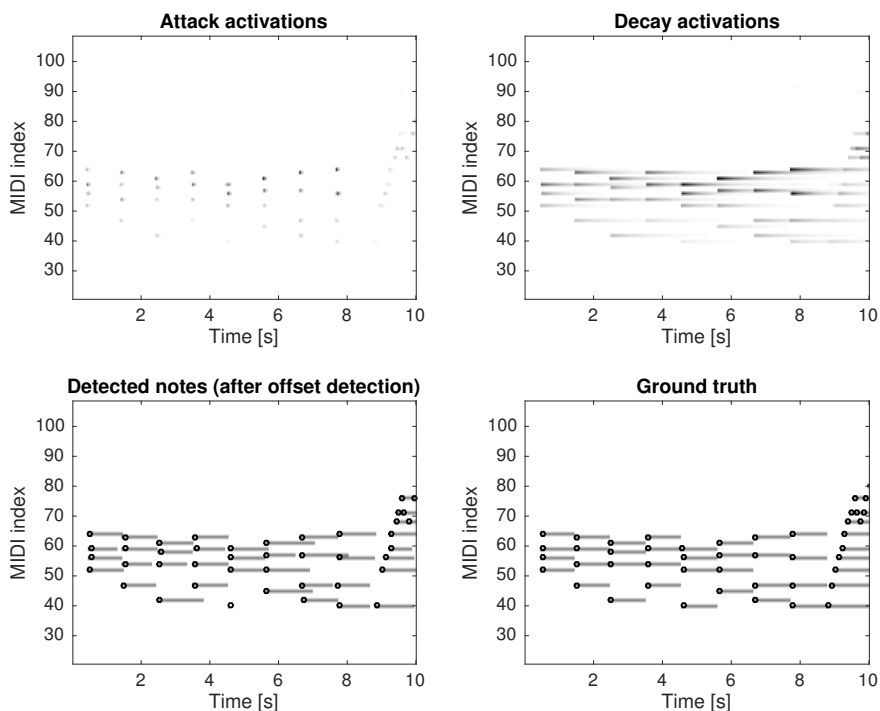


Figure 5.1: An example of output from the proposed model.

[2015] propose a note level system informed by detected onsets, which also approximates decays of piano partials with a sum of two decaying exponentials. Details of note-level systems can be found in Section 2.2.6.

The proposed method is also motivated by piano acoustics. Based on our previous studies on piano decay in Chapter 4, we know that exponential decay explains the major energy evolution for each partial in spite of various decay patterns. Here, we further simplify the decay stage using an exponential decay function and a harmonic template per pitch. We separately represent the attack stage for the percussive onset of piano sounds, as analysed in Section 2.1.2. These two stages are coupled by shared note activations. A supervised NMF framework is used to estimate note activations, and hence activations of the attack and decay stages (see Figure 5.1). The proposed model is a note-level method, which can be understood as a deconvolution method with a patch parameterised by two sets of templates and activations. Experiments show that the proposed method significantly improves supervised piano transcription, and compares favourably to other state-of-the-art techniques.

We explain the proposed model in Section 5.1. In the experiments (Section 5.2), we not only investigate the performance of the proposed model in piano transcription, but also estimate and analyse decay rates of notes with

different dynamics. Conclusions are drawn in Section 5.3.

5.1 Method

The method is composed of three main steps. We first introduce the attack and decay model for piano sounds. Parameters are estimated using a sparse NMF. The second step is to detect onsets from the attack activations by peak-picking. In the third step, offsets are detected for each pitch individually. Below we explain each step in turn.

5.1.1 A model of attack and decay

A piano sound is produced by a hammer hitting the string(s) of a key [Weinreich, 1977]. It starts with a large energy, then decays till the end of the note. At the attack stage, the strike of the hammer produces a percussive sound. It evolves quickly to an almost harmonic pitched sound, and then immediately enters the decay stage. We define a generative model for these two phases individually, in which the attack sound is generated by:

$$V_{ft}^a = \sum_{k=1}^K W_{fk}^a H_{kt}^a, \quad (5.1)$$

where \mathbf{V}^a is the reconstructed spectrogram of the attack phase, as shown in Figure 5.2(d), and \mathbf{W}^a is the percussive template (Figure 5.2(e)). $f \in [1, F]$ is the frequency bin, $t \in [1, T]$ indicates the time frame, and $k \in [1, K]$ is the pitch index. The attack activations \mathbf{H}^a (Figure 5.2(c)) are formulated by a convolution:

$$H_{kt}^a = \sum_{\tau=t-T_a}^{t+T_a} H_{k\tau} P(t-\tau), \quad (5.2)$$

where \mathbf{H} are spike-shaped note activations, shown in Figure 5.2(b), and \mathbf{P} is the amplitude attack envelope, with the typical shape shown in Figure 5.5. The range of the attack envelope is determined by the overlap for computing the spectrogram, with T_a equal to the overlap ratio (the ratio of the window size and frame hop size).

For the decay part we assume that piano notes decay approximately exponentially based on studies in Chapter 4. The harmonic decay is generated by

$$V_{ft}^d = \sum_{k=1}^K W_{fk}^d H_{kt}^d, \quad (5.3)$$

where \mathbf{V}^d is the reconstructed spectrogram of the decay phase (Figure 5.2(g)),

Table 5.1: Variable list

Descriptions	Variables
Spectrogram	\mathbf{X}
Reconstruction	\mathbf{V}
Note activations	\mathbf{H}
Attack activations	\mathbf{H}^a
Decay activations	\mathbf{H}^d
Percussive templates	\mathbf{W}^a
Harmonic templates	\mathbf{W}^d
Attack envelope	\mathbf{P}
Decay factor	α
Frequency index	$f \in [1, F]$
Time index	$t \in [1, T]$
Pitch index	$k \in [1, K]$

and \mathbf{W}^d is the harmonic template (Figure 5.2(h)). Decay activations \mathbf{H}^d in Figure 5.2(f) are generated by convolving note activations with an exponentially decaying function:

$$H_{kt}^d = \sum_{\tau=1}^t H_{k\tau} e^{-(t-\tau)\alpha_k}, \quad (5.4)$$

where α_k are decay factors, and e^{α_k} indicates the decay rate per frame for pitch k . In the NMF model, it is assumed that the energy of a note decays forever. Offsets are detected later based on the reconstructions. Then the complete model is formulated as follows:

$$\begin{aligned} V_{ft} &= V_{ft}^a + V_{ft}^d \\ &= \sum_{k=1}^K W_{fk}^a \sum_{\tau=t-T_a}^{t+T_a} H_{k\tau} P(t-\tau) + \sum_{k=1}^K W_{fk}^d \sum_{\tau=1}^t H_{k\tau} e^{-(t-\tau)\alpha_k}, \end{aligned} \quad (5.5)$$

where \mathbf{V} is the reconstruction of the whole note, as shown in Figure 5.2(i). All variables in the attack/decay model are listed in Table 5.1.

Parameters $\theta \in \{\mathbf{W}^a, \mathbf{W}^d, \mathbf{H}, \mathbf{P}, \alpha\}$ are estimated by minimising the distance between the spectrogram \mathbf{X} and the reconstruction \mathbf{V} by multiplicative update rules [Lee and Seung, 2000]. The derivative of the cost function D with respect to θ is written as a difference of two non-negative functions:

$$\nabla_{\theta} D(\theta) = \nabla_{\theta}^+ D(\theta) - \nabla_{\theta}^- D(\theta). \quad (5.6)$$

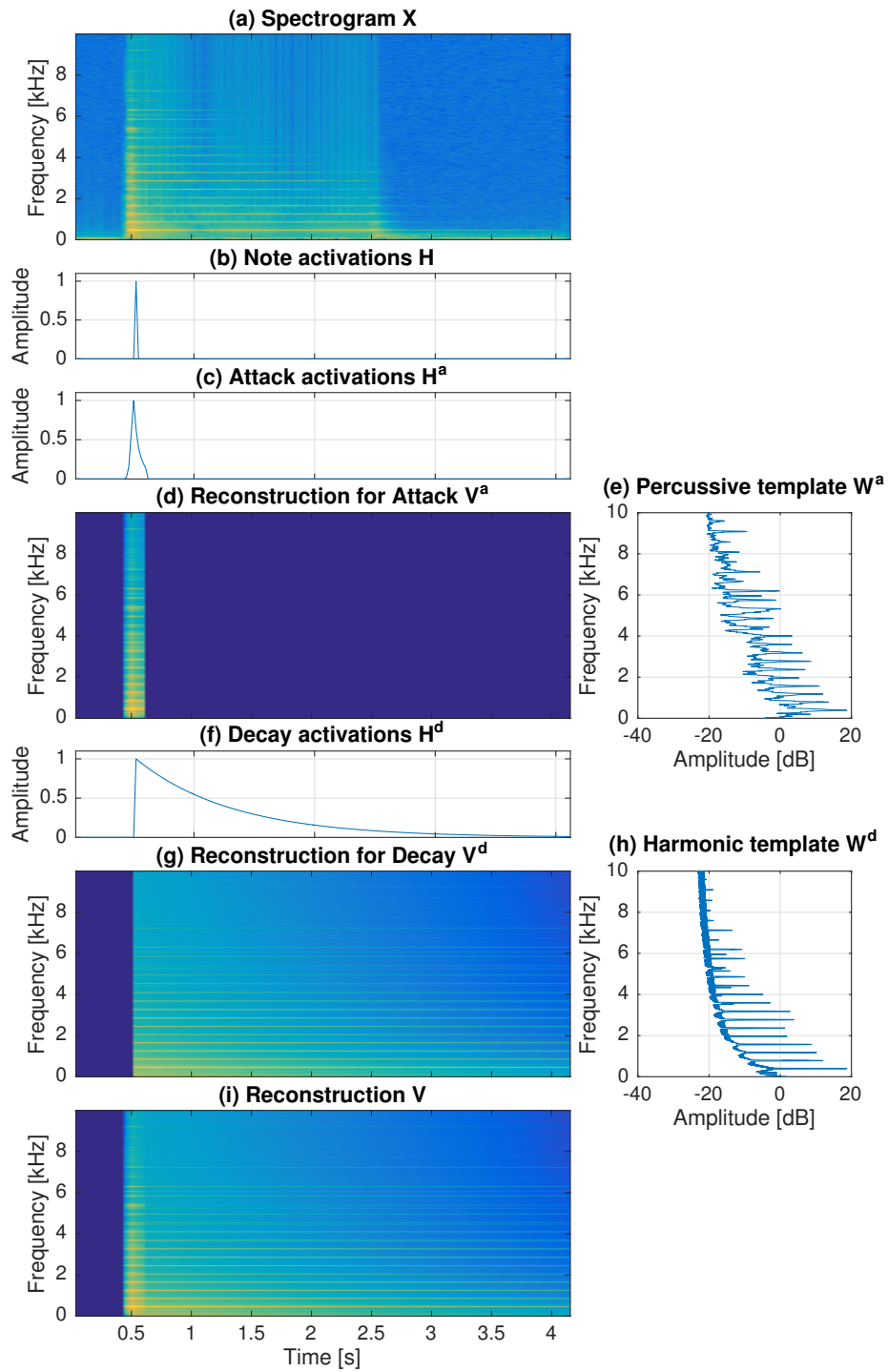


Figure 5.2: An example illustrating of the proposed model (note D3 with the MIDI index of 50).

The multiplicative algorithm is given by

$$\theta \leftarrow \theta \frac{\nabla_{\theta}^{-} D(\theta)}{\nabla_{\theta}^{+} D(\theta)}. \quad (5.7)$$

We employ the β -divergence as the cost function. The update equations are provided below.

$$W_{fk}^a \leftarrow W_{fk}^a \frac{\sum_{t=1}^T \sum_{\tau=t-T_a}^{t+T_a} H_{k\tau} P(t-\tau) (V^{\beta-2} X)}{\sum_{t=1}^T \sum_{\tau=t-T_a}^{t+T_a} H_{k\tau} P(t-\tau) V^{\beta-1}}, \quad (5.8)$$

$$W_{fk}^d \leftarrow W_{fk}^d \frac{\sum_{t=1}^T \sum_{\tau=1}^t H_{k\tau} e^{-(t-\tau)\alpha_k} (V^{\beta-2} X)}{\sum_{t=1}^T \sum_{\tau=1}^t H_{k\tau} e^{-(t-\tau)\alpha_k} V^{\beta-1}}, \quad (5.9)$$

$$\alpha_k \leftarrow \alpha_k \frac{\sum_{f=1}^F \sum_{t=1}^T W_{fk}^d \sum_{\tau=1}^t H_{k\tau} e^{-(t-\tau)\alpha_k} (t-\tau) V^{\beta-1}}{\sum_{f=1}^F \sum_{t=1}^T W_{fk}^d \sum_{\tau=1}^t H_{k\tau} e^{-(t-\tau)\alpha_k} (t-\tau) (V^{\beta-2} X)}, \quad (5.10)$$

$$H_{kt} \leftarrow H_{kt} \frac{\sum_{f=1}^F (W_{fk}^a \sum_{x=-T_a}^{T_a} P(x) + W_{fk}^d \sum_{x=0}^{T-1} e^{-x\alpha_k}) (V_{f(t+x)}^{\beta-2} X_{f(t+x)})}{\sum_{f=1}^F (W_{fk}^a \sum_{x=-T_a}^{T_a} P(x) + W_{fk}^d \sum_{x=0}^{T-1} e^{-x\alpha_k}) V_{f(t+x)}^{\beta-1}}, \quad (5.11)$$

$$P_x \leftarrow P_x \frac{\sum_{f=1}^F \sum_{t=1}^T \sum_{k=1}^K W_{fk}^a H_{kt} (V_{f(t+x)}^{\beta-2} X_{f(t+x)})}{\sum_{f=1}^F \sum_{t=1}^T \sum_{k=1}^K W_{fk}^a H_{kt} V_{f(t+x)}^{\beta-1}}, \quad (5.12)$$

where $x \in [-T_a, T_a]$ is the frame index of the attack envelope \mathbf{P} . The derivations can be found in Appendix B, with the code available online.¹ Normalisation is applied to the attack envelope \mathbf{P} (scaled to a maximum of 1) with fixed activations \mathbf{H} in the training stage. With trained templates, attack envelope and decay rates, we update the activations \mathbf{H} without normalisation in the transcription stage.

5.1.2 Sparsity

To ensure spike-shaped note activations, we simply impose sparsity on activations \mathbf{H} using element-wise exponentiation after each iteration:

$$H_{kt} \leftarrow H_{kt}^{\gamma}, \quad (5.13)$$

where γ is the sparsity factor, usually larger than 1. The larger the factor is, the sparser the activations are. This exponentiation form of sparsity constraint is usually used in the PLCA-based model [Benetos and Dixon, 2012a]. We have shown its utility in NMF in Section 2.3.2 with activations normalised to a maximum of 1. Here we use this sparsity form on activations without normalisation.

¹<https://code.soundsoftware.ac.uk/projects/decay-model-for-piano-transcription>.

In this case, sparsity is enforced by increasing activations above 1 and decreasing activations below 1.

A preliminary test confirmed that the number of peaks in activations decreases as the degree of sparsity increases. We also apply an annealing sparsity factor similar to Chapter 3, which means a continuously changing factor. We set γ to increase from 1 to $\gamma_a \in [1.01, 1.05]$ gradually within the iterations.

5.1.3 Onset detection

Different playing styles and overlapping between notes may cause a mismatch between the observed attack energy and the trained attack envelope. This results in multiple peaks around onsets in the activations. Figures 5.3(a) and (b) show note activations and attack activations of pitch G2 in a music excerpt, respectively. Attack activations indicate the actual attack envelopes of notes obtained by the proposed model. We detect onsets from attack activations by peak-picking [Wang et al., 2008]. First, we compute smoothed attack activations for each pitch, using a moving average filter with a window of 20 bins. Only peaks which exceed the smoothed attack activations by a threshold will be retained as onset candidates, as shown in Figure 5.3(b). The threshold is adapted to each piece with the parameter δ

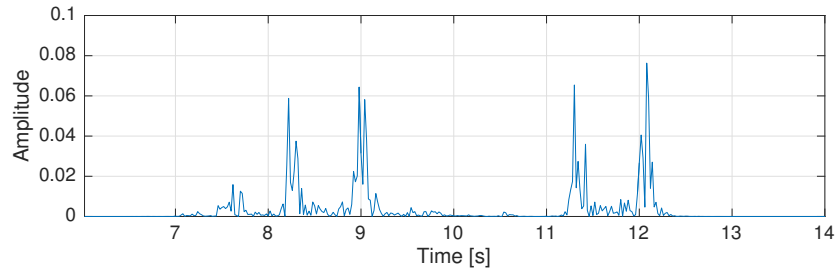
$$Thre = \delta \max_{k,t} H_{k,t}^a. \quad (5.14)$$

We test various $\delta \in \{-21\text{dB}, -22\text{dB}, \dots, -40\text{dB}\}$ in the experiment.

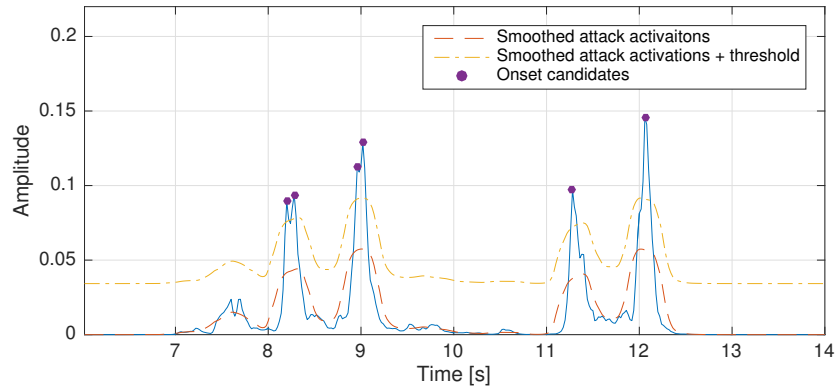
We find that there are still double peaks around onsets after thresholding. In order to deal with this problem, we simply merge pairs of peaks which are too close to each other. We set the minimal interval between two successive notes of the same pitch to be 0.1 second. If the interval between two peaks is smaller than the minimal interval, we generate a new peak. The time index of the new peak is a weighted average (weighted by amplitudes) of the indices of the two peaks, while its amplitude is the sum of that of the two peaks. Figure 5.3 (c) shows detected onsets after merging double peaks. We apply the above process again to get rid of triple peaks.

5.1.4 Offset detection

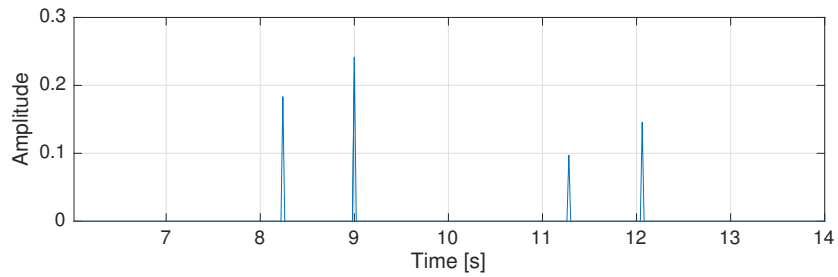
We adapt the method of Ewert et al. [2015] to detect the offsets by dynamic programming. For each pitch, there are two states $s \in \{0, 1\}$, denoting state



(a) Note activations H



(b) Attack activations H^a , showing median filtering and peak selection



(c) Detected onsets, showing result of merging of close onsets

Figure 5.3: Example of onset detection showing how activations are processed.

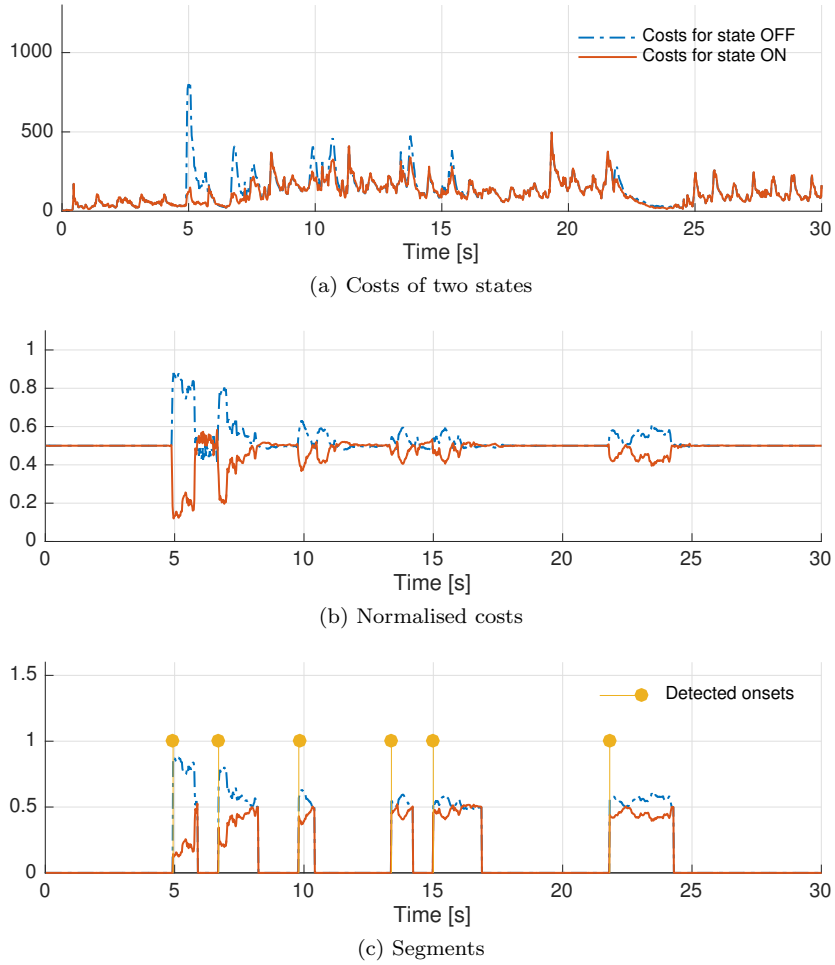


Figure 5.4: Costs and segments for pitch F3 (MIDI index 53).

‘off’ and ‘on’ respectively. The costs of the two states are defined below:

$$C_k(s, t) = \begin{cases} \sum_{f=1}^F D_{KL}(X_{ft} || V_{ft} - V_{ft}^k), & s = 0 \\ \sum_{f=1}^F D_{KL}(X_{ft} || V_{ft}), & s = 1 \end{cases} \quad (5.15)$$

where \mathbf{V}^k is the reconstruction of pitch k , and $\mathbf{V} - \mathbf{V}^k$ is the reconstruction excluding pitch k . $D_{KL}(a||b)$ denotes the KL-divergence between a and b . Then we normalise the costs per pitch to sum to 1 in all frames:

$$\widetilde{C}_k(s, t) = C_k(s, t) / \sum_{\tilde{s}} C_k(\tilde{s}, t). \quad (5.16)$$

Figures 5.4 (a) and (b) show the costs and normalised costs for pitch F3 in a music excerpt, respectively.

We can find the optimal state sequence by applying dynamic programming on the normalised costs. First, we recursively calculate the accumulated costs from the previous states to the current state. The smaller accumulated cost at each step gives the cost of the optimal path to each state, which is stored in an accumulated cost matrix:

$$A_k(s, t) = \begin{cases} \min_{\tilde{s} \in \{0,1\}} (A_k(\tilde{s}, t-1) + \widetilde{C}_k(s, t)w(\tilde{s}, s)), & t > 1 \\ \widetilde{C}_k(s, t), & t = 1 \end{cases} \quad (5.17)$$

where w is the weight matrix. In our experiment, the weights are

$$w = \begin{bmatrix} 0.5 & 0.55 \\ 0.55 & 0.5 \end{bmatrix},$$

which favours self-transitions, in order to obtain a smoother sequence. The indices of the optimal path are stored in the matrix E as follows:

$$E_k(s, t) = \arg \min_{\tilde{s} \in \{0,1\}} (A_k(\tilde{s}, t-1) + \widetilde{C}_k(s, t)w(\tilde{s}, s)), t > 1 \quad (5.18)$$

Then we trace back the optimal path from the end of sequence, with the optimal states given by

$$S_k(t) = \begin{cases} \arg \min_{\tilde{s} \in \{0,1\}} A_k(\tilde{s}, t), & t = T \\ E_k(S_k(t+1), t+1), & t \in [1, T-1] \end{cases} \quad (5.19)$$

We find that when the activation of the pitch is 0 or very small, the costs of the two states are the same or very close, and no state transition occurs. In these frames, the pitch state is expected to be off, but dynamic programming can not jump out from the previous state. Then it will be detected as state on. In order to deal with this problem we need to exclude these parts before applying dynamic programming. Figure 5.4(c) shows the segmentation by detected onsets and the costs. Each segment starts at a detected onset and ends when the difference of the smoothed normalised costs is less than a set threshold (0.05 in our experiment). We track the states of the pitch for each segment individually.

5.2 Experiments

This section is organised as follows. Experiments are described in Section 5.2.1. We analyse performance of the proposed model with different sparsity factors in Section 5.2.2, and compare to state-of-the-art methods in Section 5.2.3. In Section 5.2.4, an unsupervised transcription is applied on repeated notes of

single piano pitches to analyse performance of the proposed model in different pitch ranges and dynamics. Decay rates of isolated piano notes of different dynamics are compared in Section 5.2.5.

5.2.1 Experimental setup

We use audio files sampled at 44100 Hz. To compute the spectrogram, frames are segmented by a 4096-sample Hamming window with a hop-size of 882.² A discrete Fourier transform is performed on each frame with 2-fold zero-padding. To lessen the influence of beats in the decay stage [Cheng et al., 2015a], we smooth the spectrogram with a median filter covering 5 time frames (100 ms). During parameter estimation, we use the KL-divergence ($\beta = 1$) as the cost function. The proposed model is iterated for 50 times in all experiments to achieve convergence.

Datasets

The experiments are performed on three datasets, consisting of sounds from a real piano ('ENSTDkCl') and a synthetic piano ('AkPnCGdD') in the MAPS database [Emiya et al., 2010], and another 10 synthetic piano pieces (denoted as 'PianoE')³ [Ewert et al., 2015]. Piano sounds in the ENSTDkCl subset are recorded on a Disklavier piano. Piano sounds in the AkPnCGdD subset and PianoE dataset are synthesised using the Native Instruments Akoustik Piano and Native Instruments Vienna Concert Grand VST plugins, respectively. The main transcription experiment in Section 5.2.2 uses pieces in the ENSTDkCl subset, and the comparison experiment in Section 5.2.3 is performed on pieces in all three datasets. Both experiments use the first 30 seconds of each piece and train parameters on isolated notes produced by the same piano in the test dataset. In Section 5.2.4 the proposed method is used to detect onsets of repeated notes of single pitches in the ENSTDkCl subset. We analyse decay rates of isolated notes in three dynamics also in the ENSTDkCl subset in Section 5.2.5. Datasets used in different experiments are summarised in Table 5.2.

5.2.2 The main transcription experiment

The training stage

We train percussive and harmonic templates, decay rates and the attack envelope on the isolated notes. Note activations are updated with other parameters

²A 20 ms hop size is used to reduce computation time. For frame-wise evaluation, transcription results are represented with a hop size of 10 ms by duplicating every frame.

³<http://www.piano-e-competition.com>.

Table 5.2: Datasets used in the experiments

Experiment	Datasets
Main transcription (Section 5.2.2)	ENSTDkC1 (music pieces)
Comparison experiment (Section 5.2.3)	ENSTDkC1, AkPnCGdD and PianoE (music pieces)
Unsupervised transcription (Section 5.2.4)	ENSTDkC1 (repeated notes)
Decay rate analysis (Section 5.2.5)	ENSTDkC1 (isolated notes)

Table 5.3: Experimental configuration for the training stage

Round one	Round two
Initialisation	Initialisation
\mathbf{W}^d : random	\mathbf{W}^d : random
$\mathbf{W}^a, \alpha, \mathbf{P}$: all ones	\mathbf{W}^a, α : all ones
\mathbf{H} : set based on the ground truth	\mathbf{P} : mean of the results of round one
	\mathbf{H} : set based on the ground truth
update $\mathbf{W}^d, \mathbf{W}^a, \alpha, \mathbf{P}$	update $\mathbf{W}^d, \mathbf{W}^a, \alpha$
Parameters	Parameters
$K = 1$	same as left
sparsity: unavailable	

fixed.⁴

The training stage includes two rounds, as shown in Table 5.3. In the first round, we first fix note activations (\mathbf{H}) for each isolated note according to the ground truth, then update all other parameters ($\mathbf{W}^a, \mathbf{W}^d, \mathbf{P}$ and α). The attack envelopes are normalised to a maximum of 1 after each iteration. The attack envelopes follow a certain shape and can be shared by all pitches. So we use the average of the trained attack envelopes to reduce the number of parameters and to avoid potential overfitting. The trained attack envelopes and the average attack envelope are shown in Figure 5.5. In the second round, we fix the note activations (\mathbf{H}) and the average attack envelope (\mathbf{P}), then update all other parameters ($\mathbf{W}^a, \mathbf{W}^d$ and α).

Transcription results

For transcription, we update note activations \mathbf{H} , keeping parameters $\mathbf{W}^a, \mathbf{W}^d, \mathbf{P}$ and α fixed from the training stage. Note activations are updated using Equation 5.11 with different sparsity factors. The experimental configuration is shown in Table 5.4. Onset-only note tracking results (presented as percentages) are shown in Table 5.5 with different sparsity factors. The last column indicates

⁴The proposed model runs at about $3 \times$ real-time using MATLAB on a MacBook Pro laptop (I7, 2.2GHz, 16GB).

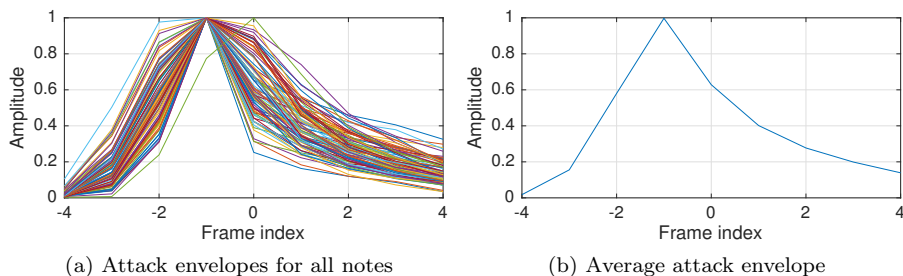


Figure 5.5: Attack envelopes.

Table 5.4: Experimental configuration I for the transcription experiments in Section 5.2.2.

Initialisation
\mathbf{W}^d , \mathbf{W}^a , α , \mathbf{P} : trained
\mathbf{H} : random
update \mathbf{H} only
Parameters
$K = 88$
sparsity: γ range from 1 to 1.05
onset threshold: optimal threshold

the optimal thresholds. We find that all F-measures with different sparsity factors are above 80% with optimal thresholds, and the optimal threshold decreases when sparsity increases. The top part of Table 5.5 contains results using fixed sparsity factors. The best results are achieved without the sparsity constraint ($\gamma = 1.00$), with an F-measure of 82.24%. The performance decreases with increasing sparsity factor. When the sparsity factor equals 1.05, the F-measure drops to 80.51%. The second part of the experiment gives results for using annealing sparsity. The best F-measure is 82.36% with the setting (1.00 \rightarrow 1.02) and the worst F-measure is 81.76% with the setting (1.00 \rightarrow 1.05). The difference between the best and the worst F-measure is only 0.6 percentage points. In general, results with annealing sparsity are slightly better than those with fixed sparsity.

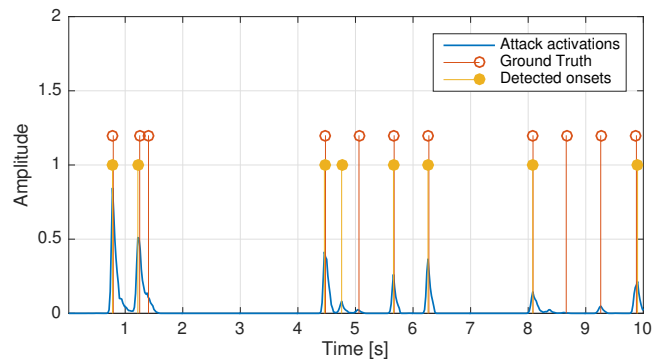
Figure 5.6 shows attack activations and detected onsets for different sparsity factors for pitch G4 for the first 10 seconds of a piano piece. Note activations are normalised to a maximum activation of 1 in that piece. With a small sparsity factor, there are more peaks in attack activations, and it is more likely to have false positives, as shown in Figure 5.6(a). In Figure 5.6(b), due to the high sparsity constraint, small peaks are more likely to disappear, resulting in an extra missed detected note (around 8 seconds). False positive peaks can be discarded

Table 5.5: Note tracking results with different fixed sparsity factors (above) and annealing sparsity factors (below).

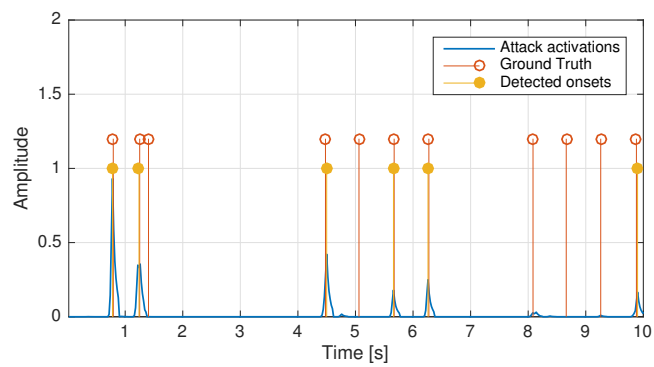
γ	P_{on}	R_{on}	F_{on}	A_{on}	$\delta(\text{dB})$
1.00	88.52	77.70	82.24	70.54	-29
1.01	87.70	78.18	82.23	70.53	-30
1.02	87.67	77.36	81.80	69.87	-30
1.03	87.22	77.31	81.62	69.66	-31
1.04	86.95	76.84	81.26	69.17	-32
1.05	86.38	75.99	80.51	68.14	-33
1 \rightarrow 1.01	87.77	78.08	82.18	70.49	-30
1 \rightarrow 1.02	88.49	77.79	82.36	70.73	-30
1 \rightarrow 1.03	88.22	77.78	82.27	70.60	-31
1 \rightarrow 1.04	87.86	77.66	82.09	70.35	-32
1 \rightarrow 1.05	86.83	77.83	81.76	69.84	-34

in the onset detection stage by thresholding and merging onsets. On the other hand if peaks disappear by imposing sparsity, they can not be recovered at later stages.

We compute the performance using thresholds ranging from -40 to -21 dB to study how performance changes with the change of thresholds. Figure 5.7(a) shows the results for different fixed sparsity factors. It is clear that precision decreases with the increase of the threshold, while recall increases. The higher the sparsity factor is, the more robust the results are to threshold changes. When decreasing the threshold from the optimal value to smaller values (moving towards -40 dB), the F-measure drops from above 82% to below 75% without sparsity, while the difference in F-measure is within 2 percentages when $\gamma = 1.05$. This is because small peaks in activations are already discounted when imposing sparsity. Lowering the threshold does not bring many false positives. Results with higher sparsity are less sensitive to reduction in the threshold. However, when the threshold becomes larger, the results with low sparsity still outperform those with high sparsity. With a larger threshold, the number of true positives decreases. There are more peaks in activations when using lower sparsity, so more true positives remain. This favours the assumption that the true positives have larger amplitudes. Figure 5.7(b) shows the robustness of using annealing sparsity factors. The transcription results are close to each other. With annealing sparsity, the results are better and more tolerant to threshold changes. The sparser the factor is, the robuster the result is to low thresholds. The reductions in F-measure for different sparsity factors are similar to those of the fixed sparsity when the threshold is increased.

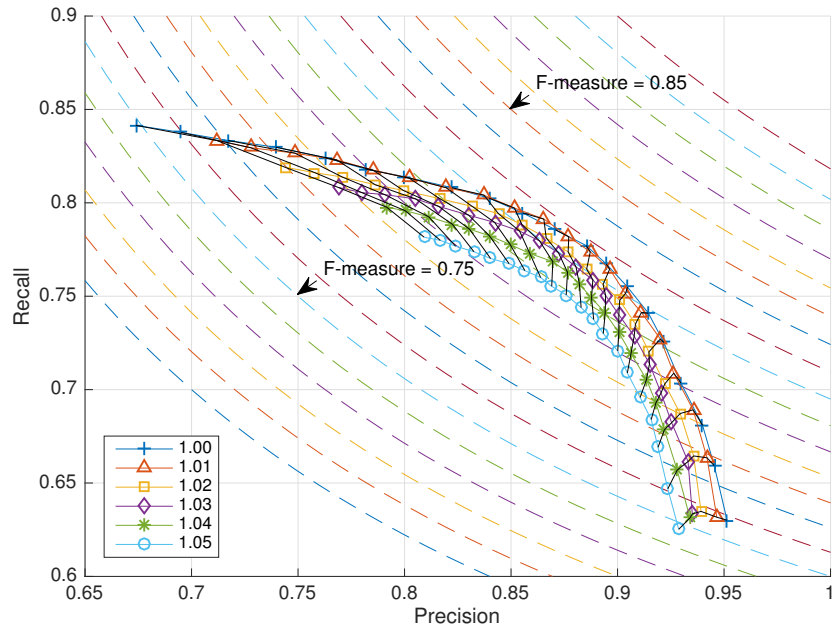


(a) Attack activations ($\gamma = 1.01$)

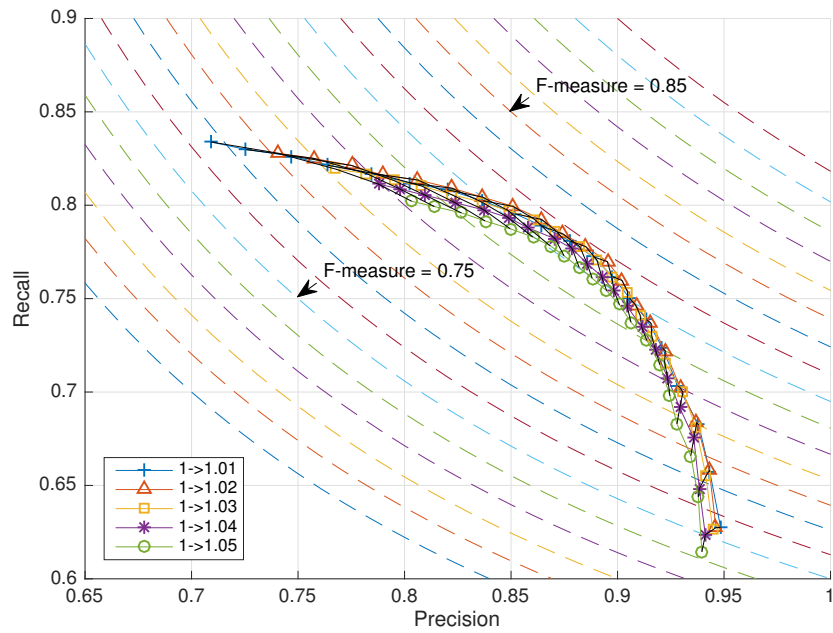


(b) Attack activations ($\gamma = 1.05$)

Figure 5.6: Detected onsets with different sparsity for pitch G4 (MIDI index 67).



(a) Results with fixed sparsity factors



(b) Results with annealing sparsity factors

Figure 5.7: Performance using different sparsity factors and thresholds. The sparsity factors are indicated by different shapes, as shown in the legends. Lines connecting different shapes are results achieved via the same threshold. The threshold of the top-left set is -40dB , and the bottom-right set is -21dB . The dashed lines show F-measure contours, with the values decreasing from top-right to bottom-left.

Table 5.6: Note tracking results (onset-offset) and frame-wise results

γ	P_{off}	R_{off}	F_{off}	A_{off}	P_f	R_f	F_f	A_f
1.00	45.29	40.28	42.39	27.74	82.90	74.43	77.54	63.74
1.01	44.68	40.48	42.27	27.80	81.19	77.70	78.61	65.24
1.02	43.66	39.24	41.14	26.97	80.14	79.21	78.96	65.75
1.03	42.84	38.67	40.49	26.53	78.89	80.58	79.03	65.89
1.04	42.27	38.07	39.91	26.11	77.97	81.34	78.94	65.84
1.05	41.49	37.27	39.10	25.52	77.22	81.62	78.66	65.53
1 \rightarrow 1.01	44.61	40.34	42.15	27.67	81.26	77.56	78.59	65.21
1 \rightarrow 1.02	44.55	39.96	41.92	27.70	80.17	79.39	79.06	65.93
1 \rightarrow 1.03	43.75	39.34	41.25	27.21	78.90	80.74	79.13	66.02
1 \rightarrow 1.04	42.64	38.46	40.28	26.47	77.72	81.95	79.12	66.03
1 \rightarrow 1.05	41.80	38.23	39.79	26.15	76.36	83.26	78.99	65.93

In the proposed model, the activation of each note decays after its onset, as shown in the decay activations of Figure 5.1. Pairs of notes in close succession are particularly hard to transcribe. When the second note has the same pitch as the first, our model tends to fail to detect the second note because of the remaining activation of the first note. Why exactly this happens still needs further study. However, when the second note has a different pitch, our model is particularly robust against the introduction of false positives at the attack of the second note, while for standard NMF, there is always some interference with the first note’s activation.

Table 5.6 shows note tracking results considering both onsets and offsets, and frame-level results computed with the optimal thresholds in Table 5.5. For all sparsity factors, the onset-offset F-measures are around 40%. Best performance is 42.39% without sparsity ($\gamma = 1$). All frame-level F-measures are above 77%, and the best one is 79.13% with annealing sparsity $\gamma = 1 \rightarrow 1.03$.

5.2.3 Comparison with state-of-the-art methods

We compare to two state-of-the-art transcription methods. Vincent et al. [2010] applies adaptive spectral bases generated by linear combinations of narrow-band spectra, so the spectral bases have a harmonic structure and the flexibility to adapt to different sounds. The method is performed in an unsupervised way, to indicate what can be achieved without training datasets. Benetos and Weyde [2015a] employ 3 templates per pitch, and the sequence of templates is constrained by a probabilistic model. We use the version of Benetos and Weyde’s method from the MIREX evaluation [Benetos and Weyde, 2015b]. We have

access to the code and train templates on isolated notes of the corresponding pianos. In the PianoE dataset, we also compare to the method of Ewert et al. [2015]. This method identifies frames in NMD patterns with states in a dynamical system. Note events are detected with constant amplitudes but various durations. The method uses template patterns trained on isolated notes. We only have access to the published data in [Ewert et al., 2015].

Based on our previous analysis, we employ the following parameters for the proposed model in comparison experiments. The sparsity factor is $\gamma = 1 \rightarrow 1.04$ by balancing among transcription results and the robustness to different thresholds. Onsets are detected with threshold $\delta = -30\text{dB}$. In the first dataset (ENSTDkCl), results of other methods are also reported with optimal thresholds with best note-wise F-measures. Then the same thresholds are used for the two synthetic piano datasets.

Results on piano pieces from the ENSTDkCl subset are shown in Table 5.7(a). The proposed model has a note tracking F-measure of 81.80% and a frame-wise F-measure of 79.01%, outperforming Vincent *et al.*'s unsupervised method by around 10 and 20 percentage points, respectively. Results of Benetos and Weyde's method are in between.

Results on the synthetic piano AkPnCGdD are shown in Table 5.7(b). In general, all methods perform better on this dataset than on the 'ENSTDkCl' dataset, especially on note tracking results. The proposed model has the best results (84.63% on note tracking F-measure and 80.81% on frame-wise F-measure), outperforming all other methods by at least 5 percentage points.

Results on the other synthetic dataset PianoE are shown in Table 5.7(c). Compared to the other datasets, note tracking results of all methods are good but frame-wise results are poor. Ewert *et al.*'s method performs the best on note tracking (88% on F-measure), and Benetos and Weyde's method is the second (83.80% on F-measure). The proposed model only outperforms Vincent *et al.*'s method, with F-measures of 81.28% and 79.41% for these two methods respectively. However, the proposed model remains the best on the frame-wise F-measure (66.77%). Pieces in this dataset are from a piano competition. Many notes have very short durations. The remaining energies of a short note in the proposed model may interfere with later notes, causing false negatives.

A supervised neural network model also has been tested on the MAPS database for piano transcription [Sigitia et al., 2016]. Besides an acoustic model, the method employs a music language model to capture the temporal structure of music. Although the method is not directly comparable, it is noticeable that our method exceeds its results by at least 5 percentage points on F-measures. When tested on the real recordings using templates trained on the synthetic piano notes, the proposed method has both frame-level and note-level F-measures

Table 5.7: Comparison of transcription results with two state-of-the-art methods on three public datasets.

(a) Transcription results on ENSTDkCl				
Method	F_{on}	A_{on}	F_f	A_f
Proposed	81.80	69.94	79.01	65.89
[Vincent et al., 2010]	72.15	57.45	58.84	42.71
[Benetos and Weyde, 2015b]	73.61	59.73	67.79	52.15

(b) Transcription results on AkPnCGdD				
Method	F_{on}	A_{on}	F_f	A_f
Proposed	84.63	74.03	80.81	68.39
[Vincent et al., 2010]	79.86	67.32	69.76	55.17
[Benetos and Weyde, 2015b]	74.05	59.57	53.94	38.65

(c) Transcription results on PianoE				
Method	F_{on}	A_{on}	F_f	A_f
Proposed	81.28	69.12	66.77	51.63
[Vincent et al., 2010]	79.41	66.39	58.59	42.45
[Benetos and Weyde, 2015b]	83.80	72.82	60.69	44.24
Ewert et al. [2015]	88			

Table 5.8: Experimental configuration II for test on repeated notes in Section 5.2.4.

Initialisation
\mathbf{W}^d, \mathbf{H} : random
$\mathbf{W}^a, \alpha, \mathbf{P}$: all ones
update all
Parameters
$K = 1$
sparsity: $\gamma = 1 \rightarrow 1.04$
onset threshold: $\delta = -30dB$

of around 65%, outperforming the method of Sigtia et al. [2016] by 10 percentage points on note-wise F-measure in a similar experiment.

5.2.4 Test on repeated notes for single pitches

We investigate the proposed model’s performance on different dynamics and pitches in this experiment. We use 66 sound clips generated according to MIDI files using the Disklavier piano in the subset ‘ENSTDkCl’ of the MAPS database [Emiya et al., 2010]. Each of the clips consists of about 15 notes of a single pitch. Notes in one clip have the same MIDI velocity, and repeat faster and faster. The larger the velocity is, the louder the sound is. The sound clips are divided into three dynamics: forte (loud), mezzo-forte (moderately loud) and piano (soft), with 22 clips in each of three dynamics.

The experimental configuration for this experiment is shown in Table 5.8. The activations are normalised to be the maximum of 1 after each iteration. We adopt the optimal parameters from the previous transcription experiment. All variables are updated during the iterations. We focus on onset-only note tracking results in this experiment. Information in some clips with soft notes is not aligned with the sounds. We manually correct onsets of these clips⁵ referring to results of the onset detection method SuperFlux [Böck and Widmer, 2013].

Table 5.9 shows detailed results of note tracking (onset-only) of repeated notes. We list the numbers of true positives, false positives and false negatives rather than precision, recall to give an intuitive aspect on the results. In general, the proposed model can find most onsets, indicated by small numbers of false negatives. The results are better for loud or moderately loud notes, with average F-measures of 88.53% and 85.38% respectively. In these two dynamics, many false positives are detected in the low pitch range, while there are few false

⁵The manually corrected onsets are given in the following link
<https://code.soundsoftware.ac.uk/projects/decay-model-for-piano-transcription>.

positives for notes in the middle and high pitch ranges (above MIDI index 50). When notes are quiet, the average F-measure is smallest (76.61%). There is no certain trend for performance associated with pitch ranges.

Figure 5.8 shows some examples of pitches in low and high range, which are played in three dynamics. There are many false positives for low pitches, as shown in the left sub-figures, possibly caused by time-varying timbre (beating especially [Cheng et al., 2015a]), reverberation and so on. There are less false positives for quiet low-pitch notes, as shown on the left of Figure 5.8(c). We find that some peaks appear around offsets of notes. This is the sound of the damper coming into contact with the string. This sound and the remaining energy are easy to be detected as another quiet note. The system works quite well for notes of high pitches, as shown in the right sub-figures. Most onsets are correct and clearly detected. There are false positives around the offsets for the quiet high-pitch note on the right of Figure 5.8(c). At the end of these clips, notes are repeated very fast. We can find that some of these notes are merged into one note, resulting in some false negatives.

In this experiment, we analyse the performance of the proposed model in different dynamics and pitch ranges. Firstly, we find the differences of performance on notes in different dynamics. The louder the notes are, the better the model performs. Secondly, the proposed model works better for notes in the middle and high pitch ranges. As indicated in the results of Section 4.3.1, the exponential decay has the worst results to fit the decay of tones in low pitch range because of the beats. This can be one reason for the bad performance for the low pitch range of the proposed model. Thirdly, the proposed model tends to merge fast-repeated notes into one note. This kind of false negatives is largely related to the simplification of ignoring note offsets at the first stage.

Table 5.9: Note tracking (onset-only) results for repeated notes in different dynamics.

Pitch	Forte						Mezzo-forte						Piano					
	N_{tp}	N_{fp}	N_{fn}	F	Pitch	N_{tp}	N_{fp}	N_{fn}	F	Pitch	N_{tp}	N_{fp}	N_{fn}	F	Pitch	N_{tp}	N_{fp}	N_{fn}
21	13	10	2	68.42	22	13	8	2	72.22	21	11	4	0	84.62				
30	13	13	2	63.41	24	12	9	3	66.67	22	8	16	1	48.48				
31	11	14	4	55.00	26	14	13	1	66.67	32	10	6	0	76.92				
37	13	4	2	81.25	27	13	8	2	72.22	38	11	4	0	84.62				
44	14	4	1	84.85	28	12	9	3	66.67	49	11	5	0	81.48				
45	13	3	2	83.87	29	13	8	2	72.22	50	10	7	0	74.07				
49	13	0	2	92.86	36	13	6	2	76.47	52	11	3	0	88.00				
53	13	0	2	92.86	52	14	2	1	90.32	54	12	5	0	82.76				
55	14	3	1	87.50	62	13	2	2	86.67	57	13	2	0	92.86				
59	13	0	2	92.86	63	14	0	1	96.55	61	10	13	1	58.82				
66	14	0	1	96.55	66	14	1	1	93.33	63	9	11	2	58.06				
71	14	1	1	93.33	68	14	2	1	90.32	67	10	11	1	62.50				
72	14	0	1	96.55	77	14	1	1	93.33	69	11	0	0	100.00				
75	13	0	2	92.86	81	14	0	1	96.55	72	12	2	2	85.71				
79	13	1	2	89.66	83	13	1	2	89.66	74	10	5	0	80.00				
84	14	0	1	96.55	89	13	2	2	86.67	79	11	3	0	88.00				
88	14	0	1	96.55	93	14	0	1	96.55	84	10	5	0	80.00				
92	14	0	1	96.55	96	14	0	1	96.55	93	8	8	4	57.14				
94	14	0	1	96.55	100	13	0	2	92.86	96	12	0	0	100.00				
102	14	0	1	96.55	103	14	0	1	96.55	100	10	0	0	100.00				
103	14	0	1	96.55	107	12	2	3	82.76	107	7	4	3	66.67				
105	14	0	1	96.55	108	14	0	1	96.55	108	4	9	6	34.78				
Average F-measure				88.53					85.38					76.61				

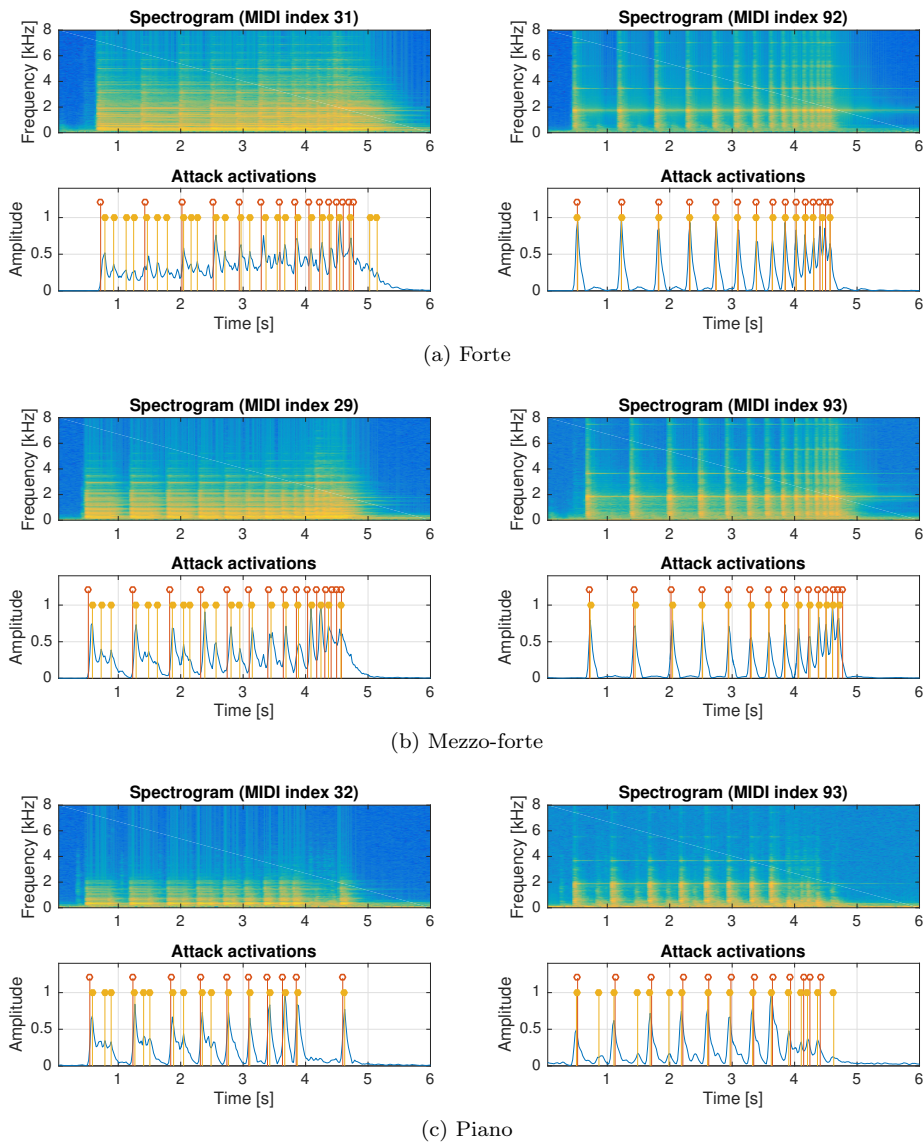


Figure 5.8: Examples of repeated note detection for low (left) and high (right) pitches at three dynamic levels. Detected onsets are shown as brown impulses, and ground truth onsets as red.

5.2.5 Analysing decay in different dynamics

In the isolated note collection, notes are also played in three different dynamics, forte (f), mezzo-forte (m) and piano (p). We use the proposed model to analyse the attack envelope and decay rates of notes in different dynamics. The process is the same as the training stage in Section 5.2.2. The only difference is that in this experiment, to obtain more accurate decay rates, we end each clip at its

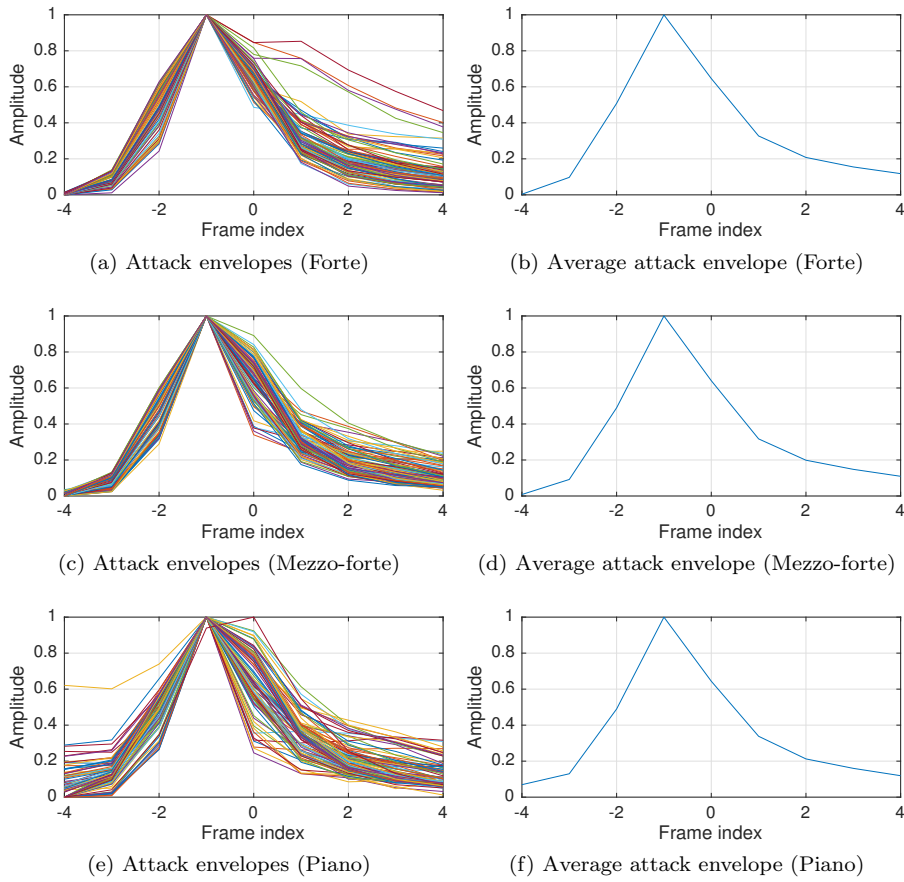


Figure 5.9: Attack envelopes of different dynamics.

offset or when its energy decreases to 50 dB below the maximum energy. For each dynamic, we first generate a note activation in form of a unit delta function with onset information for each individual note, then fix the note activation and update all other parameters. After obtaining the average attack envelope on 88 notes, we fix note activations and the average attack envelope to estimate templates and decay rates again.

Figure 5.9 shows attack envelopes and average attack envelopes for different dynamics. The attack envelopes of different pitches have clear similar shapes in all three dynamics, as shown in the left sub-figures. For quiet notes, the variance of the attack envelopes is larger than that of notes at the other two dynamics (shown in Figure 5.9(e)). The average attack envelopes (shown in the right sub-figures) resemble each other in a higher degree, especially between the shapes of loud and moderately loud notes.

We analyse the decay rates under the assumption that the note energy decays

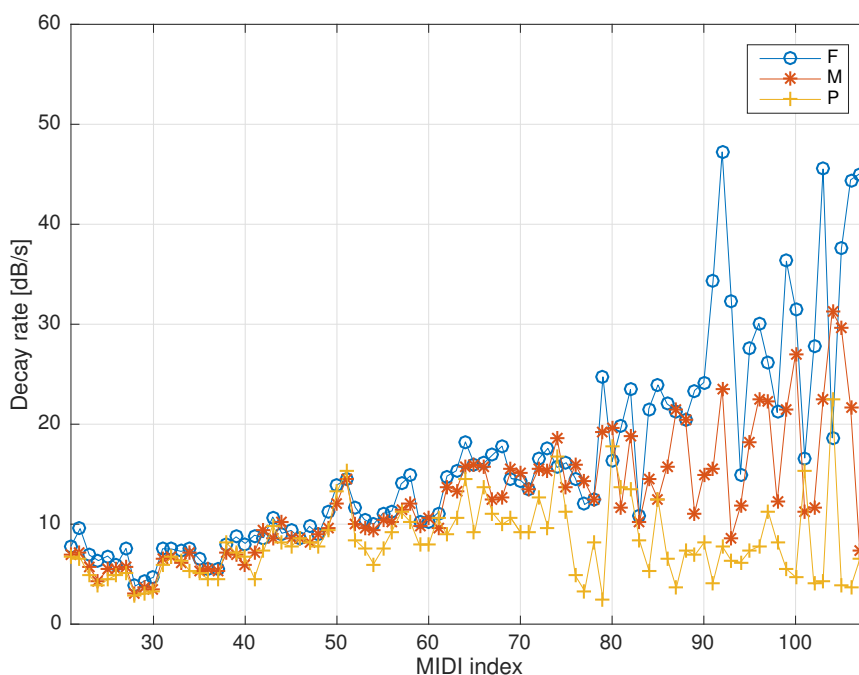


Figure 5.10: Decay rates as a function of pitch for different dynamics.

exponentially. For notes played forte, there is a trend that higher pitched notes decay faster, as shown in the blue circles in Figure 5.10. For notes of the other two dynamics, the trend is less clear. When comparing decay rates of the same pitch, we find that in the low pitch range (below 50 in MIDI index), the decay rates of the notes at different dynamics are close to each other. Dynamics barely influence decay in this pitch range. The decay rates corresponding to different dynamics begin to vary for the notes in the following two octaves. In the high pitch range (MIDI indices above 74), there are obvious differences among the decay rates, with the notes with higher energy decaying faster, while there is still more consistency in decay rates of the same note in comparison to that of other notes.

This experiment is to verify the assumption that notes of the same pitch decay at the same rate despite dynamics. The result suggests that this assumption is suitable for notes in the low and middle pitch ranges, but not for high-pitch notes.

5.3 Conclusion and future work

In this chapter we propose an attack/decay model for piano transcription. We model a piano note as having a percussive attack stage and a harmonic de-

cay stage, and the decay stage is explicitly modelled as an exponential decay. Parameters are learned using a sparse NMF, and transcription is performed in a supervised way. We detect onsets on attack activations by peak-picking and track pitch states by dynamic programming to find offsets. In the transcription experiment, the proposed model provides promising transcription results, with around 82% and 79% for note tracking and frame-wise F-measures in music pieces from a real piano in the ‘ENSTDkCl’ dataset. The best results are achieved with low sparsity, but high sparsity favours the robustness of the method to different thresholds. The annealing sparsity factor slightly improves the performance and the robustness of the proposed model.

The comparison experiment shows that the proposed model outperforms two state-of-the-art methods by a large margin on real and synthetic pianos in the MAPS database. On a different synthetic dataset, the other methods perform better on note tracking, while the proposed method remains best on frame-wise metrics.

Tests on repeated notes of single pitches show that the proposed model works better on louder notes. The assumption of exponential decay causes many false positives on notes in the low frequency range. The simplification of ignoring offsets in the NMF framework works well for long notes, but may cause false negatives on short notes. In the last experiment, we find that notes in the low pitch range have similar decay rates in different dynamics, while decay rates of a high-pitch note vary with different dynamic levels, with louder notes decaying faster. The decay rates of loud notes also show a trend that high-pitch notes decay faster.

The proposed model can also be understood as a deconvolution method by parametric patches, or as an extension of the method proposed by Berg-Kirkpatrick et al. [2014] using parametric envelopes. As a deconvolution method, the major problem is lack of sensitivity to note offsets, which usually causes false negatives. The silver lining is that we can build a note-level system by deconvolution, which has provided good transcription results [Berg-Kirkpatrick et al., 2014, Ewert et al., 2015]. In comparison to other deconvolution-based methods, the proposed model uses parametric patches, which reduces the parametric dimensionality. Secondly, we can generate arbitrarily long patches using static spectra and decay rates, so the proposed model can be applied when the training dataset only contains short notes. This makes the model more practical to available datasets. Thirdly, parameterising the decay stage also provides us with a way of analysing decay rates of piano notes.

The proposed model shows that building a note-level transcription system is more powerful than a frame-level system and reasonable parameterisation

(based on piano acoustics) makes the model more compact and practical. In the future, we would like to represent a note's decay stage by a decay filter instead of a decay rate, which is more in line with studies on piano decay in Chapter 4. Secondly, the good performance on piano music transcription is partly due to the availability of the training datasets. We would like to build an adaptive model, which could work in a more general scenario, hence more automatically. Finally, we are keen to find a way to control note offsets in the proposed model.

Chapter 6

Modelling Spectral Widths for Piano Transcription

In this chapter we make a preliminary investigation of spectral widths of partials of piano notes as a cue for automatic transcription. A piano note has different spectral distributions over its duration: it is percussive and noisy in the attack part and quasi-harmonic in the decay part. We focus on the change of the spectral width during the evolution of the sound, and use it for improving piano transcription. In order to model the spectral width in a transcription system, we first parameterise a partial by its frequency and spectral shape as modelled by a Gaussian function, with the spectral width defined as the standard deviation of the Gaussian function. Then we present a model for piano tones with time-varying spectral widths in an NMF framework. The results on isolated notes suggest that the spectral width is large in the attack part, then it decreases and remains stable in the decay part. However, there are no significant differences on the performance brought by using spectral widths in the transcription experiment. We also analyse the spectral width distributions at onsets and in the decay parts for notes in the musical pieces and show several directions of future work.

From the previous two chapters, we know that amplitudes of piano tones decay with fluctuations caused by beats. As a result, two notes played at the same dynamic level, but with different durations, will have different ending amplitudes. In order to find a more constant indicator for note tracking, Kirchhoff et al. [2014] study the relative phase offsets between partials of harmonic sounds. The method is tested on a monophonic saxophone signal and shows the phase offsets remain stable in the sustained part. In a similar attempt to find a constant indicator for note activation, we use a parametric model to rep-

resent the spectral widths for piano tones, with each partial represented by its frequency and the parameters of a Gaussian function. Hennequin et al. [2010] and Rigaud [2013] use similar parametric models to estimate the frequencies for vibratos and inharmonic tones, respectively. Here we fix the frequencies, but estimate the standard deviation of the Gaussian function to indicate the spectral distributions of difference stages of piano tones.

The rest of the chapter is structured as follows. In Section 6.1, we introduce the spectral width and represent piano tones in an NMF framework with spectral width modelled. In Section 6.2, we evaluate the proposed system in a piano transcription experiment and compare it to a baseline NMF system. Section 6.3 concludes this chapter and summarises future work.

6.1 The proposed model

6.1.1 Modelling spectral widths

Consider a harmonic signal of 10 partials at a fundamental frequency of 100 Hz ($f_0 = 100$ Hz):

$$x(t) = \sum_{h=1}^{10} \sin(2\pi f_0 h t), \quad (6.1)$$

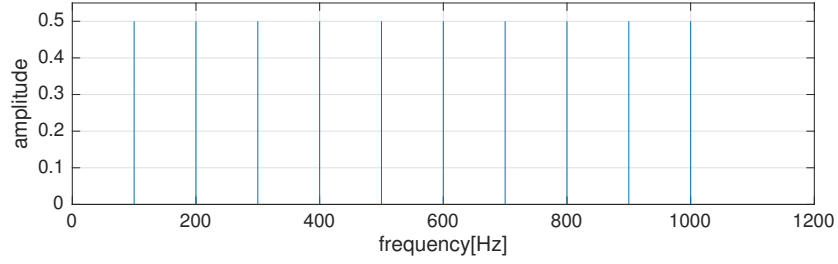
where $x(t)$ is the amplitude of the signal in time t , and h indicates the number of the partial. The theoretical magnitude spectrum of this signal is shown in Figure 6.1(a), consisting of 10 harmonic peaks at multiples of f_0 . However, the spectrum computed by the discrete Fourier transform is shown in Figure 6.1(b). The difference is due to the window function. When computing the short-time Fourier transform, the signal is first segmented and weighted by a window function, then a discrete Fourier transform is performed on the short-term signal. The spectrum of each frame is represented as a convolution of the spectrum of the signal and the window response:

$$\mathcal{F}[x(t)w(t)] = X(f) * W(f), \quad (6.2)$$

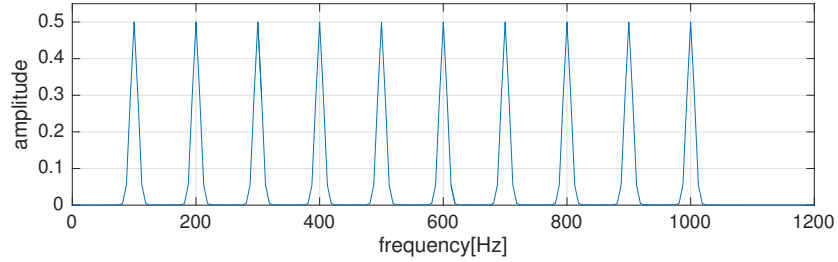
where $X(f) = \mathcal{F}[x(t)]$ and $W(f) = \mathcal{F}[w(t)]$ are the Fourier transforms of the signal $x(t)$ and window function $w(t)$, respectively.

We choose the Gaussian window for computing the STFT, because the Fourier transform of the window is also a Gaussian function, which has convenient mathematical properties. The Gaussian response is represented by the Gaussian function with a maximum of 1 as follows:

$$G(f|\sigma) = \exp\left(-\frac{f^2}{2\sigma^2}\right), \quad -3\sigma \leq f \leq 3\sigma \quad (6.3)$$



(a) The theoretical spectrum



(b) The spectrum calculated with a Gaussian window

Figure 6.1: Spectra of the signal in Equation 6.1

where σ is the standard deviation, and the function is restricted to a range of $\pm 3\sigma$, as shown in Figure 6.2. In this chapter, we define the *spectral width* of a Gaussian response as its standard deviation to avoid introducing another term.¹

6.1.2 Modelling piano notes

The beginning of a piano note is percussive and noisy. After the attack stage, the spectral width gradually reduces to a stable value and remains the same for the rest of the tone. The spectrum of pitch k in the f^{th} frequency bin and the t^{th} frame V_{ft}^k is modelled by the convolution of the spectral basis \mathbf{w}_k and the window response $G(f|\sigma_{kt})$, scaled by the current activation H_{kt} :

$$V_{ft}^k = [\mathbf{w}_k * G(f|\sigma_{kt})]_f H_{kt} = \sum_{f'=-3\sigma_{kt}}^{3\sigma_{kt}} W_{(f-f')_k} \exp\left(-\frac{f'^2}{2\sigma_{kt}^2}\right) H_{kt}, \quad (6.4)$$

where the spectral basis ($\mathbf{w}_k \in \mathbb{R}^F$) has peaks only at the partial frequencies. The whole spectrum is formulated as a sum of the spectra of all pitches:

$$V_{ft} = \sum_{k=1}^K V_{ft}^k = \sum_{k=1}^K \sum_{f'=-3\sigma_{kt}}^{3\sigma_{kt}} W_{(f-f')_k} \exp\left(-\frac{f'^2}{2\sigma_{kt}^2}\right) H_{kt}. \quad (6.5)$$

¹Usually the *spectral width* is defined as a half width at half maximum. For a Gaussian function, this value is slightly larger than the standard deviation.

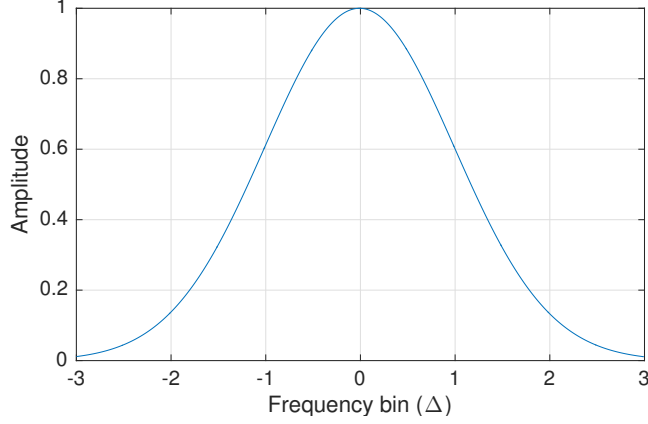


Figure 6.2: The response of a Gaussian window

Parameter estimation

In order to simplify the implementation, we restrict the Gaussian function to a fixed range, within $\pm L$ frequency bins. Then the model is formulated as follows:

$$V_{ft} = \sum_{k=1}^K V_{ft}^k = \sum_{k=1}^K \sum_{f'=-L}^L W_{(f-f')k} \exp\left(-\frac{f'^2}{2\sigma_{kt}^2}\right) H_{kt}. \quad (6.6)$$

The parameters are estimated using multiplicative update rules with β -divergence. We use the KL-divergence ($\beta = 1$) as the cost function. The update rules are listed below, with detailed derivation shown in Appendix C.

$$W_{fk} = W_{fk} \frac{\sum_{t=1}^T \sum_{f'=-L}^L \exp\left(-\frac{f'^2}{2\sigma_{kt}^2}\right) H_{kt} V_{(f+f')t}^{\beta-2} X_{(f+f')t}}{\sum_{t=1}^T \sum_{f'=-L}^L \exp\left(-\frac{f'^2}{2\sigma_{kt}^2}\right) H_{kt} V_{(f+f')t}^{\beta-1}}, \quad (6.7)$$

$$H_{kt} = H_{kt} \frac{\sum_{f=1}^F \sum_{f'=-L}^L W_{(f-f')k} \exp\left(-\frac{f'^2}{2\sigma_{kt}^2}\right) V_{ft}^{\beta-2} X_{ft}}{\sum_{f=1}^F \sum_{f'=-L}^L W_{(f-f')k} \exp\left(-\frac{f'^2}{2\sigma_{kt}^2}\right) V_{ft}^{\beta-1}}, \quad (6.8)$$

$$\sigma_{kt}^2 = \sigma_{kt}^2 \frac{\sum_{f=1}^F \sum_{f'=-L}^L W_{(f-f')k} f'^2 \exp\left(-\frac{f'^2}{2\sigma_{kt}^2}\right) V_{ft}^{\beta-2} X_{ft}}{\sum_{f=1}^F \sum_{f'=-L}^L W_{(f-f')k} f'^2 \exp\left(-\frac{f'^2}{2\sigma_{kt}^2}\right) V_{ft}^{\beta-1}}. \quad (6.9)$$

6.2 Piano transcription experiment

We evaluate the proposed method using the ‘ENSTDkCl’ subset of the MAPS database [Emiya et al., 2010], in which the piano recordings are produced by a Yamaha Disklavier upright piano. We trained the spectral templates using isolated notes played forte. The polyphonic musical pieces (the first 30 seconds)

are then transcribed with the trained templates.

6.2.1 Pre-processing

Computing STFT

The sample rate of the audio is $f_s = 44100$ Hz. To compute the STFT, each frame is weighted by a Gaussian window covering 4096 samples with a standard deviation of $N = 4096/6$ samples. In the time domain, the standard deviation of the window function is $\sigma = N/f_s$. The hop size is 882 samples. In order to locate the partial frequencies at the frequency bins, we need a high frequency resolution. Hence, we perform a 4-fold zero padding before computing the spectrum using a discrete Fourier transform (DFT).

The theoretical value of the spectral width

The Fourier transform of the window function $g_{\sigma_1}(t) = \frac{1}{\sqrt{2\pi\sigma_1^2}}e^{-t^2/(2\sigma_1^2)}$ with standard deviation of σ_1 is given by

$$G(f) = \mathcal{F}[g_{\sigma_1}](f) = e^{-2\pi^2\sigma_1^2 f^2}. \quad (6.10)$$

If we set the variance of $G(f)$ to σ_2^2 , then $e^{-f^2/(2\sigma_2^2)} = e^{-2\pi^2\sigma_1^2 f^2}$. So we can derive that $\sigma_2 = \frac{1}{2\pi\sigma_1}$. We know from the previous section that $\sigma_1 = N/f_s$. Then the standard deviation (spectral width) is $\sigma_2 = \frac{f_s}{2\pi N}$. The frequency resolution is the ratio of the sample rate f_s and the size of the DFT n_{fft} . We conclude that the spectral width covers $\frac{n_{fft}}{2\pi N}$ frequency bins. When we compute the STFT, $n_{fft} = 16384$ and $N = 4096/6$. So the theoretical value of spectral width is $\sigma = 3.82$ frequency bins.

6.2.2 Template training

We train spectral templates on isolated notes in forte from the ‘ENSTDkC1’ subset [Emiya et al., 2010]. For each pitch, we update the spectral template, activations and spectral widths via Equations 6.7, 6.8 and 6.9 with $K = 1$ for 30 iterations. The range of the Gaussian response is set to be within ± 30 frequency bins ($L = 30$).

Initialisation

In order to enforce a harmonic-comb shape for templates, we initialise the templates with the peaks of the mean spectrum. For each pitch, we first normalise the spectrum of each frame to a maximum of 1, and compute the average of the

normalised spectra. Then we detect peaks of the average normalised spectrum and use them as the initialisation of the spectral basis.

The activations are randomly initialised and the spectral widths are initialised with the theoretical value $\sigma = 3.82$.

Trained examples

There are four examples of tones of different pitches shown in Figure 6.3. We find several noticeable characteristics of the spectral width. (1) The spectral width is large around the onset, and is smaller and remains stable for the remaining duration of the note, as shown in Figure 6.3(a–c). (2) We can observe a small peak in the spectral width at the offset, as shown in Figure 6.3(b). (3) When the activation is small, the spectral width is ambiguous. The first case happens in frames before the onset and after the offset of a note, where the spectral width is theoretically undefined, hence expectedly noisy. The second case happens within the duration of the note with low amplitude. This usually occurs on high pitches. For example, as shown in Figure 6.3(d), when the amplitude is 20 dB lower than the maximum amplitude, the spectral width appears noisy.

We show the average spectral widths of all 88 notes in Figure 6.4(a). For each clip, we discard some of the silent part before the onset to make all notes start at 0.4 s, and notes end at around 2.5 s. It is clearly shown in Figure 6.4(b) that the stable average spectral width is above 6 frequency bins, and there is a major peak near the offset. Figure 6.4(c) is the histogram of the spectral width (below 20 frequency bins), indicating a mode of around 5.5 bins.

6.2.3 Post-processing

After obtaining the activations and spectral widths, we smooth both of them using a median filter covering 5 time frames. The smoothed activations are normalised to a maximum of 1 for each piece.

Onset and offset detection

Based on the training results, we know that spectral widths are less meaningful when activations are small. So we first detect active frames by thresholding on the activations for each pitch. We apply different thresholds for onsets and offsets. A note starts when the activation is larger than the onset threshold, and lasts till the activation decreases to below the offset threshold.

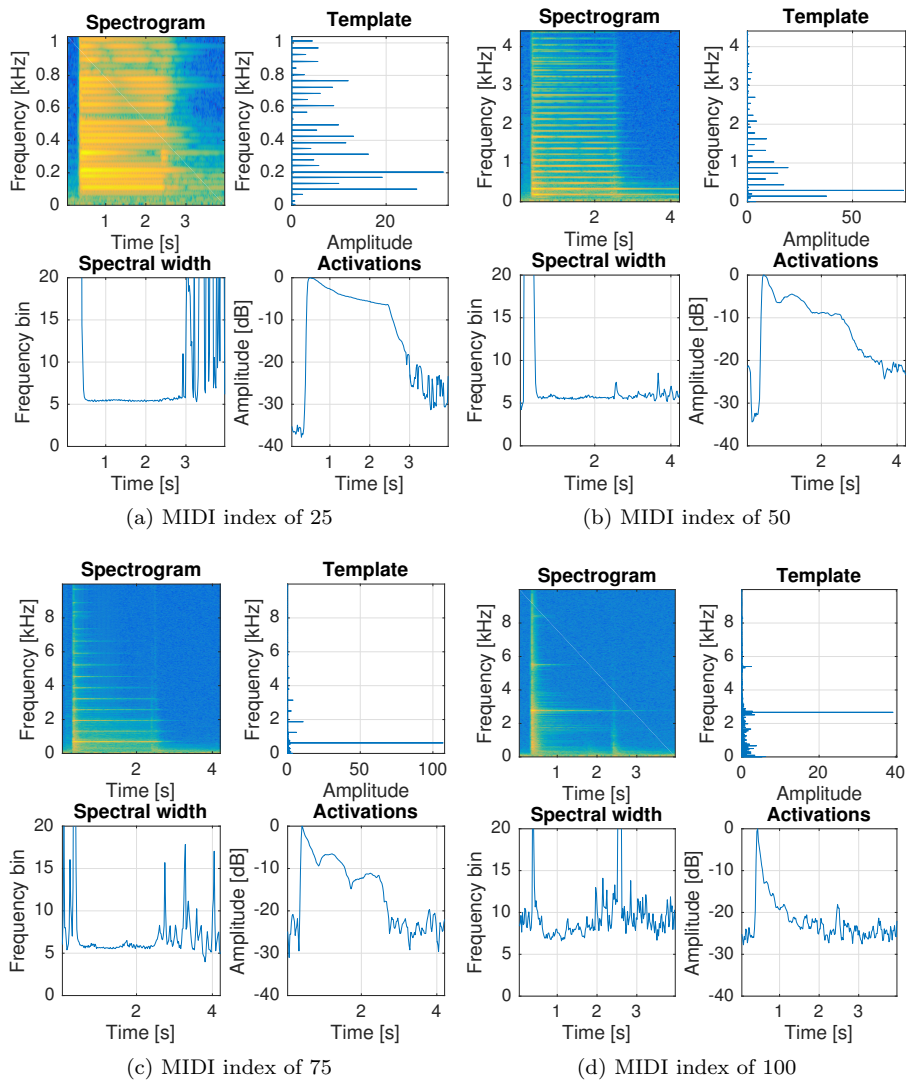


Figure 6.3: Spectrograms and extracted parameters: templates, activations and spectral widths for notes of different pitches

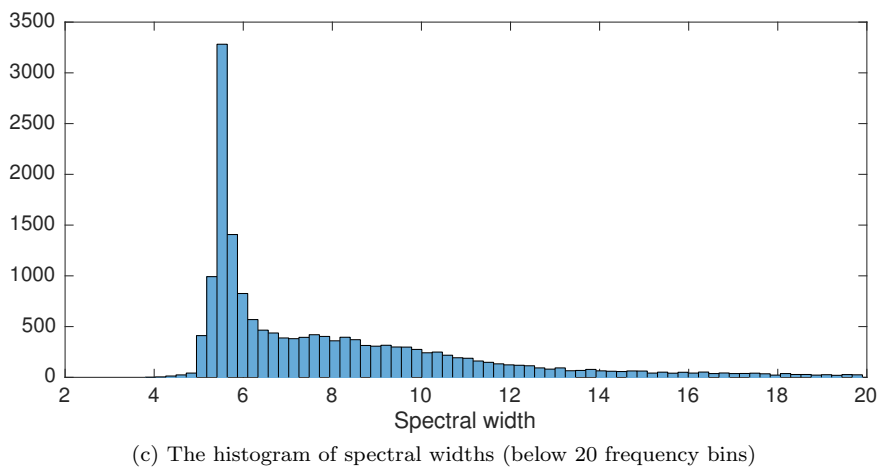
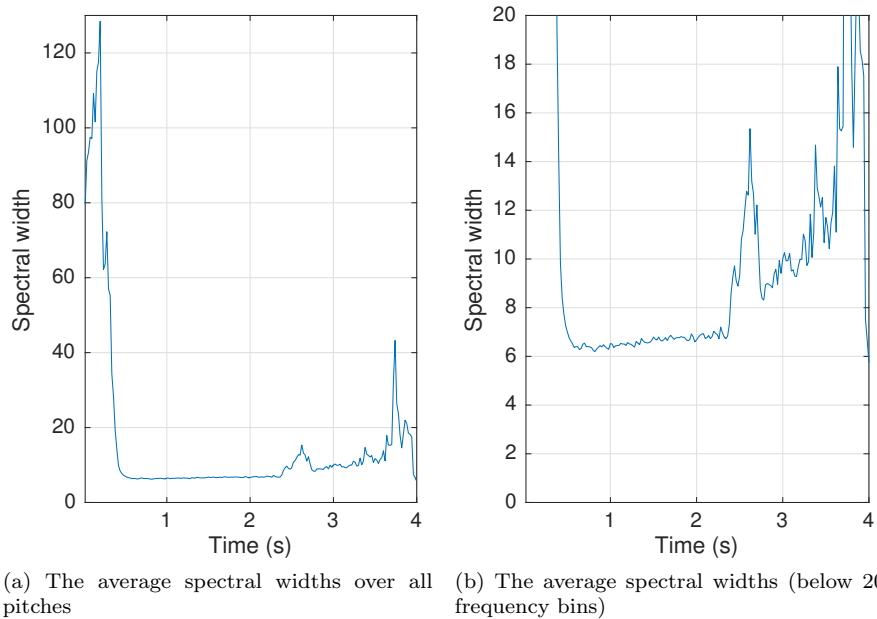


Figure 6.4: Trained spectral widths.

Spectral width constraints

After detecting the active frames, we use the spectral widths to refine onsets. We know that for isolated notes, the spectral width of a note is large around the onset. Based on this information, we first check the detected onsets. If the spectral width of an onset is smaller than M frequency bins, we delete the onsets. We test $M \in \{3, 4, 5\}$ in the experiments.

Then we detect more onsets at frames where both the activation and spectral width are large. When the normalised activation is larger than 0.3, and the spectral width is larger than N frequency bins, activation peaks are also detected as onsets. We test $N \in \{6, 7, 8\}$ in the experiments.

6.2.4 Results

In the transcription experiment, we update the activations and spectral widths with fixed spectral templates from the training stage. Spectral widths are initialised to 5.5 frequency bins, and activations are initialised randomly.

We use frame-wise metrics and onset-only note tracking metrics to evaluate the systems. A detailed explanation of the metrics is given in Section 2.4.

Transcription results

In the experiment, we compare the proposed system to a standard NMF baseline system (stdNMF). The standard NMF also uses fixed templates, which are trained using a rank-one NMF on the isolated notes. For all methods, notes are detected on activations with an optimal onset threshold and the offset threshold of -40 dB below the maximum activation of each musical piece. The optimal onset thresholds of the proposed system and the NMF system are -17 dB and -19 dB, respectively.

Table 6.1(a) shows the onset-only note tracking results. The proposed system by thresholding (SWA) has an F-measure of 76.98%. The ‘SWMX’ systems delete onsets with spectral widths smaller than X frequency bins. Systems SWM3 and SWM4 bring small improvements on the note tracking results. The results suggest that few detected onsets have spectral width smaller than 4 frequency bins. When deleting onsets with spectral widths smaller than 5 frequency bins, we find more true onsets are deleted than false onsets, resulting in a high precision and a low recall. The F-measure declines by 2.3 percentage points in this case.

The ‘SWNX’ systems add onsets whose spectral widths are larger than X frequency bins and activations larger than 0.3. These systems slightly improve the F-measure of note tracking, with decreased precisions and increased recalls.

Table 6.1: Comparison of the proposed systems with a standard NMF

(a) Note tracking results (onset-only)				
method	P_{on}	R_{on}	F_{on}	A_{on}
SWA	80.29	74.89	76.98	63.73
SWM3	80.30	74.89	76.99	63.73
SWM4	80.94	74.44	77.08	63.87
SWM5	84.85	67.41	74.69	61.02
SWN6	79.16	76.90	77.48	64.28
SWN7	80.14	75.47	77.24	64.05
SWN8	80.26	75.22	77.15	63.94
stdNMF	78.70	76.73	77.22	64.07

(b) Frame-wise results				
method	P_f	R_f	F_f	A_f
SWA	79.20	79.60	78.36	64.83
stdNMF	79.32	79.46	78.35	64.79

When the constraint on spectral width becomes larger, the difference from the SWA system is smaller, because the number of newly-detected onsets decreases with the increasing spectral width.

The F-measure of the standard NMF is 77.22%. There are no significant differences between the proposed systems and the NMF system. Only the proposed system of SWN6 has a slightly better F-measure than that of stdNMF.

The frame-wise results are listed in Table 6.1(b). Because refining onsets using spectral widths usually does not change the frame-wise results, we only show results of the proposed ‘SWA’ system. The frame-wise results of the proposed system and the NMF system are similar to each other, with F-measures of 78.4%.

The results show that refining onsets using spectral widths barely brings improvements in transcription performance, and there are no significant differences between the proposed methods and the standard NMF.

Spectral width distributions

In order to find more sophisticated methods to deal with spectral widths, we analyse their statistical characteristics. Figure 6.5 shows the distribution of spectral widths at the onsets for different pitches. We find that not all onsets have large spectral widths. The median spectral widths of most low-pitch notes are below 6 frequency bins at the onsets. The value increases for notes with

higher pitch. We suppose that it is related to the frequency interval between partials. The adjacent partials are overlapped when the spectral width is larger than a half of the fundamental frequency (frequency interval). Then the spectral widths of the onsets are limited by the fundamental frequency. Note that the observation of the spectral widths at onsets in training stage is different from that in the transcription experiment. Because in the training stage we perform a rank-one NMF, the percussive onset can only be represented by the note. Then it usually has a large onset spectral width. In the transcription experiment, the spread spectral distribution at the onset can be explained by other notes, and the spectral width is influenced more by the adjacent frequency bins of the partials.

For each pitch, the spectral widths also vary, depending on the number of notes played at the moment. If there is only one note played, the spectral width is large at the onset. If there are several notes played simultaneously, the spectral width of one note can be small because the spread energy may be represented by other notes.

This explains why we can not improve the results by simply deleting onsets with small spectral widths. In the future, we can try to extend this model in a CQT TF representation, which has constant spaces between partials for all pitches. However, we would need to deal with another problem of the model in the CQT: the spectral widths of partials of a note change with frequency.

Figure 6.6 shows the distribution of spectral widths in the decay parts. In the middle pitch range, the median value of the spectral widths is around 5 frequency bins. Notes in the low pitch range tend to have smaller spectral widths, and the spectral width is less predictable for pitches above MIDI index of 80. Even for notes of the same pitch, the range of the spectral width is large. First we know that the spectral width is closely related to the activation. When the activation is small, the spectral width is small too. Secondly the spectral width is easily influenced by notes of other pitches. For example, in Figure 6.7 the note of pitch D4 (MIDI index 62) starts at around 0.5 s and lasts till the end of the clip. When the note activations are relatively large (before 5 s as shown in Figure 6.7(b)), the spectral widths in most frames are around 5 frequency bins, as shown in Figure 6.7(a). The false peaks in the spectral width occur because notes of other pitches start.

We summarise the reasons for slight improvements by adding more onsets with large activations and spectral widths as follows. First, these onsets are easy to detect; some of the added onsets have been already detected by thresholding. Secondly, because the spectral width is influenced by the activation and other notes, there are also false onsets detected along with the true onsets. In the future, we need to reduce the dependence of the spectral widths on the

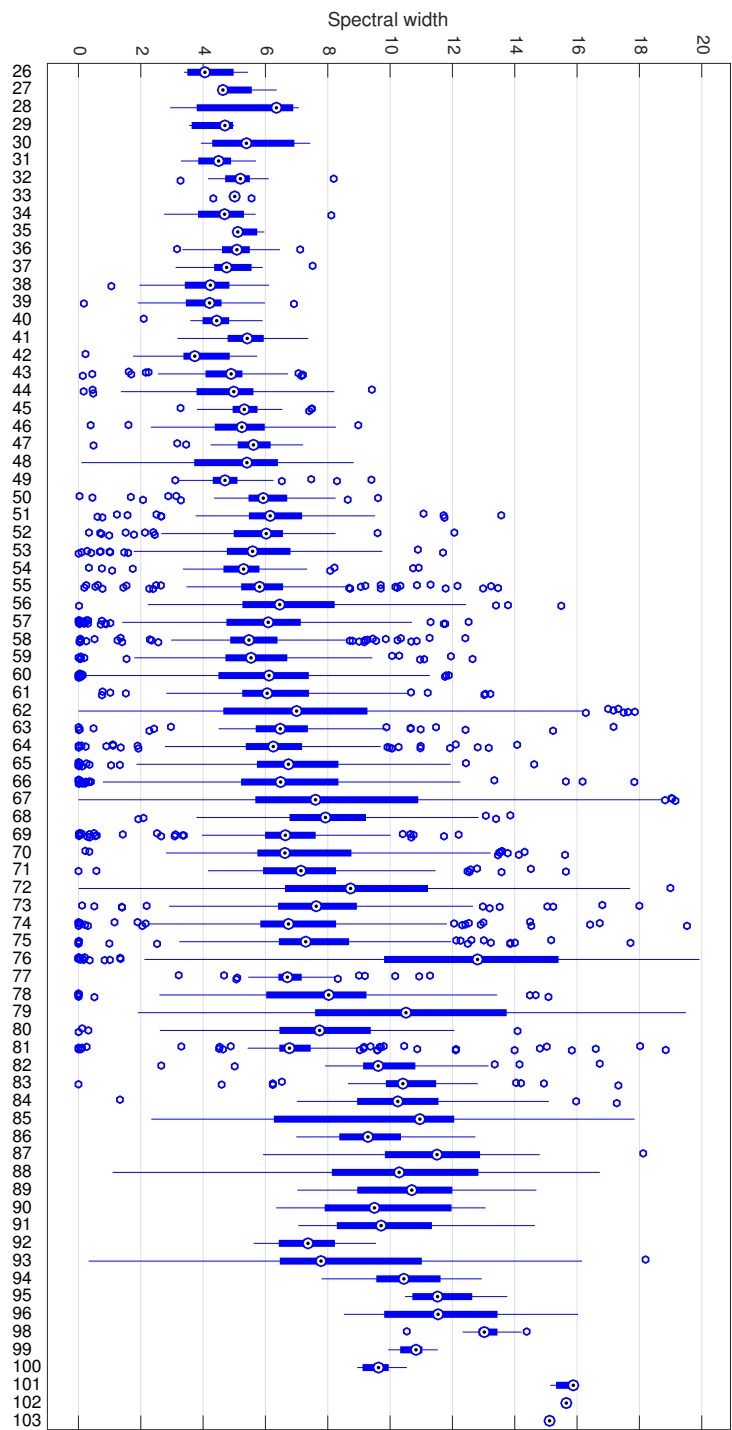


Figure 6.5: Box-and-whisker plots of spectral widths (below 20 frequency bins) at onsets, with pitch in MIDI index on the vertical axis.

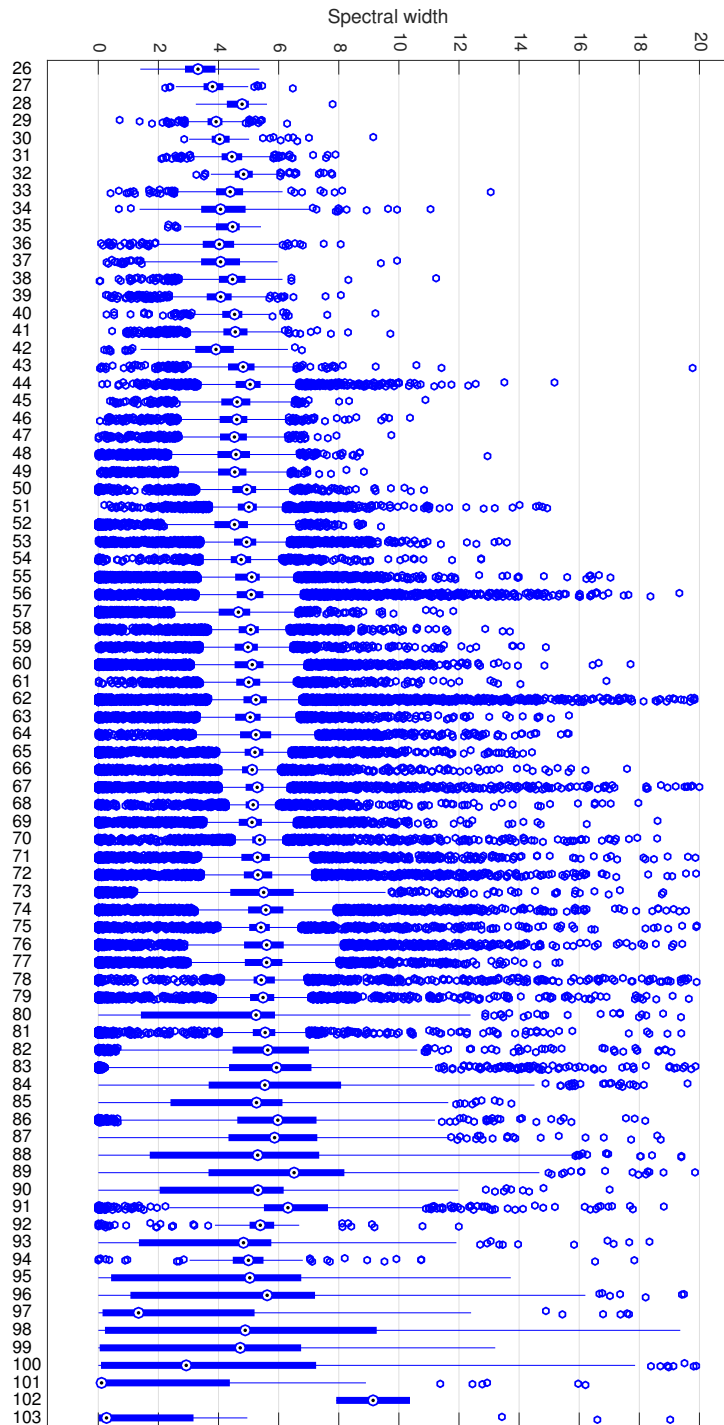


Figure 6.6: Box-and-whisker plots of spectral widths (below 20 frequency bins) in decay stages, with pitch in MIDI index on the vertical axis.

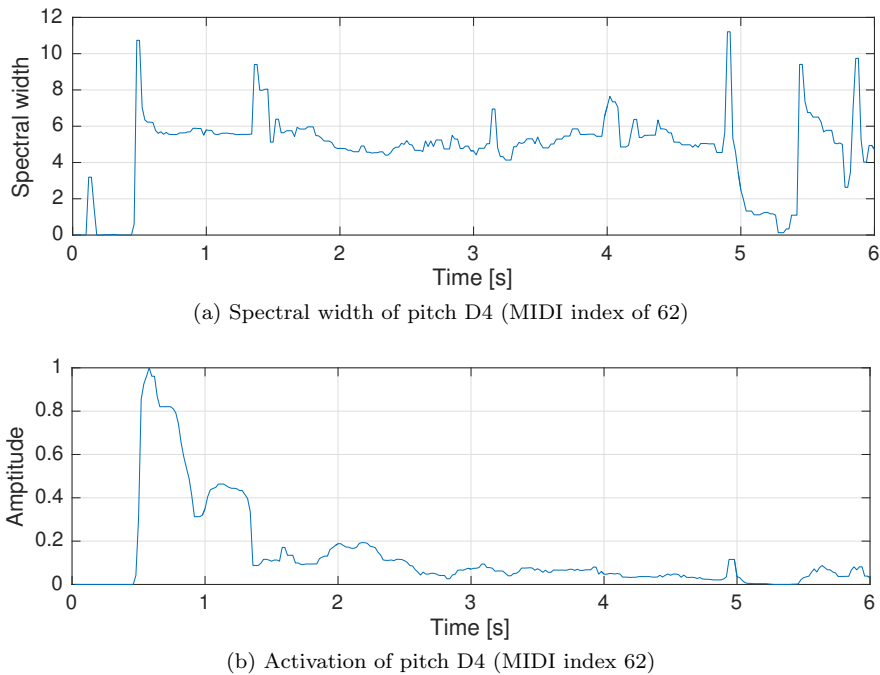


Figure 6.7: An example of the spectral width and activation for one pitch during the first 6 seconds of the piece ‘alb_se2’.

activations and impose constraints on spectral widths, such as continuity.

6.3 Conclusions and future work

In this chapter we study the spectral width for piano transcription. We first model the spectral width of a partial by the standard deviation of the Gaussian window response. Then we present the spectral basis by the convolution of a comb-shaped spectral basis and a Gaussian function. So different spectral distributions of the attack and decay parts can be modelled by different spectral widths. All unknown parameters are estimated in the NMF framework.

In the training stage we find the spectral width is large in the attack part, and is smaller and remain stable in the decay part. But the spectral width is related to the activation, which is less meaningful when the activation is small. In the transcription experiment, we find that the results of proposed systems are similar to that of a standard NMF system. Refining onsets by the spectral width shows no significant differences in the transcription performance.

The spectral width distribution at onsets shows that the spectral width is pitch-dependent at onsets in musical pieces, with a trend that higher pitch notes have larger spectral widths at onsets. The spectral width distribution

in the decay parts shows more than half of the spectral widths are around 5 frequency bins, but there are still large numbers of spectral widths outside the range.

In this chapter, we have only an exploration on the spectral width. In the future, in order to effectively use the spectral width information, we first would like to extend the method in a CQT TF representation, to deal with the pitch-dependent spectral width for onsets. In addition, the length of the frames compared to the decay time should be studied in detail to explain the spectral widths of onsets. Thirdly, we need to decouple the dependence of the spectral width on the activation. At last, we will experiment with imposing constraints on spectral widths to reduce the influence by simultaneous notes.

Chapter 7

Conclusions and Future Work

In this thesis, we study piano acoustics for automatically transcribing polyphonic music. We focus on features such as the time-varying timbre and decay amplitudes of piano notes, and model these acoustical features from different aspects with the parametric NMF. This chapter first summarises the primary work of the main chapters, then we show several directions worth future investigation.

7.1 Conclusions

In Chapter 3, we address the local minimum problem of a PLCA-based transcription method with a deterministic annealing EM algorithm. The EM-based update rules are modified by introducing a temperature parameter. A more fine-grained optimisation can be found by gradually decreasing the temperature. The results show that the proposed method improves the transcription performance. The optimisation method can also be adapted to the NMF-based model, because of the similarity between these two matrix factorisation methods. In Chapter 5, we use a similar annealing process in the proposed NMF-based model.

In Chapter 4, we study piano decay in real recordings. We first find partials by modelling their inharmonicity, and then track the decay of the partials. We focus on three decay patterns with spectral power in dB: linear decay, double decay and decay with amplitude modulations (beats) according to the theoretical studies on coupled piano strings [Weinreich, 1977]. We track first 30 partials below the Nyquist frequency of 88 notes in three dynamic levels. The results

verify that partials of higher frequencies decay faster, and the dynamic level has less impact on the decay pattern.

In Chapter 5, we propose an attack/decay model for piano transcription, with the spectra of the attack and decay parts represented by two individual spectral templates for each pitch. This method also models the amplitude envelopes for the two parts. The attack envelopes are trained on isolated notes, and we use the average attack envelope over all pitches. The decay envelope is parameterised by an exponential decay function, with the decay rate trained for each isolated note. The two parts are coupled by the note activations, which means that the decay part always occurs after the corresponding attack part. We detect onsets on attack activations by peak-picking and track pitch states by dynamic programming to find offsets.

The attack/decay model provides promising transcription results and outperform two state-of-the-art methods on the MAPS database [Emiya et al., 2010]. In the transcription experiments, we compare the fixed sparsity factors and annealing sparsity factors, based on our studies in Chapter 3. Results indicate that the annealing sparsity factor improves both performance and the robustness of the proposed model slightly. The exponential decay is a simplification of the observed decay patterns in Chapter 4, but it is sufficiently close to reality to give the observed improvement in transcription results.

We test the proposed method on repeated notes of single pitches. Results indicate that the assumption of exponential decay causes many false positives on notes in the low pitch range, due to the beats in the decay. The simplification of ignoring offsets at the first stage works well for long notes, but may cause false negatives on short notes.

The onset-offset note tracking results in Chapter 5 suggest that it is hard to detect offsets on decaying energies. In order to find a more stable indicator for note tracking, we preliminarily study the spectral widths of piano partials in Chapter 6. In the proposed model, the time-varying timbre of a piano note in the attack and decay parts is parameterised by the same spectral basis with different spectral widths. The spectral basis consists of peaks at frequencies of partials. We assume that the spectral width is large at the attack part, but is smaller and remains constant in the decay part. We represent the spectral shape of a partial by a Gaussian function. The expected value of the Gaussian function is the partial frequency and we use the standard deviation σ to indicate the spectral width. With this parametric spectral template, we can estimate spectral widths directly in the NMF framework.

In the training stage the spectral widths of most isolated notes are in line with our assumption: large in the attack part, and smaller and stable in the decay part. But when the activation of the note is small, the spectral width is

less predictable, especially for high-pitch notes. In the transcription experiment, the results of proposed systems are similar to those of a standard NMF system. No difference in transcription performance is obtained by using the spectral widths to refine the detected onsets.

In order to find the problems of this preliminary model, we analyse the spectral distribution in the attack and decay parts in polyphonic music pieces individually. The spectral width distribution at onsets shows that the spectral width is pitch-dependent at onsets in musical pieces, with higher pitch notes having larger spectral widths. The spectral width distribution in the decay parts shows more than 50% of spectral widths are around 5 frequency bins, but there are still large numbers of spectral widths outside this range.

The methods presented in this thesis are based on the matrix-factorisation method. Because the time-varying timbre and decay of energy are not well fitted by this kind of method, we extend the NMF method using cues from piano acoustics. Based on the proposed methods we can design a combined transcription system. Both models in Chapter 5 and 6 present the attack and decay parts of piano sounds separately. We can use the representation in Chapter 6 for the attack/decay model in Chapter 5: the attack part is represented by partials with large spectral widths, and the decay part by partials with small spectral widths. The method in Chapter 3 addresses the local minimum problem as an optimisation problem. It could be generalised for parameter estimation in the NMF framework.

7.2 Further work

Modelling the decay

In the attack/decay model (Chapter 5), we first simplify the note amplitudes to decay exponentially. Based on the studies in Chapter 4, we know that the decay is frequency-dependent, with upper partials usually decaying more quickly. We would like to extend the exponential decay model to be frequency-dependent by replacing the decay rate by a decay filter. Another simplification of the model is that the amplitude of a note is assumed to decay till the end of the music piece, so that we do not need to deal with offsets when we formulate the model in the NMF framework. If we consider the parametric attack and decay parts as a parametric patch, this simplification means that the parameter patches are of the same length as the music pieces. In the future, we would like to extend the model with note-varying durations, which are expected to improve the transcription performance on piano pieces with many short notes.

The idea of decay modelling can also be extended to existing methods. For example, we find that the unsupervised transcription system [Vincent et al., 2010] in the comparison experiment of Chapter 5 is a good baseline method. Each template in this method is a weighted combination of narrow-band spectral bases. We can extend the system with decay parameters to build an unsupervised system. We can further model each narrow-band spectral basis to decay at different rates to build a model which is closer to the real decay of piano notes.

Modelling spectral widths

In Chapter 6, we present a preliminary study on spectral width. The most distinguishing problem is that the spectral width is dependent on the note amplitude. The spectral width is only interpretable when the corresponding note amplitude is large enough. We need to decouple the dependence of the spectral width on the amplitude. Secondly, the spectral widths are fluctuating, and are easily influenced by simultaneous notes. We expect that this problem could be lessened by imposing constraints, such as sparsity and continuity, on activations and spectral widths. In our analysis of the spectral width distribution of the note onsets, we find that the spectral width of an note onset is related to the interval between adjacent partials. We would like to extend the method with a CQT TF representation, to deal with the pitch-dependent spectral widths of onsets.

Extension to other pianos

We would like to extend the idea of modelling acoustic features of a particular piano to a general model of an arbitrary piano in the future. The research questions associated with this direction are: what are the primary differences between two pianos, and can we share the similar parts but only model the differences when the training dataset and the test dataset are produced by different pianos?

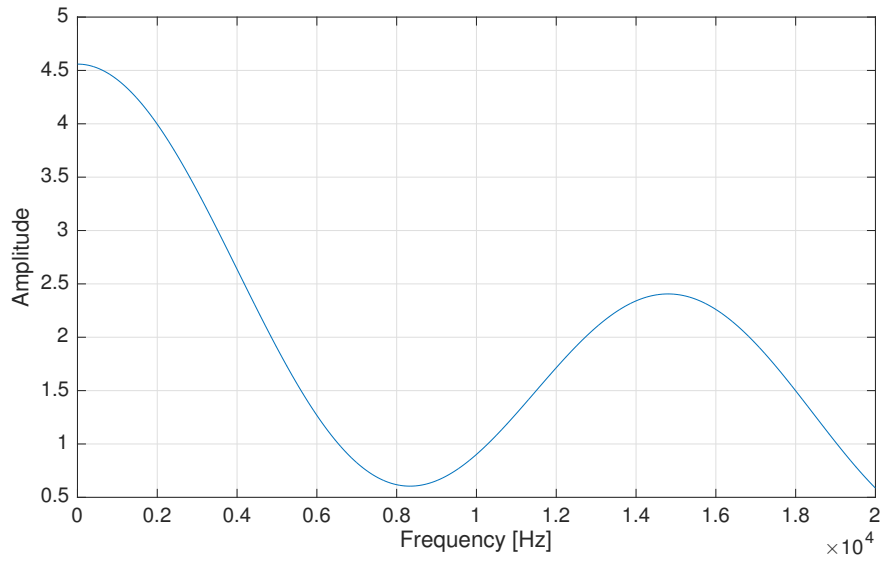
From the concept of the source-filter model, a piano has 88 sources (one for each pitch) and a filter (the soundboard). Modelling a piano with the source-filter model is not suitable, as evidenced by our previous work [Cheng et al., 2014]. For a particular piano, we can train spectral templates on each isolated note. But for another piano, can we use the same trained templates, but introduce a filter to model the difference between the frequency responses of the two pianos?

To illustrate the idea, we extended the model for spectral widths (Chapter 6) with a filter to model the frequency response difference. The filter is param-

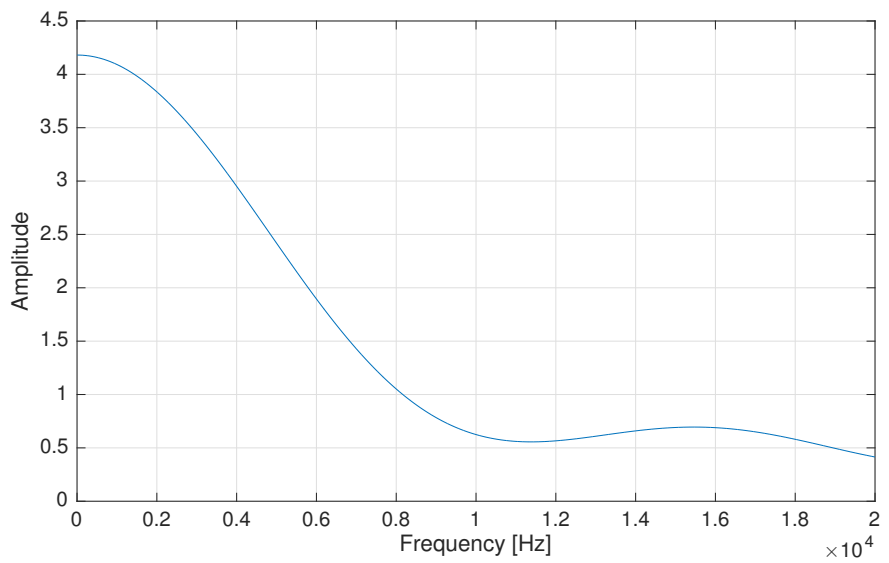
eterised using the auto-regressive moving average (ARMA) model [Hennequin et al., 2011a]. We use the templates trained on the subset ENSTDkCl subset (Disklavier piano) of the MAPS database [Emiya et al., 2010], and employ the extended model on music pieces in the ENSTDkAm subset (Disklavier piano) and the AkPnCGdD subset (synthetic piano). The estimated filters are shown in Figure 7.1. We find that there are fewer high-frequency partials resonated in the synthetic piano. Although in the preliminary test, we find no difference in transcription results with and without the filter, we would like to work further on this direction in the future.

Extension to other instruments

The proposed methods are motivated by piano acoustics. We suppose that they can be used on instruments with similar acoustical features. The attack/decay model in Chapter 5 should be apt in struck-string (for example the dulcimer) or plucked-string instruments (for instance the harpsichord and guitar), because the sounds produce by these kinds of instruments also have percussive onsets and then decaying energies. The spectral width model in Chapter 6 is more general. All harmonic sounds should have stable spectral widths, so we imagine this model could have application across a large range of instrumental sounds.



(a) The filter between ENSTDkCl and ENSTDkAm



(b) The filter between ENSTDkCl and AkPnCGdD

Figure 7.1: Filters for modelling the frequency response difference between two pianos.

Appendix A

Beating in the dB scale

In [Weinreich, 1977], the beating of two strings is represented by Equation (20), which is written as follows:

$$R(t) = \exp(-2\eta t) \times (\mu \cos \mu t - \eta \sin \mu t)^2 / \mu^2, \quad (\text{A.1})$$

where the beating frequency is 2μ and the decay rate is 2η . We know that

$$(\mu \cos \mu t - \eta \sin \mu t)^2 = (\mu^2 + \eta^2) \cos(\mu t + \varphi)^2, \quad (\text{A.2})$$

where $\varphi = \arg \tan(\eta/\mu)$. Then the equation can be rewritten as:

$$R(t) = \exp(-2\eta t) \times \frac{\mu^2 + \eta^2}{\mu^2} \times \cos(\mu t + \varphi)^2. \quad (\text{A.3})$$

We write the equation in the dB scale for curve fitting:

$$\begin{aligned} R_{dB}(t) &= 20 \log_{10}(\exp(-2\eta t) \times \frac{\mu^2 + \eta^2}{\mu^2} \times \cos(\mu t + \varphi)^2) \\ &= 20 \log_{10}(\exp(-2\eta t)) + 20 \log_{10}(\frac{\mu^2 + \eta^2}{\mu^2}) + 20 \log_{10}(\cos(\mu t + \varphi)^2) \\ &= -40\eta \log_{10}(e) \times t + 20 \log_{10}(\frac{\mu^2 + \eta^2}{\mu^2}) + 40 \log_{10}(|\cos(\mu t + \varphi)|). \end{aligned} \quad (\text{A.4})$$

We replace the parameters with $a = -40\eta \log_{10}(e)$ and $b = 20 \log_{10}(\frac{\mu^2 + \eta^2}{\mu^2})$, then the equation can be written as:

$$R_{dB}(t) = at + b + 40 \log_{10}(|\cos(\mu t + \varphi)|). \quad (\text{A.5})$$

This equation represents the purely resistive coupling of the two strings. The amplitude of the beating will change if this is not the case [Weinreich, 1977]. So we replace 40 by A , which is a parameter to estimate. We also replace μ by f to intuitively represent the frequency, and a small value ε is added to avoid taking the log of 0. Then the final equation is written as:

$$R_{dB}(t) = at + b + A \log_{10}(|\cos(ft + \varphi)| + \varepsilon), \quad (\text{A.6})$$

which is the form we use in Equation 4.5.

Appendix B

Derivations for the attack/decay model

As described in Chapter 5, the proposed model is formulated as follows:

$$\begin{aligned}
 V_{ft} &= \sum_{k=1}^K W_{fk}^a H_{kt}^a + \sum_{k=1}^K W_{fk}^d H_{kt}^d \\
 &= \sum_{k=1}^K W_{fk}^a \sum_{\tau=t-T_a}^{t+T_a} H_{k\tau} P(t-\tau) + \sum_{k=1}^K W_{fk}^d \sum_{\tau=1}^t H_{k\tau} e^{-(t-\tau)\alpha_k},
 \end{aligned} \tag{B.1}$$

where \mathbf{V} is the reconstruction of the spectrogram, $f \in [1, F]$ is the frequency bin, and $t \in [1, T]$ indicates the time frame. \mathbf{W}^a and \mathbf{W}^d are the percussive and harmonic templates, and $k \in [1, K]$ is the pitch index. \mathbf{H}^a are attack activations, generated by the convolution of note activations \mathbf{H} and the attack envelope \mathbf{P} . \mathbf{H}^d are decay activations and α_k are decay factors. In Chapter 5, we assume the harmonic phase starts at the onset time, then the maximum value of the trained attack envelope occurs at one frame before the onset.

We add a parameter T_d to control the start time of the harmonic part. Decay activations are therefore represented by:

$$H_{kt}^d = \sum_{\tau=1}^{t-T_d} H_{k\tau} e^{-(t-(\tau+T_d))\alpha_k}. \tag{B.2}$$

This indicates that the harmonic part starts at T_d frames after the onset. When the music piece is too long, we also need a parameter as the maximal duration T_{max} . Then in the convolution, $\max(1, t - T_{max}) \leq \tau \leq t - T_d$. We set $t_m =$

$\max(1, t - T_{max})$, then decay activations are represented as:

$$H_{kt}^d = \sum_{\tau=t_m}^{t-T_d} H_{k\tau} e^{-(t-(\tau+T_d))\alpha_k}. \quad (\text{B.3})$$

Then the complete proposed model is formulated as follows:

$$V_{ft} = \sum_{k=1}^K W_{fk}^a \sum_{\tau=t-T_a}^{t+T_a} H_{k\tau} P(t-\tau) + \sum_{k=1}^K W_{fk}^d \sum_{\tau=t_m}^{t-T_d} H_{k\tau} e^{-(t-(\tau+T_d))\alpha_k}. \quad (\text{B.4})$$

In Chapter 5, we use a simplified model with $T_d = 0$ and $T_{max} = T$, then $t_m = 1$. Here we work on the complete model.

The parameters are estimated by minimising the distance between the spectrogram and the reconstruction by multiplicative update rules [Lee and Seung, 2000]. The derivative of the cost function with respect to (w.r.t.) θ is written as a difference of two non-negative functions:

$$\nabla_{\theta} D(\theta) = \nabla_{\theta}^+ D(\theta) - \nabla_{\theta}^- D(\theta). \quad (\text{B.5})$$

The multiplicative algorithm is given by $\theta \leftarrow \theta \cdot \nabla_{\theta}^- D(\theta) / \nabla_{\theta}^+ D(\theta)$. We minimise the β -divergence between the spectrogram \mathbf{X} and the reconstruction \mathbf{V} , with the β -divergence given as follows [Févotte, 2011]:

$$d_{\beta}(x|y) = \begin{cases} \frac{1}{\beta(\beta-1)}(x^{\beta} + (\beta-1)y^{\beta} - \beta xy^{\beta-1}) & \beta \in \mathbb{R} \setminus \{0, 1\}, \\ x \log \frac{x}{y} - x + y & \beta = 1, \\ \frac{x}{y} - \log \frac{x}{y} - 1 & \beta = 0. \end{cases} \quad (\text{B.6})$$

The derivative of the β -divergence w.r.t. θ is given by [Févotte, 2011]:

$$\begin{aligned} \nabla_{\theta} D(\theta) &= \nabla_{\theta} d_{\beta}(X|V(\theta)) \\ &= (V(\theta)^{\beta-1} - XV(\theta)^{\beta-2}) \nabla_{\theta} V(\theta). \end{aligned} \quad (\text{B.7})$$

The update rule is [Févotte, 2011]

$$\theta \leftarrow \theta \cdot \frac{V(\theta)^{\beta-1} \nabla_{\theta}^- V(\theta) + XV(\theta)^{\beta-2} \nabla_{\theta}^+ V(\theta)}{XV(\theta)^{\beta-2} \nabla_{\theta}^- V(\theta) + V(\theta)^{\beta-1} \nabla_{\theta}^+ V(\theta)}. \quad (\text{B.8})$$

The derivative of V_{ft} w.r.t. W_{fk}^a is

$$\nabla_{W_{fk}^a} V_{ft} = \nabla_{W_{fk}^a}^+ V_{ft} = \sum_{\tau=t-T_a}^{t+T_a} H_{k\tau} P(t-\tau), \quad (\text{B.9})$$

then the update rule of W_{fk}^a is

$$W_{fk}^a \leftarrow W_{fk}^a \frac{\sum_{t=1}^T \sum_{\tau=t-T_a}^{t+T_a} H_{k\tau} P(t-\tau) (V_{ft}^{\beta-2} X_{ft})}{\sum_{t=1}^T \sum_{\tau=t-T_a}^{t+T_a} H_{k\tau} P(t-\tau) V_{ft}^{\beta-1}}. \quad (\text{B.10})$$

The derivative of V_{ft} w.r.t. W_{fk}^d is

$$\nabla_{W_{fk}^d} V_{ft} = \nabla_{W_{fk}^d}^+ V_{ft} = \sum_{\tau=t_m}^{t-T_d} H_{k\tau} e^{-(t-(\tau+T_d))\alpha_k}, \quad (\text{B.11})$$

then the update rule of W_{fk}^d is

$$W_{fk}^d \leftarrow W_{fk}^d \frac{\sum_{t=1}^T \sum_{\tau=t_m}^{t-T_d} H_{k\tau} e^{-(t-(\tau+T_d))\alpha_k} (V_{ft}^{\beta-2} X_{ft})}{\sum_{t=1}^T \sum_{\tau=t_m}^{t-T_d} H_{k\tau} e^{-(t-(\tau+T_d))\alpha_k} V_{ft}^{\beta-1}}. \quad (\text{B.12})$$

The derivative of V_{ft} w.r.t. α_k is

$$\nabla_{\alpha_k} V_{ft} = \nabla_{\alpha_k}^- V_{ft} = W_{fk}^d \sum_{\tau=t_m}^{t-T_d} H_{k\tau} e^{-(t-(\tau+T_d))\alpha_k} (t - (\tau + T_d)), \quad (\text{B.13})$$

then the update rule of α_k is

$$\alpha_k \leftarrow \alpha_k \frac{\sum_{f=1}^F \sum_{t=1}^T W_{fk}^d \sum_{\tau=t_m}^{t-T_d} H_{k\tau} e^{-(t-(\tau+T_d))\alpha_k} (t - (\tau + T_d)) V_{ft}^{\beta-1}}{\sum_{f=1}^F \sum_{t=1}^T W_{fk}^d \sum_{\tau=t_m}^{t-T_d} H_{k\tau} e^{-(t-(\tau+T_d))\alpha_k} (t - (\tau + T_d)) (V_{ft}^{\beta-2} X_{ft})}. \quad (\text{B.14})$$

We set $x = t - \tau$, then the reconstruction is given by replacing t with $\tau + x$

$$V_{f(\tau+x)} = \sum_{k=1}^K W_{fk}^a \sum_{\tau=t-T_a}^{t+T_a} H_{k\tau} P(x) + \sum_{k=1}^K W_{fk}^d \sum_{\tau=t_m}^{t-T_d} H_{k\tau} e^{-(x-T_d)\alpha_k} \quad (\text{B.15})$$

We derive the ranges of the two summations with respect to x . In the first one $t - T_a \leq \tau \leq t + T_a \Rightarrow t - T_a \leq t - x \leq t + T_a$, so $-T_a \leq x \leq T_a$. In the second one the upper limit is $\tau \leq t - T_d \Rightarrow t - x \leq t - T_d$, so $x \geq T_d$. The lower limit is $\tau \geq \max(1, t - T_{max})$. If $t - T_{max} > 1 \Rightarrow t - x \geq t - T_{max}$, so $x \leq T_{max}$. If $t - T_{max} \leq 1 \Rightarrow \tau \geq 1$, which gives no restriction to the range of x . Then the range is determined by the following restriction: $t \leq T_{max} + 1 \Rightarrow \tau + x \leq T_{max} + 1$, so $1 \leq \tau \leq T_{max} + 1 - x \Rightarrow x \leq T_{max}$. Combining these two conditions, we have $T_d \leq x \leq T_{max}$. With these two ranges, the reconstruction is rewritten as

$$V_{f(\tau+x)} = \sum_{k=1}^K W_{fk}^a \sum_{x=-T_a}^{T_a} H_{k\tau} P(x) + \sum_{k=1}^K W_{fk}^d \sum_{x=T_d}^{T_{max}} H_{k\tau} e^{-(x-T_d)\alpha_k} \quad (\text{B.16})$$

We replace τ with t to obtain more consistent equations:

$$V_{f(t+x)} = \sum_{k=1}^K W_{fk}^a \sum_{x=-T_a}^{T_a} H_{kt} P(x) + \sum_{k=1}^K W_{fk}^d \sum_{x=T_d}^{T_{max}} H_{kt} e^{-(x-T_d)\alpha_k} \quad (\text{B.17})$$

The derivative of V_{ft} w.r.t. H_{kt} is

$$\nabla_{H_{kt}} V_{f(t+x)} = \nabla_{H_{kt}}^+ V_{f(t+x)} = W_{fk}^a \sum_{x=-T_a}^{T_a} P(x) + W_{fk}^d \sum_{x=T_d}^{T_{max}} e^{-(x-T_d)\alpha_k}, \quad (\text{B.18})$$

then the update rule of H_{kt} is

$$H_{kt} \leftarrow H_{kt} \frac{\sum_{f=1}^F (W_{fk}^a \sum_{x=-T_a}^{T_a} P(x) + W_{fk}^d \sum_{x=T_d}^{T_{max}} e^{-(x-T_d)\alpha_k}) (V_{f(t+x)}^{\beta-2} X_{f(t+x)})}{\sum_{f=1}^F (W_{fk}^a \sum_{x=-T_a}^{T_a} P(x) + W_{fk}^d \sum_{x=T_d}^{T_{max}} e^{-(x-T_d)\alpha_k}) V_{f(t+x)}^{\beta-1}}. \quad (\text{B.19})$$

The derivative of V_{ft} w.r.t. $P(x)$ with Equation B.17 is :

$$\nabla_{P(x)} V_{f(t+x)} = \nabla_{P(x)}^+ V_{f(t+x)} = \sum_{k=1}^K W_{fk}^a H_{kt}, \quad (\text{B.20})$$

then the update rule of $P(x)$ is

$$P(x) \leftarrow P(x) \frac{\sum_{f=1}^F \sum_{t=1}^T \sum_{k=1}^K W_{fk}^a H_{kt} (V_{f(t+x)}^{\beta-2} X_{f(t+x)})}{\sum_{f=1}^F \sum_{t=1}^T \sum_{k=1}^K W_{fk}^a H_{kt} V_{f(t+x)}^{\beta-1}}. \quad (\text{B.21})$$

Appendix C

Derivations for modelling spectral widths

In Chapter 6, we propose a parametric NMF model with time-varying spectral widths for each pitch. The Gaussian function representing the spectral shape for partials of pitch k at the t^{th} frame is given by:

$$G(f|\sigma_{kt}) = \exp\left(-\frac{f^2}{2\sigma_{kt}^2}\right), -3\sigma_{kt} \leq f \leq 3\sigma_{kt} \quad (\text{C.1})$$

where σ_{kt} is the time-varying standard deviation (spectral width), and the Gaussian function has a maximum value of 1 and is restricted in a range of $\pm 3\sigma_{kt}$. The spectrum of pitch k in the f^{th} frequency bin and the t^{th} frame V_{ft}^k is modelled by the convolution of the spectral basis \mathbf{w}_k and the Gaussian window response $G(f|\sigma_{kt})$, scaled by the current activation H_{kt} :

$$V_{ft}^k = [\mathbf{w}_k * G(f|\sigma_{kt})]_f H_{kt} = \sum_{f'=-3\sigma_{kt}}^{3\sigma_{kt}} W_{(f-f')k} \exp\left(-\frac{f'^2}{2\sigma_{kt}^2}\right) H_{kt}, \quad (\text{C.2})$$

where the spectral basis ($\mathbf{w}_k \in \mathbb{R}^F$) only has peaks at the partial frequencies. The whole spectrum is formulated as a sum over all pitches:

$$V_{ft} = \sum_{k=1}^K V_{ft}^k = \sum_{k=1}^K \sum_{f'=-3\sigma_{kt}}^{3\sigma_{kt}} W_{(f-f')k} \exp\left(-\frac{f'^2}{2\sigma_{kt}^2}\right) H_{kt}. \quad (\text{C.3})$$

Parameter estimation

In order to simplify the implementation, we restrict the Gaussian function in a fixed range, within $\pm L$ frequency bins. Then the model is formulated as follows:

$$V_{ft} = \sum_{k=1}^K V_{ft}^k = \sum_{k=1}^K \sum_{f'=-L}^L W_{(f-f')k} \exp\left(-\frac{f'^2}{2\sigma_{kt}^2}\right) H_{kt}. \quad (\text{C.4})$$

The parameters are estimated using multiplicative update rules with β -divergence as in Appendix B. The derivative of the β -divergence w.r.t. θ is given by the subtraction of two non-negative parts:

$$\nabla_{\theta} D(\theta) = (\mathbf{V}(\theta)^{\beta-1} - \mathbf{X}\mathbf{V}(\theta)^{\beta-2}) \nabla_{\theta} \mathbf{V}(\theta), \quad (\text{C.5})$$

where \mathbf{X} the observed spectrogram. The update rule for θ is

$$\theta \leftarrow \theta \cdot \frac{\mathbf{V}(\theta)^{\beta-1} \nabla_{\theta}^{-} \mathbf{V}(\theta) + \mathbf{X}\mathbf{V}(\theta)^{\beta-2} \nabla_{\theta}^{+} \mathbf{V}(\theta)}{\mathbf{X}\mathbf{V}(\theta)^{\beta-2} \nabla_{\theta}^{-} \mathbf{V}(\theta) + \mathbf{V}(\theta)^{\beta-1} \nabla_{\theta}^{+} \mathbf{V}(\theta)}. \quad (\text{C.6})$$

We first derive the update rule for W_{fk} as follows:

$$V_{(f+f')t} = \sum_{k=1}^K \sum_{f'=-L}^L W_{fk} \exp\left(-\frac{f'^2}{2\sigma_{kt}^2}\right) H_{kt}, \quad (\text{C.7})$$

$$\frac{\partial V_{(f+f')t}}{\partial W_{fk}} = \sum_{f'=-L}^L \exp\left(-\frac{f'^2}{2\sigma_{kt}^2}\right) H_{kt}. \quad (\text{C.8})$$

Then the update rule for W_{fk} is:

$$W_{fk} \leftarrow W_{fk} \frac{\sum_{t=1}^T \sum_{f'=-L}^L \exp\left(-\frac{f'^2}{2\sigma_{kt}^2}\right) H_{kt} V_{(f+f')t}^{\beta-2} X_{(f+f')t}}{\sum_{t=1}^T \sum_{f'=-L}^L \exp\left(-\frac{f'^2}{2\sigma_{kt}^2}\right) H_{kt} V_{(f+f')t}^{\beta-1}}. \quad (\text{C.9})$$

The derivative of the reconstruction V_{ft} w.r.t. H_{kt} is given by:

$$\frac{\partial V_{ft}}{\partial H_{kt}} = \sum_{f'=-L}^L W_{(f-f')k} \exp\left(-\frac{f'^2}{2\sigma_{kt}^2}\right), \quad (\text{C.10})$$

so the update rule for H_{kt} is:

$$H_{kt} \leftarrow H_{kt} \frac{\sum_{f=1}^F \sum_{f'=-L}^L W_{(f-f')k} \exp\left(-\frac{f'^2}{2\sigma_{kt}^2}\right) V_{ft}^{\beta-2} X_{ft}}{\sum_{f=1}^F \sum_{f'=-L}^L W_{(f-f')k} \exp\left(-\frac{f'^2}{2\sigma_{kt}^2}\right) V_{ft}^{\beta-1}}. \quad (\text{C.11})$$

The derivative of the reconstruction V_{ft} w.r.t. σ_{kt}^2 is given by:

$$\begin{aligned}\frac{\partial V_{ft}}{\partial \sigma_{kt}^2} &= \sum_{f'=-L}^L W_{(f-f')k} \frac{\partial \exp(-\frac{f'^2}{2\sigma_{kt}^2})}{\partial \sigma_{kt}^2} H_{kt} \\ &= \frac{H_{kt}}{2(\sigma_{kt}^2)^2} \sum_{f'=-L}^L W_{(f-f')k} f'^2 \exp(-\frac{f'^2}{2\sigma_{kt}^2}),\end{aligned}\quad (\text{C.12})$$

so the variance σ_{kt}^2 is updated by:

$$\sigma_{kt}^2 \leftarrow \sigma_{kt}^2 \frac{\sum_{f=1}^F \sum_{f'=-L}^L W_{(f-f')k} f'^2 \exp(-\frac{f'^2}{2\sigma_{kt}^2}) V_{ft}^{\beta-2} X_{ft}}{\sum_{f=1}^F \sum_{f'=-L}^L W_{(f-f')k} f'^2 \exp(-\frac{f'^2}{2\sigma_{kt}^2}) V_{ft}^{\beta-1}}.\quad (\text{C.13})$$

Bibliography

- S. A. Abdallah and M. D. Plumbley. Polyphonic music transcription by non-negative sparse coding of power spectra. In *5th International Conference on Music Information Retrieval (ISMIR)*, pages 318–325, 2004.
- M. Aramaki, J. Bensa, L. Daudet, P. Guillemin, and R. Kronland-Martinet. Resynthesis of coupled piano string vibrations based on physical modeling. *Journal of New Music Research*, 30(3):213–226, 2001.
- B. Bank. Physics-based sound synthesis of the piano. Master’s thesis, Budapest University of Technology and Economics, Hungary, 2000.
- B. Bank. Accurate and efficient modeling of beating and two-stage decay for string instrument synthesis. In *MOSART Workshop on Current Research Directions in Computer Music*, pages 134–137, 2001.
- M. Bay, A. F. Ehmann, and J. S. Downie. Evaluation of multiple-F0 estimation and tracking systems. In *10th International Society for Music Information Retrieval Conference (ISMIR)*, pages 315–320, 2009.
- M. Bay, A. F. Ehmann, J. W. Beauchamp, P. Smaragdis, and J. S. Downie. Second fiddle is important too: Pitch tracking individual voices in polyphonic music. In *13th International Society for Music Information Retrieval Conference (ISMIR)*, pages 319–324, 2012.
- J. M. Becker, C. Sohn, and C. Rohlfig. NMF with spectral and temporal continuity criteria for monaural sound source separation. In *European Signal Processing Conference (EUSIPCO)*, pages 316 – 320, 2014.
- E. Benetos. *Automatic transcription of polyphonic music exploiting temporal evolution*. PhD thesis, Queen Mary University of London, 2012.
- E. Benetos and S. Dixon. A shift-invariant latent variable model for automatic music transcription. *Computer Music Journal*, 36(4):81–94, 2012a.

- E. Benetos and S. Dixon. Multiple-F0 estimation and note tracking for MIREX 2012 using a shift-invariant latent variable model. In *Music Information Retrieval Evaluation eXchange (MIREX)*, 2012b.
- E. Benetos and S. Dixon. Multiple-instrument polyphonic music transcription using a temporally constrained shift-invariant model. *The Journal of the Acoustical Society of America*, 133(3):1727–1741, 2013.
- E. Benetos and T. Weyde. An efficient temporally-constrained probabilistic model for multiple-instrument music transcription. In *16th International Society for Music Information Retrieval Conference (ISMIR)*, pages 701–707, 2015a.
- E. Benetos and T. Weyde. Multiple-F0 estimation and note tracking for MIREX 2015 using a sound state-based spectrogram factorization model. In *Music Information Retrieval Evaluation eXchange (MIREX)*, 2015b.
- E. Benetos, S. Cherla, and T. Weyde. An efficient shift-invariant model for polyphonic music transcription. In *6th International Workshop on Machine Learning and Music*, 2013a.
- E. Benetos, S. Dixon, D. Giannoulis, H. Kirchhoff, and A. Klapuri. Automatic music transcription: challenges and future directions. *Journal of Intelligent Information Systems*, 41(3):407–434, 2013b.
- E. Benetos, R. Badeau, T. Weyde, and G. Richard. Template adaptation for improving automatic music transcription. In *15th International Society for Music Information Retrieval Conference (ISMIR)*, pages 175–180, Taipei, 2014.
- J. Bensa, S. Bilbao, R. Kronland-Martinet, and J. O. Smith. The simulation of piano string vibration: From physical models to finite difference schemes and digital waveguides. *The Journal of the Acoustical Society of America*, 114(2):1095–1107, 2003.
- T. Berg-Kirkpatrick, J. Andreas, and D. Klein. Unsupervised transcription of piano music. In *Advances in Neural Information Processing Systems 27*, pages 1538–1546, 2014.
- N. Bertin, R. Badeau, and E. Vincent. Fast Bayesian NMF algorithms enforcing harmonicity and temporal continuity in polyphonic music transcription. In *IEEE Workshop on Applications of Signal Processing to Audio and Acoustics (WASPAA)*, pages 29–32, 2009a.
- N. Bertin, C. Févotte, and R. Badeau. A tempering approach for Itakura-Saito non-negative matrix factorization. With application to music transcription. In

- IEEE International Conference on Acoustics, Speech, and Signal Processing (ICASSP)*, pages 1545–1548, 2009b.
- N. Bertin, R. Badeau, and E. Vincent. Enforcing harmonicity and smoothness in Bayesian non-negative matrix factorization applied to polyphonic music transcription. *IEEE Transactions on Acoustics, Speech, and Signal Processing*, 18(3):538–549, 2010.
- E.D. Blackham. The physics of the piano. *Scientific American*, 213(6), 1965.
- S. Böck and M. Schedl. Polyphonic piano note transcription with recurrent neural networks. In *IEEE International Conference on Acoustics, Speech and Signal Processing (ICASSP)*, pages 121–124, 2012.
- S. Böck and G. Widmer. Local group delay based vibrato and tremolo suppression for onset detection. In *14th International Society for Music Information Retrieval Conference (ISMIR)*, pages 589–594, November 2013.
- J. C. Brown. Calculation of a constant Q spectral transform. *The Journal of the Acoustical Society of America*, 89(1):425434, 1991.
- J. J. Burred. *The acoustics of the Piano*. PhD thesis, Professional Conservatory of Music Arturo Soria, 2004.
- B. Capleton. False beats in coupled piano string unisons. *The Journal of the Acoustical Society of America*, 115(2):885–892, 2004.
- A. T. Cemgil. Bayesian inference for nonnegative matrix factorisation models. *Computational Intelligence and Neuroscience*, 2009.
- A. Chaigne and J. Kergomard. *Acoustics of Musical Instruments*. Springer-Verlag New York, 2016.
- Z. Chen, G. Grindlay, and D. P. W. Ellis. Transcribing multi-instrument polyphonic music with transformed eigeninstrument whole-note templates. In *Music Information Retrieval Evaluation eXchange (MIREX)*, 2012.
- T. Cheng, S. Dixon, and M. Mauch. A deterministic annealing EM algorithm for automatic music transcription. In *14th International Society for Music Information Retrieval Conference (ISMIR)*, pages 475–480, 2013.
- T. Cheng, S. Dixon, and M. Mauch. A comparison of extended source-filter models for musical signal reconstruction. In *International Conference on Digital Audio Effects (DAFx)*, pages 203–209, 2014.

- T. Cheng, S. Dixon, and M. Mauch. Modelling the decay of piano sounds. In *IEEE International Conference on Acoustics, Speech and Signal Processing (ICASSP)*, pages 594–598, 2015a.
- T. Cheng, S. Dixon, and M. Mauch. Improving piano note tracking by HMM smoothing. In *European Signal Processing Conference (EUSIPCO)*, pages 2009–2013, 2015b.
- M. Christensen and A. Jakobsson. *Multi-Pitch Estimation*. Morgan & Claypool, 2009.
- A. Cogliati and Z. Duan. Piano music transcription modeling note temporal evolution. In *IEEE International Conference on Acoustics, Speech and Signal Processing (ICASSP)*, pages 429–433, 2015.
- A. Cont. Realtime multiple pitch observation using sparse non-negative constraints. In *7th International Conference on Music Information Retrieval (ISMIR)*, pages 206–211, 2006.
- A. Cont, S. Dubnov, and D. Wessel. Realtime multiple-pitch and multiple-instrument recognition for music signals using sparse non-negative constraints. In *International Conference on Digital Audio Effects (DAFx)*, pages 85–92, 2007.
- A. de Cheveigné. Cancellation model of pitch perception. *The Journal of the Acoustical Society of America*, 103(3):1261–1271, 1998.
- A. de Cheveigné. Multiple f0 estimation. In *Computational Auditory Scene Analysis, Algorithms and Applications*. IEEE Press/Wiley, New York, 2006.
- A. de Cheveigné and H. Kawahara. YIN, a fundamental frequency estimator for speech and music. *The Journal of the Acoustical Society of America*, 111(4):1917–1930, 2002.
- A. Dessein, A. Cont, and G. Lemaitre. Real-time polyphonic music transcription with non-negative matrix factorization and beta-divergence. In *11th International Society for Music Information Retrieval Conference (ISMIR)*, pages 489–494, 2010.
- S. Dixon. On the computer recognition of solo piano music. In *Australasian Computer Music Conference*, pages 31–37, 2000.
- K. Dressler. Pitch estimation by the pair-wise evaluation of spectral peaks. In *Audio Engineering Society Conference: 42nd International Conference on Semantic Audio*, pages 278–290, 2011.

- Z. Duan and D. Temperley. Note-level music transcription by maximum likelihood sampling. In *15th International Society for Music Information Retrieval Conference (ISMIR)*, pages 181–186, 2014.
- Z. Duan, B. Pardo, and C. Zhang. Multiple fundamental frequency estimation by modeling spectral peaks and non-peak regions. *IEEE Transactions on Audio, Speech, and Language Processing*, 18(8):2121–2133, 2010.
- N. Q. K. Duong, E. Vincent, and R. Gribonval. Under-determined reverberant audio source separation using local observed covariance and auditory-motivated time-frequency representation. In *9th International Conference on Latent Variable Analysis and Signal Separation*, pages 73–80, 2010.
- J. Eggert and E. Körner. Sparse coding and NMF. In *IEEE International Joint Conference on Neural Networks*, pages 2529–2533, 2004.
- V. Emiya, B. David, and R. Badeau. A parametric method for pitch estimation of piano tones. In *IEEE International Conference on Acoustics, Speech and Signal Processing (ICASSP)*, volume 1, pages 249–252, 2007.
- V. Emiya, R. Badeau, and B. David. Multipitch estimation of piano sounds using a new probabilistic spectral smoothness principle. *IEEE Transactions on Audio, Speech, and Language Processing*, 18(6):1643–1654, 2010.
- S. Ewert, M. D. Plumbley, and M. Sandler. A dynamic programming variant of non-negative matrix deconvolution for the transcription of struck string instruments. In *IEEE International Conference on Acoustics, Speech and Signal Processing (ICASSP)*, pages 569–573, 2015.
- C. Févotte. Majorization-Minimisation algorithm for smooth Itakuro-Saito non-negative matrix factorization. In *IEEE International Conference on Acoustics, Speech and Signal Processing (ICASSP)*, pages 1980–1983, 2011.
- C. Févotte, N. Bertin, and J.-L. Durrieu. Nonnegative matrix factorization with the Itakura-Saito divergence: With application to music analysis. *Neural Computation*, 21(3):793–830, 2009.
- T. Fillon and J. Prado. A flexible multi-resolution time-frequency analysis framework for audio signals. In *International Conference on Information Science, Signal Processing and their Applications (ISSPA)*, pages 1124–1129, 2012.
- H. Fletcher, E. D. Blackham, and R. Stratton. Quality of piano tones. *The Journal of the Acoustical Society of America*, 34(6):749–761, 1962.

- N. H. Fletcher and T. D. Rossing. *The Physics of Musical Instruments*. Springer New York, 1998.
- J. Fox and S. Weisberg. Nonlinear regression and nonlinear least squares in R. In *Appendix to An R Companion to Applied Regression, second edition*, pages 1–20, 2010.
- D. Gerhard. Pitch extraction and fundamental frequency: History and current techniques. Technical report, Dept. of Computer Science, University of Regina, 2003.
- M. Goto. A real-time music-scene-description system: predominant-f0 estimation for detecting melody and bass lines in real-world audio signals. *Speech Communication*, 43(4):311–329, 2004.
- M. Goto, H. Hashiguchi, T. Nishimura, and R. Oka. RWC Music Database: Music Genre Database and Musical Instrument Sound Database. In *4th International Conference on Music Information Retrieval (ISMIR)*, pages 229–230, 2003.
- G. Grindlay and D. P. W. Ellis. Transcribing multi-instrument polyphonic music with hierarchical eigeninstruments. *IEEE Journal on Selected Topics in Signal Processing*, 5(6):1159–1169, 2011.
- G. Grindlay and D. P. W. Ellis. A probabilistic subspace model for multi-instrument polyphonic transcription. In *11th International Society for Music Information Retrieval Conference (ISMIR)*, pages 81–94, 2012.
- R. Hennequin, R. Badeau, and B. David. Time-dependent parametric and harmonic templates in non-negative matrix factorization. In *International Conference on Digital Audio Effects (DAFx)*, pages 246–253, 2010.
- R. Hennequin, R. Badeau, and B. David. NMF with time-frequency activations to model nonstationary audio events. *IEEE Transactions on Audio, Speech, and Language Processing*, 19(4):744–753, 2011a.
- R. Hennequin, B. David, and R. Badeau. Score informed audio source separation using a parametric model of non-negative spectrogram. In *IEEE International Conference on Acoustics, Speech and Signal Processing (ICASSP)*, pages 45–48, 2011b.
- D. J. Hermes. Measurement of pitch by sub-harmonic summation. *The Journal of the Acoustical Society of America*, 83(1):257–264, 1988.
- W. Hess. *Pitch Determination of Speech Signals*. Springer-Verlag, Berlin, 1983.

- M. C. Hirschhorn. Dynamic model of a piano action mechanism. Master’s thesis, University of Waterloo, Canada, 2004.
- M. Hoffman, D. Blei, and P. Cook. Bayesian Nonparametric Matrix Factorization for Recorded Music. In *27th International Conference on Machine Learning (ICML)*, pages 439–446, 2010.
- T. Hofmann. Probabilistic latent semantic analysis. In *Uncertainty in Artificial Intelligence*, pages 289–296, 1999.
- P. O. Hoyer. Non-negative sparse coding. In *12th IEEE Workshop on Neural Networks for Signal Processing*, 2002.
- P. O. Hoyer. Non-negative matrix factorization with sparseness constraints. *Journal of Machine Learning Research*, 5:1457–1469, 2004.
- Y. Itaya, H. Zen, Y. Nankaku, C. Miyajima, K. Tokuda, and T. Kitamura. Deterministic annealing EM algorithm in acoustic modeling for speaker and speech recognition. *IEICE Transactions on Information and Systems*, E88-D (3):425–431, 2005.
- H. Järveläinen, V. Välimäki, and M. Karjalainen. Audibility of the timbral effects of inharmonicity in stringed instrument tones. *Acoustics Research Letters Online*, 2(3):79–84, 2001.
- H. Kameoka, T. Nishimoto, and S. Sagayama. Harmonic-temporal structured clustering via deterministic annealing EM algorithm for audio feature extraction. In *6th International Conference on Music Information Retrieval (ISMIR)*, pages 115–122, 2005.
- H. Kameoka, T. Nishimoto, and S. Sagayama. A multipitch analyzer based on harmonic temporal structured clustering. *IEEE Transactions on Audio, Speech, and Language Processing*, 15(3):982–994, 2007.
- H. Kameoka, N. Ono, K. Kashino, and S. Sagayama. Complex NMF: A new sparse representation for acoustic signals. In *IEEE International Conference on Acoustics, Speech and Signal Processing (ICASSP)*, pages 3437–3440, 2009.
- M. Karjalainen, P. Antsalo, A. Mäkipirta, T. Peltonen, and V. Välimäki. Estimation of modal decay parameters from noisy response measurements. *Journal of the Audio Engineering Society*, 50(11):867–878, 2002.
- H. Kirchhoff. *A User-assisted Approach to Multiple Instrument Music Transcription*. PhD thesis, Queen Mary University of London, 2013.

- H. Kirchhoff, R. Badeau, and S. Dixon. Towards complex matrix decomposition of spectrograms based on the relative phase offsets of harmonic sounds. In *IEEE International Conference on Acoustics, Speech and Signal Processing (ICASSP)*, pages 1572–1576, 2014.
- A. Klapuri. Analysis of musical instrument sounds by source-filter-decay model. In *IEEE International Conference on Audio, Speech and Signal Processing (ICASSP)*, pages 53–56, 2007.
- A. Klapuri and M. Davy, editors. *Signal Processing Methods for Music Transcription*. Springer-Verlag, New York, 2006.
- A. P. Klapuri. Multiple fundamental frequency estimation based on harmonicity and spectral smoothness. *IEEE Transactions on Speech and Audio Processing*, 11(6):804–816, 2003.
- A. P. Klapuri. A perceptually motivated multiple-f₀ estimation method. In *IEEE Workshop on Applications of Signal Processing to Audio and Acoustics (WASPAA)*, pages 291–294, 2005.
- D. Lee and H. Seung. Algorithms for non-negative matrix factorization. In *Neural Information Processing Systems (NIPS)*, pages 556–562, 2001.
- D. D. Lee and H. S. Seung. Learning the parts of objects by non-negative matrix factorization. *Nature*, 401:788–791, 1999.
- D. D. Lee and H. S. Seung. Algorithms for non-negative matrix factorization. In *Advances in Neural Information Processing Systems 13*, pages 556–562, 2000.
- N. Lee, J. O. Smith, and V. Välimäki. Analysis and synthesis of coupled vibrating strings using a hybrid modal-waveguide synthesis model. *IEEE Transactions on Audio, Speech and Language Processing*, 18(4):833–842, 2010.
- D. Livelybrooks. Physics of Sound and Music, Course PHYS 152, Lecture 16. University Lecture, 2007. URL <http://hendrix2.uoregon.edu/~dlivelyb/phys152/116.html>.
- S. McAdams. Perspectives on the contribution of timbre to musical structure. *Computer Music Journal*, 23(2):96–113, 1999.
- P. McLeod and G. Wyvill. A smarter way to find pitch. In *International Computer Music Conference (ICMC)*, pages 138–141, 2005.
- J. Meyer. *Acoustics and the Performance of Music*. Springer-Verlag, New York, 2009.

- MIREX. Multiple Fundamental Frequency Estimation & Tracking in Music Information Retrieval Evaluation eXchange (MIREX), 2016. URL http://www.music-ir.org/mirex/wiki/2016:Multiple_Fundamental_Frequency_Estimation_%26_Tracking.
- K. Miyamoto, H. Kameoka, T. Nishimoto, N. Ono, and S. Sagayama. Harmonic-Temporal-Timbral Clustering (HTTC) for the analysis of multi-instrument polyphonic music signals. In *IEEE International Conference on Acoustics, Speech and Signal Processing (ICASSP)*, pages 113–116, 2008.
- N. Mohammadiha, W. B. Kleijn, and A. Leijon. Gamma hidden Markov model as a probabilistic Nonnegative Matrix Factorization. In *European Signal Processing Conference (EUSIPCO)*, pages 1–5, 2013.
- B. C. J. Moore and B. R. Glasberg. A revision of Zwicker’s loudness model. *Acta Acustica*, 82:335–345, 1996.
- J. A. Moorer. *On the Segmentation and Analysis of Continuous Musical Sound by Digital Computer*. PhD thesis, Stanford University, CA, USA, 1975.
- G. J. Mysore, P. Smaragdis, and B. Raj. Non-negative hidden Markov modeling of audio with application to source separation. In *International Conference on Latent Variable Analysis and Signal Separation*, pages 140–148, 2010.
- M. Nakano, J. Le Roux, H. Kameoka, Y. Kitano, N. Ono, and S. Sagayama. Nonnegative matrix factorization with Markov-chained bases for modeling time-varying patterns in music spectrograms. In *International Conference on Latent Variable Analysis and Signal Separation*, pages 149–156, 2010.
- J. Nam, J. Ngiam, H. Lee, and M. Slaney. A classification-based polyphonic piano transcription approach using learned feature representations. In *12th International Society for Music Information Retrieval Conference (ISMIR)*, 2011.
- T. Necciari, P. Balazs, N. Holighaus, and P. L. Sondergaard. The ERBlet transform: An auditory-based time-frequency representation with perfect reconstruction. In *IEEE International Conference on Acoustics, Speech and Signal Processing (ICASSP)*, pages 498–502, 2013.
- A. M. Noll. Cepstrum pitch determination. *The Journal of the Acoustical Society of America*, 41(2):293–309, 1967.
- K. O’Hanlon and M. D. Plumbley. Automatic music transcription using row weighted decompositions. In *IEEE International Conference on Acoustics, Speech and Signal Processing (ICASSP)*, pages 16–20, 2013.

- A. V. Oppenheim and R. W. Schaffer. From frequency to quefrency: a history of the cepstrum. *IEEE Signal Processing Magazine*, 21(5):95–106, 2004.
- A. Ozerov, C. Févotte, and M. Charbit. Factorial scaled hidden Markov model for polyphonic audio representation and source separation. In *IEEE Workshop on Applications of Signal Processing to Audio and Acoustics (WASPAA)*, pages 121–124, 2009.
- G. Peeters. Music pitch representation by periodicity measures based on combined temporal and spectral representations. In *IEEE International Conference on Acoustics Speech and Signal Processing Proceedings (ICASSP)*, 2006.
- R. Peharz and F. Pernkopf. Sparse nonnegative matrix factorization with l0-constraints. *Neurocomputing*, 80(1):38–46, 2012.
- J. R. Pierce. *The science of musical sound*. New York: Scientific American Library, 1983.
- R. Plomp. Timbre as a multidimensional attribute of complex tones. In *Frequency Analysis and Periodicity Detection in Hearing*. A. W. Sijthoff, Leiden, 1970.
- R. Plomp. Timbre of complex tones. In *Aspects of Tone Sensation: A Psychophysical Study*. Academic Press, 1976.
- M. D. Plumbley and S. A. Abdallah. An independent component analysis approach to automatic music transcription. In *Audio Engineering Society Convention 114*, 2003.
- G. E. Poliner and D. P. W. Ellis. A discriminative model for polyphonic piano transcription. *EURASIP Journal on Applied Signal Processing*, 2007(1), 2007.
- L. R. Rabiner. On the use of autocorrelation analysis for pitch detection. *IEEE Transactions on Acoustics, Speech, and Signal Processing*, 25(1):24–33, 1977.
- L. R. Rabiner. A tutorial on hidden Markov models and selected applications in speech recognition. *Proceedings of the IEEE*, 77(2):257–286, 1989.
- S. Raczyński, N. Ono, and S. Sagayama. Multipitch analysis with harmonic nonnegative matrix approximation. In *8th International Conference on Music Information Retrieval (ISMIR)*, pages 381–386, 2007.
- S. Raczyński, E. Vincent, and S. Sagayama. Dynamic Bayesian networks for symbolic polyphonic pitch modeling. *IEEE Transactions on Audio, Speech, and Language Processing*, 21(9):1830–1840, 2013.

- F. Rigaud. *Models of music signals informed by physics. Application to piano music analysis by non-negative matrix factorization*. PhD thesis, Télécom ParisTech, 2013.
- F. Rigaud, B. David, and L. Daudet. Piano sound analysis using Non-negative Matrix Factorization with inharmonicity constraint. In *European Signal Processing Conference (EUSIPCO)*, pages 2462–2466, 2012.
- F. Rigaud, B. David, and L. Daudet. A parametric model and estimation techniques for the inharmonicity and tuning of the piano. *The Journal of the Acoustical Society of America*, 133(5):3107–3118, 2013a.
- F. Rigaud, A. Falaize, B. David, and L. Daudet. Does inharmonicity improve an NMF-based piano transcription model? In *IEEE International Conference on Acoustics, Speech, and Signal Processing (ICASSP)*, pages 11–15, 2013b.
- J. G. Roederer. *The Physics and Psychophysics of Music: an Introduction*. Springer-Verlag, New York, 2009.
- M. J. Ross, H. L. Shaffer, A. Cohen, R. Freudberg, and H. J. Manley. Average magnitude difference function pitch extractor. *IEEE Transactions on Acoustics, Speech, and Signal Processing*, 22(5):353–363, 1974.
- T. D. Rossing. *The Science of Sound*. Addison-Wesley Publishing Company, 1990.
- M. P. Ryyänänen and A. Klapuri. Polyphonic music transcription using note event modeling. In *IEEE Workshop on Applications of Signal Processing to Audio and Acoustics (WASPAA)*, pages 319–322, 2005.
- R. Schachtner, G. Poeppel, A. M. Tomé, and E. W. Lang. A Bayesian approach to the Lee-Seung update rules for NMF. *Pattern Recognition Letters*, 45: 251–256, 2014.
- C. Schörkhuber and A. Klapuri. Constant-Q transform toolbox for music processing. In *7th Sound and Music Computing Conference*, 2010.
- C. Schörkhuber, A. Klapuri, N. Holighaus, and M. Döfler. A Matlab Toolbox for Efficient Perfect Reconstruction Time-Frequency Transforms with Log-Frequency Resolution. In *Audio Engineering Society Conference: 53rd International Conference on Semantic Audio*, pages 1–8, 2014.
- O.H. Schuck and R.W. Young. Observations on the vibrations of piano strings. *The Journal of the Acoustical Society of America*, 15(1), 1943.

- S. Sigtia, E. Benetos, S. Cherla, T. Weyde, A. d'Avila Garcez, and S. Dixon. An RNN-based music language model for improving automatic music transcription. In *15th International Society for Music Information Retrieval Conference (ISMIR)*, pages 53–58, 2014.
- S. Sigtia, E. Benetos, N. Boulanger-Lewandowski, T. Weyde, A. d'Avila Garcez, and S. Dixon. A hybrid recurrent neural network for music transcription. In *IEEE International Conference on Acoustics, Speech and Signal Processing (ICASSP)*, pages 2061–2065, 2015.
- S. Sigtia, E. Benetos, and S. Dixon. An end-to-end neural network for polyphonic piano music transcription. *IEEE/ACM Transactions on Audio, Speech, and Language Processing*, 24(5):927–939, 2016.
- P. Smaragdis. Relative-pitch tracking of multiple arbitrary sounds. *The Journal of the Acoustical Society of America*, 125(5):3406–3413, 2009.
- P. Smaragdis and J. C. Brown. Non-negative matrix factorization for polyphonic music transcription. In *IEEE Workshop on Applications of Signal Processing to Audio and Acoustics (WASPAA)*, pages 177–180, 2003.
- P. Smaragdis and B. Raj. Shift-invariant probabilistic latent component analysis. Technical report, Mitsubishi Electric Research Laboratories, 2007.
- P. Smaragdis, B. Raj, and M. Shashanka. Sparse and shift-invariant feature extraction from non-negative data. In *IEEE International Conference on Acoustics, Speech and Signal Processing (ICASSP)*, pages 2069–2072, 2008.
- P. Smaragdis, C. Fevotte, G. J. Mysore, N. Mohammadiha, and M. Hoffman. Static and Dynamic Source Separation Using Nonnegative Factorizations: A unified view. *IEEE Signal Processing Magazine*, 31(3):66–75, 2014.
- J. O. Smith. Physical modeling using digital waveguides. *Computer Music Journal*, 16(4):74–91, 1992.
- D. Talkin. A robust algorithm for pitch tracking (RAPT). In *Speech Coding and Synthesis*. Elsevier Science B. V., 1995.
- G. Tambouratzis, K. Perifanos, I. Voulgari, A. Askenfelt, S. Granqvist, K. F. Hansen, Y. Orlarey, D. Fober, and S. Letz. VEMUS: An Integrated Platform to Support Music Tuiton Tasks. In *8th IEEE International Conference on Advanced Learning Technologies*, pages 972–976, 2008.
- T. F. Tavares, J. G. A. Barbedo, and R. Attux. Unsupervised note activity detection in NMF-based automatic transcription of piano music. *Journal of New Music Research*, 45(2):118–123, 2016.

- N. Ueda and R. Nakano. Deterministic annealing EM algorithm. *Neural Networks*, 11(2):271 – 282, 1998.
- V. Välimäki, J. Huopaniemi, M. Karjalainen, and Z. Jánosy. Physical modeling of plucked string instruments with application to real-time sound synthesis. *Journal of the Audio Engineering Society*, 44(5):331–353, 1996.
- E. Vincent. Musical source separation using time-frequency priors. *IEEE Transactions on Audio, Speech and Language Processing*, 14(1):91–98, 2006.
- E. Vincent and X. Rodet. Music transcription with ISA and HMM. In *International Symposium on Independent Component Analysis and Blind Signal Separation*, pages 1197–1204, 2004.
- E. Vincent, N. Bertin, and R. Badeau. Harmonic and inharmonic nonnegative matrix factorization for polyphonic pitch transcription. In *IEEE International Conference on Acoustics, Speech and Signal Processing (ICASSP)*, pages 109–112, 2008.
- E. Vincent, N. Bertin, and R. Badeau. Adaptive harmonic spectral decomposition for multiple pitch estimation. *IEEE Transactions on Acoustics, Speech, and Signal Processing*, 18(3):528–537, 2010.
- T. Virtanen. Monaural sound source separation by nonnegative matrix factorization with temporal continuity and sparseness criteria. *IEEE Transactions on Acoustics, Speech, and Signal Processing*, 15(3):1066–1074, 2007.
- T. Virtanen, A. T. Cemgil, and S. Godsill. Bayesian extensions to non-negative matrix factorisation for audio signal modelling. In *IEEE International Conference on Acoustics, Speech and Signal Processing (ICASSP)*, pages 1825–1828, 2008.
- W. Wang, Y. Luo, J. A. Chambers, and S. Sanei. Note onset detection via nonnegative factorization of magnitude spectrum. *EURASIP Journal on Advances in Signal Processing*, 2008(1), 2008.
- W. Wang, A. Cichocki, and J. A. Chambers. A multiplicative algorithm for convolutive non-negative matrix factorization based on squared euclidean distance. *IEEE Transactions on Signal Processing*, 57(7):2858–2864, 2009.
- G. Weinreich. Coupled piano strings. *The Journal of the Acoustical Society of America*, 62(6):1474–1484, 1977.
- C. Yeh, A. Roebel, and X. Rodet. Multiple fundamental frequency estimation and polyphony inference of polyphonic music signals. *IEEE Transactions on Audio, Speech, and Language Processing*, 18(6):1116–1126, 2010.

K. Yoshii and M. Goto. Infinite composite autoregressive models for music signal analysis. In *13th International Society for Music Information Retrieval Conference (ISMIR)*, pages 79–84, 2012.